INFORMATION TO USERS

This reproduction was made from a copy of a manuscript sent to us for publication and microfilming. While the most advanced technology has been used to photograph and reproduce this manuscript, the quality of the reproduction is heavily dependent upon the quality of the material submitted. Pages in any manuscript may have indistinct print. In all cases the best available copy has been filmed.

The following explanation of techniques is provided to help clarify notations which may appear on this reproduction.

1. Manuscripts may not always be complete. When it is not possible to obtain missing pages, a note appears to indicate this.

2. When copyrighted materials are removed from the manuscript, a note appears to indicate this.

3. Oversize materials (maps, drawings, and charts) are photographed by sectioning the original, beginning at the upper left hand corner and continuing from left to right in equal sections with small overlaps. Each oversize page is also filmed as one exposure and is available, for an additional charge, as a standard 35mm slide or in black and white paper format.*

4. Most photographs reproduce acceptably on positive microfilm or microfiche but lack clarity on xerographic copies made from the microfilm. For an additional charge, all photographs are available in black and white standard 35mm slide format.*

*For more information about black and white slides or enlarged paper reproductions, please contact the Dissertations Customer Services Department.

U·M·I Dissertation Information Service

University Microfilms International
A Bell & Howell Information Company
300 N. Zeeb Road, Ann Arbor, Michigan 48106

Wickramasekara, Lee

SYNTHESIS OF SAMARIUM-TITANIUM-IRON AND NEODYMIUM-IRON-BORON MAGNETIC FILMS WITH SPECIAL ANISOTROPIES

City University of New York PH.D. 1986

PLEASE NOTE:

In all cases this material has been filmed in the best possible way from the available copy. Problems encountered with this document have been identified here with a check mark __✓__.

1. Glossy photographs or pages _____
2. Colored illustrations, paper or print _____
3. Photographs with dark background _____
4. Illustrations are poor copy _____
5. Pages with black marks, not original copy _____
6. Print shows through as there is text on both sides of page _____
7. Indistinct, broken or small print on several pages ✓
8. Print exceeds margin requirements _____
9. Tightly bound copy with print lost in spine _____
10. Computer printout pages with indistinct print _____
11. Page(s) _____ lacking when material received, and not available from school or author.
12. Page(s) _____ seem to be missing in numbering only as text follows.
13. Two pages numbered _____. Text follows.
14. Curling and wrinkled pages _____
15. Dissertation contains pages with print at a slant, filmed as received _____
16. Other _____

_____

_____

University
Microfilms
International

SYNTHESIS OF Sm-Ti-Fe AND Nd-Fe-B MAGNETIC FILMS WITH SPECIAL ANISOTROPIES

by

LEE WICKRAMASEKARA

A dissertation submitted to the Graduate Faculty in Physics in partial fulfillment of the requirements for the degree of Doctor of Philosophy, The City University of New York.

1986

This manuscript has been read and accepted for the Graduate Faculty in Physics in satisfaction of the dissertation requirement for the degree of Doctor of Philosophy.

9/30/86
date

Fred J. Cadieu
Chairman of Examining Committee

9/30/86
date

Executive Officer

Prof. Fred J. Cadieu

Prof. Rutherford C. Fischer

Prof. Mark Miksic

Prof. Fred H. Smith

Dr. Jerry J. Cuomo

Supervisory Committee

The City University of New York

ABSTRACT

SYNTHESIS OF Sm-Ti-Fe AND Nd-Fe-B MAGNETIC FILMS

WITH SPECIAL ANISOTROPIES

by

LEE WICKRAMASEKARA

Adviser: Professor Fred J. Cadieu

Rare earth-transition metal film magnets of Nd-Fe-B and several new phases of Sm-Ti-Fe system have been synthesised by special sputtering methods to utilize the high magnetic anisotropies of these alloys. The magnetic properties of these film magnets were observed to be strongly dependent on the film textures. Thus, by varying the sputtering conditions we were able to synthesize films with crystal textures which gives rise to special anisotropies. Crystalline films of $Sm(FeTi)_2$ and $SmCo_3$ were synthesized with large perpendicular anisotropy of 10^6 erg/cc, whereas $(SmTi)Fe_5$ and $Sm_2(FeCoZr)_{17}$ were synthesized with inplane anisotropy and static energy product of 20 MG-Oe. The $Nd_2Fe_{14}B$ film system is unique due to the fact that it can be synthesized with large perpendicular anisotropy of $1.5x10^7$ erg/cc with 9 kG remanent and 16 kOe coercive force or inplane anisotropy with 16 MG-Oe static energy product by controlling the sputtering rate. In addition, $SmCo_5$, $(SmTi)Fe_5$, and $Sm_2(FeCoZr)_{17}$ film systems were synthesized in amorphous states in the presence of inplane magnetic field of 2.5 kOe

and exibited large uniaxial inplane anisotropy of 10^6 erg/cc. In particular, upon annealing from the amorphous state in the same magnetic field, the $SmCo_5$ phase exhibited a coercive force larger than 22 kOe and its moment could not be rotated within the film plane with a 22 kOe external field, thus increasing the uniaxial inplane anisotropy constant to at least 10^7 erg/cc.

ACKNOWLEDGEMENTS

I am grateful to my supervisor, Professor Fred J. Cadieu, for his continuous support and encouragement throughout this work. I am indebted to Dr. Tak D. Cheung for his invalueable guidance and help. My thanks are also extended to all the members of our research group and ex-colleague Dr. Samy H. Aly.

I would also like to thank the members of my Supervisory Committee. It is my pleasure to extend my sincere thanks to all members of the Faculty and Staff, colleagues, and friends at the Department of Physics, Queens College.

I would also like to thank my friend Sajoo Samuel for his support and contribution. I take this opportunity to thank my wife Ranmal for her continuous moral support and for bearing with me throughout the period of this research.

My thesis is part of the research program, studying rare earth transition metal permanent magnet systems, principally supported by grants from the U.S. Army Research Office to Professor Cadieu (Grant #: DAAG29-80-K-0094 & DAAG29-83-K-0114). I was also supported in part, by funds from the PSC-BHE Faculty Research Award Program of CUNY grants of Professor Cadieu.

TABLE OF CONTENTS

LIST OF TABLES

LIST OF FIGURES

relative Fe.

Figure 7.2 Hysteresis loops measured perpendicular (a) and parallel to film plane (b) for $Sm(Fe,Ti)_2$ sample.

Figure 7.3 X-Ray diffractometer trace, Cu radiation, of $Sm(Fe,Ti)_2$ film.

Figure 7.4 Remanent moment as a function of angle away from the film normal after (a) initially being magnetized perpendicular to plane, and (b) in the film plane. The sample was rotated in the zero field after initial magnetization to observe relaxation of moment.

Figure 7.5 Hysteresis loop measured normal to the film plane (solid line)and in the film plane (dotted line) for Nd-Fe-B directly crystallized at 700 C with 0.9 A/sec sputtering rate.

Figure 7.6 X-Ray diffraction trace, Cu radiation, of the same sample.

Figure 7.7 Hysteresis loop measured normal to the film plane (solid line) and in the film plane (dotted line) for Nd-Fe-B directly crystallized at 700 C with 2 A/sec sputtering rate.

Figure 7.8 X-Ray diffraction trace, Cu radiation, of the same sample.

Figure 7.9 Hysteresis loop measured normal to the film plane (solid line) and in the film plane (dotted line) for Nd-Fe-B direct crystallized at 800 C with 0.6 A/sec sputtering rate. The cross points show 4*Pi*M versus internal effectie field after correcting the solid curve for the demagnetization factor (normal to the film plane).

Figure 7.10 X-Ray diffraction trace, Cu radiation, of the same sample.

Figure 7.11 Hysteresis loop measured normal to the film plane (solid line) and in the film plane (dotted line) for $SmCo_3$ sample directl crystallized at 600 C.

Figure 7.12 X-Ray diffraction trace, Cu radiation, of the same sample.

Chapter 1

INTRODUCTION

Rare earth-transition metal alloys have attracted considerable attention due to their exceptional magnetic properties and technical importance. Light rare earth transition metal rich compounds form several new classes of high performance permanent magnet materials such as Co based alloys of $SmCo_5$, Sm_2Co_{17} with added trace elements and Fe based $Nd_2Fe_{14}B$. Cobalt based permanent magnet materials are characterized by their high magnetic ordering temperature (T_c of $SmCo_5$ = 1000 K) while the highest known energy product have been attained by Fe based $Nd_2Fe_{14}B$ (BH_{max}=45 MG-Oe) even though its Curie temperature is low (T_c of $Nd_2Fe_{14}B$ = 600 K).

Since the discovery of the extremely high magneto crystalline anisotropy of YCo_5 in 1966 there has been rapidly increasing interest in the development of cobalt-rare earth alloys as permanent magnets. But the actual fabrication of R-TM permanent magnets was not possible till the discovery of $SmCo_5$ in the late 60's. This hard magnetic phase had an anisotropy field of 400 kOe which is the

highest among all known materials. In order to be a potentially good permanent magnet material a system must exhibit reasonably high saturation magnetization and Curie temperature with large easy axis anisotropy energy. Since cubic materials have high crystal symmetry and exhibit low anisotropy,non cubic materials with unique crystal axis such as hexagonal,tetragonal are prefered. In uniaxial materials with easy plane anisotropy, the prefered direction of magnetization in a plane is perpendicular to the c-axis and are not suitable because the energy barrier for magnetization reversal will then reduce to that for rotation in the plane and it is usually very low. In order to fully utillize the high anisotropy of R-TM alloys, the materials must be prepared in defect free fine particle form (single domains) such that magnetization reversal take place by coherent rotation against the anisotropy field. Then the material's intrinsic coercivity (resistance to demagnetization) is limited only by the anisotropy field. Even though RCo_5 compounds where R= Y,La,Ce,Pr,Sm and mischmetal seems to have favorable properties to be good permanent magnet materials[1], only $SmCo_5$ could be developed into a high quality permanent magnet material. In $R-Co_5$ compounds magnetization reversal take place mainly by nucleation and domain wall rotation because it is difficult to prepare fine particles without defects and the observed coercivity is very small except $SmCo_5$. The intrinsic coercivity of $SmCo_5$ magnets are about 40 kOe, which is still about 1/10 of the theorical upper limit. The R_2Co_{17}

seems to have higher saturation moment and Curie temperature comparable to 1:5 compounds. The principle drawback of the 2:17 cobalt compound is that coercivity is limited by low magnetocrystalline anisotropy. Among the R_2Co_{17} compounds,only those with Sm, Er, Tm, and Yb exhibit the easy axis anisotropy with Sm_2Co_{17} being the most anisotropic(H_a= 65 kOe). Pure Sm-Co 2:17 cannot be fabricated into permanent magnet because of its low coercivity.(about 2 kOe). However preferential substitution of Mn,Cr,Zr into the so called "dumb-bell" Co sites increase the anisotropy and coercivity[2-4] of Sm_2Co_{17}. High energy product (> 25MG-Oe) permanent magnet have been made with $Sm_2(Co,Fe,Cu)_{17}$ systems and energy product have been further improved with small additions of Zr, V, Hf, Ti, Nb, etc. Once again Sm and Co are the basic elements to get good permanent magnet materials. The principle characteristic of the $SmCo_5$ (1:5) type is extremely high intrinsic coercivity and the main feature of the 2:17 type is high induction. Since cobalt is comparatively scarce and expensive, attention was set on cobalt free permanent magnet materials. These investigation were carried out in rare earth iron rich compounds because Fe is more abundant and has a very close ionic radii. In comparison to SmCo system RFe_5 does not exist in bulk form and R_2Fe_{17} compounds do not exhibit hard magnetic properties, i.e., it has relatively low Curie temperatures and favors easy plane

anisotropy. The Curie temperature of R_6Fe_{23} and RM_2 are higher than those of R_2Fe_{17}, but it's crystal structures are cubic. Since R-Fe binary compounds does not have potential to be good permanent magnet materials, one may have to study ternary and or quarternary compounds for practical materials. The development of Co free R-TM permanent magnet material has been a highly active research area for the last decade.

The Pure Sm-Fe system exhibits only 1-2, 1-3, and 2-17 phases in both bulk[5] and film form.[6] The Sm_2Fe_{17} does not have hard magnetic properties to qualify as a permanent magnet material, eg. Sm-Fe 2:17 exhibit easy plane anisotropy and has fairly low Curie temperature of 385 K. In contrast to Sm-Co system ,the important 1:5 phase does not exists in pure Sm-Fe system.

However the close proximity of Fe and Co in the periodic table(very close ionic radii) suggest an interesting basic research problem of the absence of $SmFe_5$ phase and a challenging new question of whether it is possible to synthesize a 1:5 phase with third element additions. This thesis will be directed to the investigation of the ternary phase of Sm-Fe-M (M=non magnetic) with special emphasis on (Sm,M):Fe or Sm:(FE,M) =1:5 composition. The Sm-Fe-M system with M= Ti,O exhibited an additional magnetic phase in Fe rich region with a higher intrinsic coercivity[7]. In

particular, the Sm-Ti-Fe film magnet system exhibits interesting magnetic properties for two different Fe concentrations. We have discovered a new magnetic phase in Fe rich region with composition (Sm+Ti):Fe = 1:5 with coercivities up to 24 kOe which open a new possibility for Co free permanent magnets.[8] For lower Fe concentrations as in $Sm(Fe,Ti)_2$, we successfully fabricated film magnets that exhibited perpendicular anisotropy[9] with easy axes of magnetization aligned perpendicular to the plane of the film. In order to establish easy axis perpendicular to the film plane intrinsic anisotropy must be large enough to overcome demagnetization energy of $4*Pi*M^2$ due to shape anisotropy. $Sm(Fe,Ti)_2$ exhibited a large perpendicular remanent of 3.5 kG, effective anisotropy constant of $4x\ 10^6$ erg/cc and Q value (= $k/2*Pi*M^2$) of 5.

It is known that it is not possible to substitute iron for cobalt for more than 1 wt. % in RCo_5 compounds because the RFe_5 compounds do not form by usual melting methods.[10] By sputtering from 2 $SmCo_5$,one $(Sm+Ti)Fe_5$ targets we synthesized a phase of $(Sm_{13}Ti_3)(Co(47)Fe_{33})_5$ which contains 33 at. % of Fe with the addition of 3 at. % Ti. This phase exhibited a static energy product of 15 MG-Oe as compared to 18 MG-Oe of $SmCo_5$ sputtered films[8,11]. However the highest energy product that we had achieved

is 21 MG-Oe in the $Sm_2(Co,Fe,Zr)_{17}$ phase with 35 at. % Fe.[11]

Generally Nd-Fe rich compounds do not have easy axis anisotropy because Nd ions favor basal plane anisotropy. But in ternary phase $Nd_2Fe_{14}B$, both Nd and Fe exhibit uniaxial anisotropy and permanent magnet with energy product 30 to 45 MG-Oe(theoretical upper limit=60 MG-Oe) were reported.[12,13] presently fabrication of $Nd_2Fe_{14}B$ magnets are done by two distinct methods: The Powder metallurgy method, as used for $SmCo_5$magnets and hot-pressing of rapidly solidified ribbons. Even though the raw materials for Nd-Fe-B magnets are relatively cheap there is a major draw back,that the magnetic properties are strongly temperature dependent due to its low Curie temperature(300 C). The Curie temperature can be raised by replacing Fe with Co.[14] This thesis will also investigate the fabrication of Nd-Fe-B in thin film magnet form. We have successfully synthesized $Nd_2Fe_{14}B$ film with static energy product of 15.6 MG-Oe from the procedure of sputtering amorphous and then annealed. We have discovered that c-axes alignment onto film plane depends on the sputtering rate. The c-axes of these polycrystalline $Nd_2Fe_{14}B$ are preferentially aligned onto film plane for high sputtering rates[15] (>1.8 A/sec) and are preferentailly aligned perpendicular to film plane for lower rates (< 1.8 A/sec). Using low rate sputtering we synthesized $Nd_2Fe_{14}B$ phase[16] with magnetic moments normal to the

film plane and a large effective perpendicular anisotropy constant of 1.2 x 10^7 erg/cc and Q value of 5. This switching of perpendicular to plane anisotropies by different sputtering rates were not observed in the analogous $SmCo_5$ system. Nevertheless in the $SmCo_5$ sputtering, we found that low rate (<1A/sec) gave preferential 110 texture and high rate (>2A/sec) gave preferential 200 texture. That is, only textures switching were observed in the inplane anisotropy $SmCo_5$ sputtered films by different sputtering rates.[17]

In addition to above hard magnetic films, we have synthesized amorphous R-TM alloy films in the presence of inplane applied field of 1.75 and or 2.5 kOe. Magnetic measurements within film plane, reveals square hysteresis loops when measured parallel to $H_{sputter}$ and incline hysteresis loops when measured perpendicular to $H_{sputter}$ indicating a prefered direction of magnetization within the film plane. We have achived the highest inplane anisotropy of any amorphous material known 2x10 ^{6} erg/cc.[18] This was observed in amorphous $SmCo_5$, Sm_2Co_{17}, and $(SmTi)Fe_5$ phases and are potential candidate for longitudinal digital recording.

In this thesis, special anisotropies as well as other magnetic properties in relation to our sputtering parameters will be presented.

Chapter 2

INTERMETALLIC COMPOUNDS of RARE EARTH ELEMENTS AND Ni,Co,or Fe

Intermetalic compounds of R-TM, where R is a light rare earth, form the high performance permanent magnets when compared to any other systems. Energy product in the 45 MG-Oe is reached by $Nd_2Fe_{14}B$ and high Curie temperature is characterized by Co alloys such as $SmCo_5$(T_c=1000 K). The emergence of this class of materials in the late 1960's were probably due to the discovery of large magneto crystalline anisotropy of YCo_5 and availability of pure rare earth elements in a large scale. Among 104 stable elements only three transition elements (Fe,Co and Ni) and one rare earth element (Gd) are ferromagnetic near room temperature. The transition metal elements Fe,Co and Ni are characterized by their high Curie temperature but low coercivity. On the other hand the rare earth elements possesses high magnetic moment per atom, strong single ion magneto crystalline anisotropy and extremely low ordering temperatures. In their elemental form, neither rare earth nor transition metals, are suitable for hard magnetic material. However

the combination, i.e., RE-TM alloys benefit from intrinsic properties of both partners, namely high single ion anisotropy of rare earth partner and high magneto coupling strength (high ordering temperatures) of 3d transition metal partner. Because of the difference in atomic radii between rare earth and Fe,Co and Ni atoms very little terminal solubility exists in rare earth transition element systems. Thus the probability of forming new ductile magnetic alloy is small and one must study intermetallic compounds for practical materials. Due to this limited solubility of rare earth elements into transition metals the thermodynamic equilibrium crystal structure exists only as a delicate balance between the attractive ionic energy and repulsive electronic energy. This delicate requirement readily demonstrated by the fact that $SmFe_5$ does not exist in bulk form, whereas the $SmCo_5$ bulk is a stable hexagonal structure that exhibits a magnetic anisotropy field about 400 kOe,at room temperature, the highest value among all known ferromagnetic materials.

2.1 The Crystal Structure Of R-TM Compounds

Table 1 gives a general survey of the various structures of observed in binary R-M compounds.[19-21] The series of compounds RM_2,

RM_3, R_2M_7, RM_5 AND R_2M_{17} of special interest crystal structure of these compounds are related and originated from the hexagonal lattice of $CaCu_5$ type, from which they arise through of simple substitution accompanied by layer shifts. Therefore this series can serve as a base for the study of different type of magnetic interactions operating on R-TM systems.

The unit cell of $CaCu_5$ type shown in Fig. 2(a). There are two type of layers: In the lowest layer both R and M atoms found whereas in the next layer only M atoms are found. A extended view of the layer containing R and M atoms are shown in 2(b). Here ABCD indicates again the basal plane of the unit cell with unit cell edge a. The R_2M_{17} structure arises from the RM_5 lattice via replacement of one-third of all atoms by the pair of M atoms (so called dumb-bell pairs). The new unit cell edge in the basal plane now is a (3a). If, in the basal plane replacement mentioned, occurs at site A, then it will occur at site C in the next layer containing R atoms. In the following layer containing R atoms it may occur at site A, leading to hexagonal structure, or at site F, leading to a rhombohedral structure. These two possible stacking sequences are shown Fig. 2(c).

In order to obtain the structure of compounds R_2M_7, RM_3 and RM_2 one has to replace M atoms by R atoms in RM_5. This is shown for RM_3

compounds in Fig.2(d). In the basal plane of each second RM_5 unit cell one of the two M atoms are replace by R atom followed by a shift and minor rearrangement of the atoms. This leads to a RM_3 unit cell which has same unit cell edge in the a-direction but c-axis is 4 times as long. Also for RM_3 one has two modifications. The corresponding stacking arrangements are shown in Fig. 1(e). In similar way one obtains the structure for the R_2M_7 and RM_2 compounds. Their stacking arrangements shown in Fig. 2(f). For those structure types which give rise to two modifications one often observes both forms in the same sample. The difference in stability between two forms is probably small and transition from one form into other can proceed without diffusion.

2.2 Magnetic Properties of R-TM Compounds

2.2.1 Magnetic Interactions

The magnetic properties of R-M compounds are determined by following three types of magnetic interactions:

(1) the R-R interaction

(2) the M-M interaction

(3) the R-M interaction

These three types of interactions will be discussed separately

2.2.2 R-R Interaction

The interaction between the magnetic moment of the rare earth atoms is by far the weakest one. Due to small spacial extension of wave function the magnetic coupling has to proceed indirectly since there is virtually no overlap of the 4f wave functions. One of the possible path of the interaction is the spin polarization of the s conduction electrons. Each localized 4f moments located elsewhere in the crystal lattice will fell this polarization and orient themselves accordingly. The conduction electron porization due to given 4f moment is not uniform in space. It is oscillatory in character and its absolute value decreases with increasing distance. This implies that it lead to parallel as well as antiparallel coupling between moments. This known as Ruderman-Kittel-Kasuya-Yosida (RKKY) interaction.[22] The strength of this coupling depends on structure type and the number conduction electrons. The much stronger M-M interaction usually obscures the

R-R interaction. Experimental evidence that the R-R interaction in the R-M compounds is indeed weak can be obtained through the low values of the ordering temperatures measured in the cases where the M atoms do not carry a magnetic moment.[24]

2.2.3 M-M Interaction

The M-M interaction is the strongest one operative in R-M compounds. This is a direct consequence of the much larger special extent of 3d wave functions as compared to 4f wave functions. The M-M interaction can be studied in which the component is non magnetic, i.e., R = La,Y or Lu. The observed high ordering temperatures of these compounds is the experimental evidence for the stronger M-M interaction.

The strong overlap between 3d wave functions suggested itinerant electron models based on the 3d band structure to be devoloped,[24] on the other hand more localized models have been suggested as well to explain the magnetic properties of these compounds.[25,26] Experimental work including NMR and Mossabauer on one side and magnetovolume effects on the other side and gave indications of the localized and itinerant nature of the 3d electrons respectively.

2.2.4 R-M Interaction

The order of magnitude of R-M interaction lies between the R-R and M-M interactions. The observed saturation moments and temperature dependance of magnetization can be interpreted as being the result of an antiparallel coupling between R and M sublattice if R is a heavy rare earth and a parallel coupling if R is a light rare earth element. These observations are consistent with the idea that the 3d moments always couples antiferromagnetically with the spin moment of R component. The observed difference in behavior between compounds in which R is a light or heavy rare earth element then follow from the fact that in the former the total rare earth angular momentum is given by J = L - S while in the latter J = L + S. The Antiparallel coupling between the 3d and 4f spin magnetic moment has been accounted for using different models.[25,27-29]

2.2.5 Magnetic Anisotropies

Even though the exchange coupling between the electron spin is the main feature of ferromagnetic materials, magnetic anisotropies controls most of the macroscopic properties of these materials. Anisotropy of magnetic properties means that the free energy is a

function of Magnetization. The directions where energy is minimum(i.e. easy to magnetize) is called easy axis while the directions of highest energy is called hard direction. The energy involve in the anisotropy is much smaller than exchange energy. Anisotropies can be classified as magnetocrystalline, shape, strain, and pair ordering.

2.3 Amorphous R-TM Compounds

Amorphous R-TM alloys can be prepared without an addition of a glass forming element,and are found to retain relatively high T_c (often above room temperature) and magnetic moment comparable with those of their crystalline counterparts. Amorphous R-TM alloys are of great technical interest due to their potential application in thermomagnetic information storage,[30] bubble devices,[31] and as precursor material for preparation of permanent magnets.[32]

In general amorphous magnetic alloys can be prepared by sputter deposition method using high sputtering rate and low substrate temperature. In fact sputtering at liquid He temperature with sputtering rate of few A/sec always produce amorphous films. Wheather or not the film crystallize on heating to room temperature

can be predicted from consideration of atomic and composition range. This charectertic make amorphous material precursor material for permanent magnet fabrication. Our highest coercive force films is produced by this method which we shall discuss in later chapters.($SmCo_5$ H_c > 22 kOe ; $(SmTi)Fe_5$ H_c= 24 kOe)

From theoretical view point amorphous magnetic alloys is the most disordered system where the atom position,spin position and spin magnitude are all random.[33] The simple case, spin glass which consist of a dilute solution of magnetic element in a non magnetic host, atom position are fixed but spin random.

The structure of amorphous alloys can be describe by two principle models;dence random packing and microcrytallites.[34] Systems like Gd-Co,TbFe are describe by dence random packing and systems such as $HoCo_5$ described by micro crystallites model. In general R-TM amorphous alloys still contain major feature of d band and give rise to long range magnetic order.

Chapter 3

EXPERIMENT

3.1 FILM SYNTHESIS

All the films reported here in this thesis were synthesized by RF sputtering in an Ar/Kr environment. Sputtering deposition is a common method in thin film preparation and are well documented in the literature.[35,36,37] The major characteristic features of our sputtering techniques that were different from the common approach were the selectively thermaliztion of the different spices of sputtered atoms. This selective thermalization method originally used by my adviser, Professor Cadieu, in producing superconducting films with high T_c : Nb_3Ge (T_c= 22 K).[38] We extended this thermalization scheme into magnetic thin film sputtering. Details of which, are described later. The other characteristic feature included, the application of a magnetic field, $H_{sputter}$, 1.75 or

2.5 kOe in the substrate plane during deposition in a temperature environment of 300 k to 1100 K. The advantage of $H_{sputter}$ during deposition was to promote easy axis alignment during film growth.[39]

There were basically 2 type of targets that we used, namely, uniform composition targets and gradient composition targets. These targets were arranged in a co-linear fashion spanning the length of the substrate. In the Sm-Co based and $Nd_2Fe_{14}B$ sputtering, reported in this thesis, uniform targets were used. They were $SmCo_5$ bulk, TDK ($Sm_2(CoFeZr)_{17}$), bulk obtained from Colt Industries. In the Sm-Fe-Ti films sputterings, both type of targets were used. For gradient targets, we usually employed one Sm and two (Fe-Ti) targets with fixed Fe to Ti ratio. Those alloy targets were button shape ingot that we arc-melted in our specially designed arc-melter with dynamic flush-cleaning action which was especially necessary for those reactive rare-earth elements. Details of which were reported earlier by Cadieu et.al.[40]

3.2 SELECTIVE THERMALIZATION

In the sputtering process, high energy ions bombarded the surface of a sputtering target and ejected the surface atoms by

momentum transfer. Those ejected surface atoms (sputtered atoms) were predominately neutral atoms with an asymmetric energy distribution center approximately 5-10 ev and extending up to 100 ev. Thermalization means simply,the removal of excess momentum and kinetic energy of the sputtered atoms and to lower the sputtered atom temperature to that of the substrate before they arrive at the substrate,by collision with the sputtering gas atoms. The use of selectively thermalized sputtering allows a delicate and or metastable phase to be replicated by the subsequently arriving sputtered atoms.The model used for such calculations treat the collision between the sputtered atoms and sputtering gas atoms as elastic collisions between spheres having maxwellian velocity distribution corresponding to temperatures T_1 and T_2 respectively. The average energy loss of the sputtered atoms per collision normalized to the average energy of the sputtered atoms is given by 41

$$f = 8\, M_1M_2(1-T_2/T_1)/3(M_1+M_2)^2.$$

The fractional energy remaning is given by

$$b = 1-f.$$

Then the energy in K of sputtered atoms after *n* collisions is given by[38]

$$E = (E_0-T_2)b^n + T_2,$$

where E_0= initial energy, and n = $P*S*L/T_2$ is the number of collisions suffered over a distance L, where P is the sputtering gas pressure in millitorr, and S is the scattering cross section. This model can easily extended to a mixture of two sputtering gases and equation becomes

$$E = (E_0 - T_2)\, b_1^{n} b_2^{q} + T_2$$

In Fig. 3.1, we show the calculated change in sputtered atom energy as the sputtered atoms progress from the target to the substrate, using the above model. As indicated in Fig. 3.2, the pressures of 5 millitorr or less which is the most commonly use values in sputtering work is not large enough to thermalized the sputtered atoms for a target to substrate distance of few centimeters. A sputtering gas pressure of 150 millitorr Ar had been used for most of the films reported in this thesis. This pressure is large enough to thermalized sputtered atoms to substrate temperature before arrival at substrate as shown in Fig. 3.1 and Fig. 3.2.

3.3 THE EFFECT OF APPLIED FIELD DURING DEPOSITION

The effect of an applied magnetic field, which we term $H_{sputter}$, during deposition is to break the symmetry in the film plane and induce a magnetic anisotropy. If the deposition temperature is below the magnetic ordering temperature, then the sputtered films would have an induce magnetic anisotropy after the sputtering. The application of a magnetic field during film synthesis has been used previously by several other groups either to promote perpendicular texturing for crystalline Sm-Co films[42] or to promote uniaxial inplane anisotropy for flash evaporated amorphous Sm-Co films[43]. In this work we have applied inplane magnetic field of either 1.75 kOe or 2.5 kOe during the synthesis of R-TM film systems. Our objective was to induce an uniaxial anisotropy in the film plane of amorphous R-TM film systems and to enhance the preferential alignment of easy axes of polycrystalline R-TM film systems. The effect is most marked in the case of $SmCo_5$ films. We were able to induce uniaxial inplane anisotropy of 2.6×10^6 erg/cc in the amorphous $SmCo_5$ films when sputtered onto water cooled substrate under the influence of $H_{sputter}$ of 2.5 kOe.[18] The effect

of $H_{sputter}$ of different amorphous film systems are listed in table 2. The induced anisotropy constant were roughly constant for these systems at (1.4-2.6) x 10^6 erg/cc. This suggests that the induced inplane anisotropy is related predominently to $H_{sputter}$ and only slightly to the details of the different compositions. When annealing these samples in the presence of H(sputter) it was found that the in the film plane anisotropy increased to at least 10^7 erg/cc. Fig. 3.3 shows magnetization as a function of inplane angle for the annealed $SmCo_5$. It is clear that the applied external measuring field of 22 kOe is not large enough to rotate the magnetization by any significant amount away from the induced easy axis (direction of $H_{sputter}$ during synthesis). Thus the induced uniaxial inplane anisotropy must be extremely large and high field measurements are needed to determine the anisotropy of this sample. The effect of $H_{sputter}$ on those films which were sputtered onto hot substrate for direct crystallization is less drastic.[39] The variation of magnetization as a function of angle is only about 15 % as shown in Fig 3.4. This is probably due to the relatively large thermal energy of the deposited atoms at the hot substrate which then suppressed the magnetic energy. We also noticed that the effect of $H_{sputter}$ in the direct hot substrate sputtering disappears as the grain size got smaller than about 350 A. The film shown in fig. 3.4 had a grain size of about 500 A. Thus we can conclude that

the use of $H_{sputter}$ in inducing magnetic anisotropy was highly effective in the diffusion processes in the amorphous annealing processes and less effective in the stacking processes during the hot substrate deposition. No attempts were made at this moment to calculate these differences although the differences would be qualitatively understood in the following manner. The diffusion processes within a media usually has much less energy when compared to the stacking processes of the formation of that media and thus the $H_{sputter}$ can influence the diffusion processes readily. The thermal energy (kT) is roughly 10^{-13} erg given a substrate temperature of 1000 K. The magnetic energy (uH) per atom is roughly 10^{-17} erg given a $H_{sputter}$ of 2 kOe. For a grain size of 250 A, it would contain 10^5 atoms assuming a 5 A separation between atoms. The magnetic energy of this cluster would be about 10 times larger than the thermal energy. Since there is also a cos(0) term where 0 is the angle between the moment and the H field, the magnetic energy of this cluster is probably only a few times larger than the thermal energy. In any event, the effect of $H_{sputter}$ should be noticeable for grain size of roughly 250 A or larger, that is, a cluster size of more than 10^5 atoms. of course, we assume that it is a single crystal within a grain. In the annealed film, the X-Ray diffraction yielded a grain size of about 300 A in $SmCo_5$, to be discussed in details later, therefore the $H_{sputter}$ should influence the easy axis

alignment readily. On the contrary, in the direct hot substrate sputtering the layers are replicating themselves according to the already deposited layers. Because of this stacking procedure, the effective cluster would be more like a 2 dimensional area rather than a 3 dimensional volume as in the annealing case where the films were already deposited. For a 2 dimensional area, a grain of 500 A is needed to give 10^4 atoms which then would bring the magnetic energy to be roughly the same as the thermal energy. Therefore in the direct hot substrate sputtering, grain size of 500 A or more is needed for $H_{sputter}$ to exert noticeable influence. It should be noted that small grain is essential for high coercive force as discussed in later sections. We also assume that the substrate temperature during deposition or annealing is lower than the Curie temperature in the above discussion. If the deposition temperature is near or above the Curie temperature, the exchange energy would be very small and the correlation length would then be much smaller than the grain size. In fact we did not observe any noticeable $H_{sputter}$ induced anisotropy effect in the synthesis of low Curie temperature phases such as $Nd_2Fe_{14}B$ and $Sm_2Fe_{14}Ti$.

3.4 THICKNESS MEASUREMENTS

The film thickness was usually determined by the relation tAd = w, where t was the thickness, A was the area, and d was the density of the film. The major contribution of error in those parameters was the uncertainity in the density of the deposited materials. The density of the bulk could be different from that of the film by a few percents due to slightly different lattice parameters and the presence of empty space. The necessary corrections for the lattice parameter differences were obtained from our X-Ray diffraction results. Investigations using scanning electron microscopy were required to detect the presence of empty spaces in films. All SEM work reported in this thesis were done at Fort Monmouth,NJ. For those selected films that were investigated under the SEM, they all revealed dense packing suggesting that the error in using the X-Ray density as the actual overall density was at most few percent. On the whole, this thickness relation gave an error of at most 5% in the worst cases. The thickness could also be checked by measuring the saturation flux of the magnetic film and it was consistent for those films that we could saturate. (Most of our films required high field of up to 100 kOe or more for saturation.) The other

method that we could use for thickness measurement was by measuring the reflection of beta electrons from the film using various beta decay sources that gave different beta electron energies. By using different calibration standards, thickness measurement was possible. Since we were measureing rare earth transition metal compounds, calibration standards were difficult to prepare and this method gave again an error of about 5%.

3.5 ATOM COMPOSITION

The atom compositions were generally checked by X-Ray fluorescence for heavy elements and Auger electron spectroscopy for light elements. Details of those complimentary techniques were well documented in the literature.[44-49] For the AES, elemental sensitivity factor chart was used for calibrating atomic ratios. For the X-Ray fluorescence, calibration standards made from dilute solution of the film atoms onto the Al_2O_3 substrate were used. The common method of dilute solutions on filter paper was not used in our case because the rare earth L lines were strongly absorbed by the filter paper as compared to the transition metal K lines. In the Sm-Ti-Fe system, it was impossible to dissolve the three elements together so Sm-Fe calibration was obtained experimentally

and then Ti effect was calculated. The absorption of the Sm L_a in a pure Fe matrix and a Fe-Ti matrix was calculated from standard formula. The Fe K_a was much less affected by the Ti addition For the TDK sputtered films, because of the presence of five elements, no calibration standard was prepared. The X-Ray fluorescence results were also within 5% of the TDK bulk results. For the $Nd_2Fe_{14}B$ films, X-Ray fluorescence results were also within 5% of the bulk counterpart.

The X-Ray fluorescence was performed on all the films and the depth profile AES was only performed on selected films.Some of those results were confirmed using electron microprobe. The electron microprobe was able to separate the K_{a1} and K_{a2} lines of the transition metals as well as the complicated rare earth L lines due to its high energy resolution. This was important in our particular application since the rare earth L lines and transition metal K lines were very close to each other and the electron microprobe resolved it clearly by using a crystal diffractometer . The X-Ray fluorescence used a Si(Li) detector of 200 ev resolution. Again the techniques of the electron microprobe is well established in the literature.[50-52]

The X-Ray fluorescence experiment consists of a GE X-Ray machine with a Princeton Gamma Tech Si(Li) detector. The schematic diagram of the X-Ray energy dispersive apparatus is shown in Fig.

3.5. The electron microprobe was performed with a Norelco AMR-3 microprobe and the AES was performed with a Varian cylindrical mirror analyzer.

3.6 LATTICE PARAMETER MEASUREMENTS

Our films were mostly hexagonal or tetragonal in structure. The a and c were performed by standard X-R ay diffraction method using a GE diffractometer. Our detector, Si(Li) crystal, gave good discrimination against the Co background in the X-Ray diffraction of Co based films using Cu K_a lines. Our data, count versus angle, were collected by MCA and then stored in a microcomputer for later data processing. The lattice parameters were calculated by minimizing the following function for various a and c pairs.[53]

$$F=\{1/\sin(22.5)*\tan(22.5)\}*\{(1/N)\mathrm{SUM}[\langle A_{exp}-A_{cal}\rangle*\sin(A)*\tan(A)]^2\}^{1/2},$$

where the sum is over N observed reflections at the angles 2A. Essentially we are looking for the vortex point in the F versus a and c 3-dimensional graph shown in fig. 3.6 and 3.7

The grain size was determined by the well known Warren method which gives t = 0.9 * wave length / { cos(0)*B}.[54]

3.7 MAGNETIC MEASUREMENTS

The films were cut into different regions for magnetic measurements. It was performed by a Foner vibrating sample magnetometer manufactured by Princeton Applied Research (PAR). The field was supplied by a conventional water cooled electromagnet up to 22 kOe. Curie temperature was measured in the high temperature oven supplied by PAR. All the high field data beyond 22 kOe were performed at Fort Monmouth and at the National Magnetic Laboratory. Our Al_2O_3 substrate was diamagnetic with an isotropic magnetic susceptibility(at room temperature) of $-0.4+0.1x10^{-6}$ emu/gm. The total moment of a typical sample size of 0.04 cm^2 was measured to be $-5x10^{-4}$ emu at magnetic field of 20 koe. This was about 1% of the magnetization of our film sample and hence the substrate contribution to the moment had been neglected.

Chapter 4

$Sm(Co_xFe_{1-x})$ BASED AND Sm-Ti-Fe HIGH ENERGY PRODUCT FILMS

4.1 INTRODUCTION

In our investigation of $Sm(Co_xFe_{1-x})$ based and SmTiFe based films, we have achieved the following four highlights:

1. sputtered the hightest energy product magnetic film ---in the 20 MG-Oe range with the $Sm_2(CoFeZr)_{17}$ films.

2. achieved the highest coercive force Co free magnetic film: 24 kOe in SmTiFe films.

3. achieved the highest coercive force with square hysteresis loop in SmCo5 annealed films---Hc> 22 kOe.

4. can substitute up to 33% Fe into $SmCo_5$ with Ti stabilization while retaining 15 MG-Oe energy product.

These will be discussed in the following sections accordingly.

The development of hard magnetic materials in bulk form have always been parallel with the investigation of thin film form. After the discovery of the $SmCo_5$ phase, $SmCo_5$ films were sputtered that had coercivities of 40 kOe,[55] but with BH_{max} 4 MG-Oe due to S shape hysteresis loops. The S shape hysteresis loop feature must be overcome to achive high static energy product values.We had directly sputtered $SmCo_5$ films onto hot substrate in a magnetic field and produced flat-topped hysteresis loops with coercive forces 8.9 kOe.[39] Later we extended the coercive forces to the 20 kOe range while maintaining the flat-topped hysteresis loops either by directly sputtering onto hot substrate in the presence of an inplane field magnetic field or by sputtering an amorphous state and then crystallizing in a magnetic field.[11] In addition, we have applied these techniques to $Sm_2(Co,Fe,Zr)_{17}$ system. The directly crystallized samples exhibit BH_{max}= 21 MG Oe while samples,crystallized from amorphous state have shown large increase in coercivity.

RESULTS AND DISCUSSION

In Fig. 4.1, the hysteresis loop measured inplane and parallel

to $H_{sputter}$ for a $SmCo_5$ sample measured at -63 C up to 90 kOe is shown. This film was sputtered onto heated substrate at 600 C with an inplane field of 1.75 kOe. A maximum coercive force of 23 kOe and BH_{max} = 18 MG-Oe was observed. It was observed that an optimum sputtering rate of 1.5 A/sec was necessary to produce such high coercivities. Altering the sputtering rate to either lower or higer than optimum rate produced coercivities in the 12 k Oe range. However, the flat-topped hysteresis loop characteristic was retained. The X-Ray diffraction patterns in Fig. 4.2 shows the (200) and (100) lines indicating that the films were highly textured with the c-axis aligned into the film plane. It was noted that the high coercivity arises from very fine grain size, 150 A, and from the (110) texture associated with the Co 2-c sites which have high anisotropy.

In Fig. 4.3, the demagnetization curve of a $SmCo_5$ film measured at room temperature up to 22 kOe is shown. It is clear that the flat-top nature is manifested. This film was sputtered onto water cooled substrate in the amorphous state in an inplane field of 2.5 kOe and then crystallzed by heating in that same field at 700 C for 60 min. The X-Ray diffraction pattern in Fig. 4.4 shows (200) and (110) lines only and an average grain size of 150 A was indicated. In this sputtered amorphous and crystallized procedure, any correlation between coercivity and sputtering rate is not obvious as in contrast to sputtered hot sample procedure.

In Fig. 4.5, the hysteresis loop measured inplane and parallel to $H_{sputter}$ for a $Sm_2(Co,Fe,Zr)_{17}$ film is shown. This sample was sputtered onto a 600 C substrate in an inplane field of 2.5 kOe. The perpendicular to the plane moment at 18 kOe applied field was only 3 kG. X-Ray diffraction data (Fig. 4.6) indicates the (110) and (111) reflections with a grain size of 350 A. The high moment values due to the inclusion yielded an inplane energy product for this loop of 21 MG-Oe with $_iH_c$= 7 kOe. This film has the highest static energy product of any sputtered film as far as we know. The sputtering targets were TDK type mixtures of the 1-5 and 2-17 phases. The X-Ray diffraction pattern of the sputtered film was identical to that of the TDK targets but with a slightly higher (110) to (111) ratio suggesting that the c-axis more align to the film plane.

In Fig. 4.7, the hysteresis loop of a $Sm_2(Co,Fe,Zr)_{17}$ film made by crystallizing an amorphous film sputtered onto water cooled substrates in an inplane field of 2.5 kOe is shown. Heat treatments at 700 C of from 40 to 60 minutes yielded coercive forces 16 to 20 kOe respectively. The X-Ray diffraction patterns in Fig. 3.8 exhibited (110), (111) and (201) lines with an average grain size of about 200 A. Although the coercivities of these TDK type films were increased to the 20 kOe range, the flat-top nature of the hysteresis loops is less pronounced and only yeilds a BH_{max} of about 15 MG-Oe.

Further improvement of the loop squareness should bring the BH(max) nearer its theoretical limit of above 33 MG-Oe. For the $SmCo_5$ and $Sm_2(Co,Fe,Zr)_{17}$ films that were sputtered amorphous and crystallized the film surfaces were mirror like. In contrast, those sputtered hot, showed a darker matted finish, indicating that columnar growth is the general surface morphology. This was also confirmed in our SEM studies.[17]

4.2 TEXTURE STUDY OF $SmCo_5$

It is noted that, in the deposition of $SmCo_5$ films, the c-axis always prefer to align into the plane. This is confirmed by X-Ray diffraction in which (hkl) reflection with none zero l was never observed.[11,17] This could be understood in the following manner. In the case where c-axis is perpendicular to the plane, the inplane atoms exhibit a hexagonal net. On the contrary, when the c-axis is onto the plane, the inplane atoms exhibit a rectangular net. These are illustrated in the following diagram.

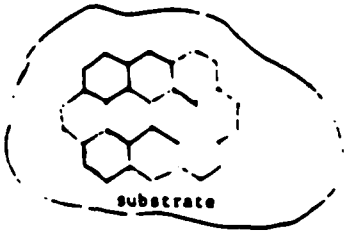

C axis is perpendicular to substrate plane.

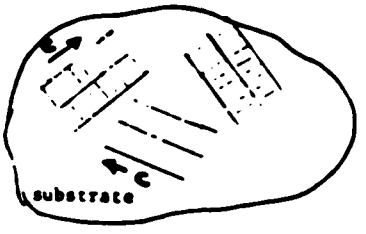

C axis on the plane of the substrate.

The experimental results indicate that (002) is not favorable and never observed, suggesting that the deposited atom prefer lower in-plane symmetry. The lower entropy (002) orientation is not

favorable.

The absence of (002) orientation is also consistent with the surface bonding picture. Since our substrate is Al_2O_3, the bonding perpendicular to the surface must be covalent. On the other hand the bonding along the surface must be metallic. The given lattice parameters with a short c-axis allows more covalent bonding with the substrate in a rectangular net fashion as compared to the larger a-axis that gives less atoms, ie. less bonding per unit length. The covalent bonding is prefered in the interface is conformed by the fact that deposition onto stainless steel or Mo substrate is possible only when a thin layer of Al_2O_3 was coated onto the surface first. It must be pointed out that deposition directly onto Cu or Ni is possible simply because $Sm(CoNi)_5$, $Sm(CoCu)_5$ compounds exists.

Also, from the energy point of view, the c-axis coming out of the plane texturing is not favorable due to large demagnetization energy involved. To establish c-axis perpendicular to the film plane system has to overcome demagnetization energy of $2*Pi*M^2$. Thus the c-axis onto the film plane texturing is more favorable. If a and c differ too much the situation will be entirely different and texturing in these phases will be discussed at the end of this section.

Within the prefered (200)/(110) orientations, we also find that these two orientations could be controlled by varying the Argon incoming flux during deposition via the sputtering rate. The (200) and (110) stacking sequences are respectively illustrated in Fig. 4.9. By controlling the Ar bombardment rate onto the surface, the (200) sequence can be compacted to become the (110) sequence. Experimentally this means that high sputtering rate (relatively low Ar bombardment) produce (200) orientation whereas low sputtering rates (relative high Ar bombardment) produce (110) orientation. Calculations shows that (110) should carry more coercive force than (200) due to the inplane arrangements of atoms of the high anisotropy Co, 2c sites in the (110) stacking sequence. However in actual sputtering it is found that moderate rate of sputtering (1.5 A/sec) where the grain size is smallest together with (110) ,(200) presence gives the highest coercive force of 23 kOe. This illustrates the importance of grain size in achieving high coercivity.

The texture response to sputtering parameters is most drastic when $H_{sputter}$ is applied during the annealing procedure. For those samples that are deposited amorphous and then annealed, external field of up to 22 kOe is not able to rotate moment within the plane. The X-Ray diffraction indicates (110),(200) only. When anneal in the absence of $H_{sputter}$, X-Ray diffraction reveal patterns that resemble random powder pattern with (111),(200) and (110)

reflections. Not only texturing is achieved in the presence of $H_{sputter}$ during annealing, but some c-axis alignment in the direction of $H_{sputter}$ is also achieved. The coercivity is > 22 kOe in the presence of $H_{sputter}$ as compared to 2 kOe in the absence of $H_{sputter}$ during annealing.

In contrast to $SmCo_5$, the other film systems such as tetragonal $Nd_2Fe_{14}B$, and $Sm_2Fe_{14}Ti$ have been synthesized with the c-axis preferentially align onto the film plane as well as align perpendicular to the film plane. In particular it was observed that in $Nd_2Fe_{14}B$ low sputtering rate produced perpendicular anisotropy while high rate sputtering produced inplane anisotropy(to be discussed in chapter 7). Thus the c-axis alignment in tetragonal Nd-Fe-B system is sputtering rate dependant while hexagonal $SmCo_5$ is not. This can be explained qualitatively as follows. When the c-axis of $Nd_2Fe_{14}B$ is onto the plane, the inplane atoms exhibit a rectangular net with sides 8.8 A by 12.2 A compared to the almost square 5 A by 4 A $SmCo_5$ net with c-axis on the film plane. In addition within the rectangular net the complicated $Nd_2Fe_{14}B$ phase contains much more atoms as compared to the simple $SmCo_5$ phase. Therefore at low sputtering rate it would be very difficult to replicate these large Nd-Fe-B rectangular nets in order to produce inplane anisotropy $Nd_2Fe_{14}B$ due to continuous bombardment of the

high Ar flux. In contrast if the c-axis is coming out of the plane, the inplane atoms exhibit square net with sides 8.8 A and contains less number of atoms than the rectangular 8.8 A by 12.2 A net. Thus at low sputtering rate the c-axis will preferentially align normal to the film plane inspite of demagnetization energy. At high rate replication of inplane anisotropy stacking sequence is possible and also more favorable due to absence of large demagnetization energy. These film systems showed multiple stacking sequences by the presence of many diffraction lines, to be discussed later, and consequently preferential alignment of the c-axis in or out of the plane cannot be easily interpreted with any single (hkl) texturing in contrary to the simple $SmCo_5$ case.

4.3 Fe SUBSTITUTION INTO $SmCo_5$ SPUTTERED FILMS

INTRODUCTION

It has been establised that Fe substitution in SmCo5 bulk is possible only up to about 1 wt.% Fe because $SmFe_5$ does not form by usual melting methods[10]. One of the objective of this work is to see if a greater amount of Fe can be incorporated into a sputtered

1:5 phase than have been possible by bulk methods. Selectively thermalized sputtering have been used to directly crystalize these samples onto heated substrates with a gradient in Fe to Co composition. By the use of thermalized sputtering we enhance the possibility of forming delicate and or metastable phases to be replicated by the subsequently arriving sputtered atoms.

First, we have been able to increase the Fe content to 5 at.% in SmCo5 films without any third element additions. Further increase in Fe content is possible in thin film form because $(Sm+Ti)Fe_5$ and $(Sm+Ti)Co_5$ exists in thin form. Up to 33 at.% Fe substitution is possible with 3 at.% Ti replacing Sm sites.[8] X-Ray diffraction pattern of these samples reasonably sharp and indicate a simple pattern of 1:5 hexagonal phase. Flat topped nature of the hysteresis loop retained and exhibit a energy product of 15 MG-Oe at 33 at.% Fe substituted phase compared to 18 MG-Oe for pure SmCo5 films.

RESULTS AND DISCUSSION

In Fig. 4.10, hysteresis loop measured inplane and parallel to H sputter for $Sm(Fe_{.05}Co_{.95})_5$ sample measured at room temperature is shown. This film was sputtered on to a substrate at 600 C with an inplane field of 1.75 kOe. The inplane remanent after magnetizing to a 18 kOe external field was 6.9 kG. Flat topped nature of the

hysteresis loop retained and exhibited a coercive force of 6 kOe and static energy product of 10 MG-Oe.

In Fig. 4.11, hysteresis loop measured inplane and parallel to H sputter for $(Sm_{13}Ti_3)(Fe_{33}Co_{47})$ sample measured at room temperature is shown. At a 18 kOe magnetizing field in the plane flux was 11 kG. This sample exhibited a large remanent of 9.5 kG due to increased transition metal contribution from Fe sub-lattice. The maximum coercive force was 4.5 kOe and had an energy product of 15 MG-Oe as compared to 18 MG-Oe for pure $SmCo_5$. Anisotropy field of this phase was about 100 kOe in contrast to 400 kOe for $SmCo_5$. The extremely large anisotropy in $SmCo_5$ is due to uniaxial contribution from both Sm and Co sub-lattices. The reduced anisotropy in Fe substituted phase may be due to reduction in Co and Sm concentration.

Fig. 4.12, is the X-Ray diffraction data of $(SmTi)(FeCo)_5$ phase. These were identified as (110),(200) and (111) reflections of 1:5 hexagonal phase. The X-Ray lines shifted to a slightly lower angles indicating an increase in d spacing. The lattice parameters a and c increased by about 1%. As Fe content in the samples increases the intensity ratio of (111)/(200) reflections increases.

Fig. 4.13, is the plot of Fe fraction versus remanent ratio for $(SmTi)(FeCo)_5$ samples. As Fe content increases this ratio increases

from .02 to .25. This was correlated with emergence of the (111) peak indicating that c-axis out of plane alignment was increasing as Fe content was increased.

4.4 MAGNETIC PROPERTIES OF (Sm+Ti):Fe = 1:5 PHASE FILMS

INTRODUCTION

Pure Sm-Fe system exhibits only 1-2, 1-3, and 2-17 phases in both film[6] and bulk[5] form. In contrast to Sm-Co system, the important 1:5 phase is not known to exist in pure Sm-Fe system while the other possible candidate 2:17 does not possess hard magnetic properties to qualify as a permanent magnet material. eg. Sm_2Fe_{17} phase has a low coercivity of only .1 kOe[56] at 4.2 K and fairly low Curie point of 385 K.

Previously we have reported the successful synthesis of a metastable $SmFe_5$ phase with Ti additions by selectively thermalized sputtering.[7] Then we have extended our investigations by synthesizing this new phase with 1-15 at. % of Ti measured relative to the Fe content. The grain size is fairly large and estimated to

be 400 A (20%). The intrinsic coercive force of these samples, sputtered onto hot substrates exhibits a maximum of 6.2 kOe and a static energy product of 5.5 MG-Oe at 10 at.% of Ti (Ti:Fe = 1:9) as measured with an initial magnetizing field of 18 kOe at room temperature. High field measurements up to 90 kOe made on 5 at. % samples gave coercive force of 10 kOe with a energy product of 12 MG-Oe at -63 C. The Curie temperatures of 5,10,15 at.% Ti samples are found to be 608+10 K,630+10 K,and 650+10 K respectively. To enhance the Curie point we replaced some of the Fe in the sample by Co. A 5 at. % Co substitute 1-5 phase shows an intrinsic coercivity of 4 kOe and a Curie temperature of 726+10K.

Since we could not synthesize finer grain samples (to get higer coercivity) by direct crystalization on to hot substrates, we tried the alternate way, ie. sputtered amorphous first and then crystalized, and succeeded in synthesizing samples having room temperature coercivities of 24 kOe.[8] This value is among the highest of all Co free magnetic materials.

RESULTS AND DISCUSSION

In Fig. 4.14, the film plane hysteresis loop and a loop for the magnetometer field applied perpendicular to the film plane for a Sm-Ti-Fe (0.075,.091,.833) sample are shown. The inplane loop exhibit an intrinsic coercivity equal to 6.2 kOe and static energy

product of 5.5 MG-Oe.

In Fig. 4.15, the diffraction pattern for the previous sample (Fe:Ti = 9:1) is shown. This pattern is indexed on the basis of a Ti stabilized hexagonal $SmFe_5$ phase.

In Fig. 4.16, the hysteresis loop for a $Sm_{0.087}Ti_{0.046}Fe_{0.867}$ (5 at. % Ti for Fe) sample is shown at -100 C for a field up to 90 kOe. The $_iH_c$ was 10 kG and BH_{max} was 12 MG-Oe. The coercive force remain fairly constant up to -30 C with 90 kOe maximum applied field. This sample was sputtered from elemental targets so as to create a gradient in the (Sm+Ti) to Fe concentration. The data is for the sub region of the film with the stated composition. The sample was directly crystalized onto a substrate at 600 C with an applied field, $H_{sputter}$, of 1.75 kOe. This target arrangement enabled us to synthesize a metastable state which may not exit in the bulk form. As we reported earlier we identify this phase as a Ti stabilized $SmFe_5$ hexagonal phase.[7] It was observed that sputtering produced a composition gradient promoted growth of large grains of about 400 A in $SmCo_5$ samples.[6] This was also the grain size of these (SmTi)Fe samples which may explain the relatively lower coercive forces of these $(SmTi)Fe_5$ samples versus the $SmCo_5$ samples. The $SmCo_5$ subregions from substrates sputtered with a composition gradient gave a $_iH_c$ of 8.9 kOe versus $_iH_c$ in the 20 kOe

range for uniform composition films.[11] Controlling the grain size in the $(SmTi)Fe_5$ samples should increase the $_iH_c$.

In Fig. 4.17, the hysteresis loop of a new ternary Sm-Ti-Fe phase is shown. This sample was amorphous as sputtered and then annealed in-situ at 800 C. This was done as a part of our attempt to control the grain size of $(SmTi)Fe_5$ phase. Although this sample contains both hard and soft magnetic phases, it is estimated from the magnetic data that 80 % by volume is of the hard magnetic phase. High field data obtained at the National Magnet Laboratory, courtesy of Grumman Corporation, gave a room temperature $_iH_c$ of 24 kOe. In the film plane 4*Pi*M values at 145 kOe parallel and perpendicular to $H_{sputter}$ were 12.8 and 11.8 kG respectively. The easy axis was in the film plane in contrast to hot sputtered samples. This also agreed with X-Ray indexing. Since this sample exhibited inplane anisotropy at an applied field of 145 kOe, the anisotropy field associated with this phase must be greater than 145 kOe. X-Ray diffractometer trace (Fig. 4.18) with Cu radiation showed strong reflections for the (212), (220), (310), (320), (231), (400) lines based on tetragonal indexing and a = 8.290± 004 A and c =12.500 ± .005 A. We had tenatively identyfy this hard magnetic phase as tetragonal $Sm_2Fe_{14}Ti$ in analogus to $R_2Fe_{14}B$ system. The estimated saturation flux using two sub-lattice model was about 16 kG at room temperature and this value agrees with our amorphous

results. It is not surprising that both $Nd_2Fe_{14}B$ and $Sm_2Fe_{14}Ti$ have comparable flux because most contribution to the moment comes from the Fe sublattice. The Curie temperature of this new phase was found to be 630 K and about 50 C higher than that of $Nd_2Fe_{14}B$. The roughly estimated grain size about 150 A. As expected decrease in grain size resulted in large increase in coercivity. This new phase could be a very good candidate for a high energy product Co free permanent magnet material.

In Fig. 4.19, the magnetization as a function of temperature is shown for a $Sm_{0.084}Ti_{0.084}Fe_{0.833}$ (10 at. % Ti for Fe) sample measured in an applied field of 5 kOe.

CONCLUSION

Our group had discovered a new ternary hard magnetic phase at about 83 at.% Fe with Ti addition and I included it as part of my thesis proposal in 1983. Presently, we found that the annealing process gave the $Sm_2Fe_{14}Ti$ tetragonal phase with 24 kOe coercive force and the hot substrate direct sputtering gave the $Sm_2Ti_1Fe_{15}$ hexagonal phase where the Sm/Ti ratio could be a variable because the Sm and the Ti occupied only the rare earth sites of the hexagonal phase. This is similiar to the Sm_2Co_{17} phase where both the hexagonal or the rhombohedral phases could be synthesized.[17]

Chapter 5

$Nd_2Fe_{14}B$ High Energy Product Films

INTRODUCTION

The $Nd_2Fe_{14}B$ iron based permanent magnet material have been successfully sputtered in thin film with energy product of 16 MG-Oe and intrinsic coercivity of 15 kOe.[15] Our sputtering technique have two unique features, namely we have applied field of 1.75 kOe in the substrate plane during the deposition and our sputtering pressure is high enough to achive thermalization before their arrival at the substrate. These sputtering features are essential in sputtering Sm-Co based film magnets that have high energy products(> 20 MG-Oe range) as we reported earlier.[11] In contrast to the $SmCo_5$ hexagonal system, the $Nd_2Fe_{14}B$ has a lower anisotropy and lower $_iH_c$, and structurally $Nd_2Fe_{14}B$ is a rather complicated tetragonal structure. It is expect that the sputtering parameters for producing high energy product $SmCo_5$ based film magnets to be different from that

for producing $Nd_2Fe_{14}B$ films. Indeed we found that c-axis alignment onto film plane depends on the sputtering rate incontrast to $SmCo_5$. c-axis of $Nd_2Fe_{14}B$ is align onto film plane for high sputtering rates(>2 A/s) while for lower rates (<.8 A/s) align perpendicular to film plane. Also to achive coercivities over 10 kOe much higher deposition temperatures were needed. In this chapter various condition for synthesizing high energy product type $Nd_2Fe_{14}B$ film magnets are reporting. The synthesis of perpendicular anisotropy $Nd_2Fe_{14}B$ film magnets will be discussed in chapter 7.

RESULTS AND DISCUSSION

In Fig. 5.1, hysteresis loop of a sample made at 700 C is shown. This sample exhibits a static energy product of 7 Mg-Oe and a intrinsic coersivity of 8 kOe at magnetization field of 18 kOe. The observed coercivity of films made 600 C under similar condition is about 6 kOe. At this temperature, the analogous $SmCo_5$ film could be sputtered with coercivity in the 15 kOe range and flat topped square hysteresis loop as we reported earlier.[11] It is clear that the $Nd_2Fe_{14}B$ film needed a higher deposition temperature for optimum magnetic properties. The estimated grain size of the above mention two samples were about 500 A(20% error) range. This grain size must be reduced to achive higher coercivity.

In Fig. 5.3, a hysteresis loop of a sputtered $Nd_2Fe_{14}B$ film deposited at 750 C substrate temperature is shown. Only minor hysteresis loops could be obtained with a maximum external field of 20 kOe. The in the film plane $_iH_c$ in this case was 16 kOe. From the X-Ray diffraction pattern, the grain size is estimated to be 200 A.

In Fig. 5.4, hysteresis loop of a sample first made amorphous and crystallized is shown. This sample has been pulse at 50 kOe before measuring at maximum dc field of 20 kOe. The flat topped nature were similar to the case of $SmCo_5$ films and exhibited a large intrinsic coercivity. Energy product and intrinsic coercivity is 16 MG-Oe and 15 kOe respectively. It is clear that this measured loop is a minor loop. The observed flux of 10 kG is much lower than the expected saturation value of 16.4 kG $Nd_2Fe_{14}B$ phase.

Chapter 6

LARGE INPLANE ANISOTROPY AMORPHOUS FILMS

INTRODUCTION

Amorphous films of $SmCo_5$, $Sm_2(CoFeZr)_{17}$, $(SmTi)Fe_5$ and $Nd_2Fe_{14}B$ compositions have been synthesized by RF sputtering onto water cooled substrates with a magnetic field, $H_{sputter}$, of 2.5 kOe applied in the film plane during the deposition.[18] Originally we had made the first use of an inplane $H_{sputter}$ field to directly crystallized onto hot substrates high energy product Co based films and to synthesize a new $(Sm,Ti)Fe_5$ phase.[39,7] The objective in using a $H_{sputter}$ field has been to obtain a certain degree of preferential alignment of the c-axis of these systems within the plane of the substrates. By using these methods we have produced films with in the film plane static energy product in the 21 MG-Oe range.[11] In this work we investigate the magnetic properties of these amorphous compositions made with an inplane field of 2.5 kOe. All the the

hysteresis loops when measured in the film plane and parallel to $H_{sputter}$ are square and flat topped; but exhibit inclined loops when measured in the film plane but perpendicular to $H_{sputter}$. The in the film plane anisotropy constants for these systems are in the range of 10^6 erg/cc. These anisotropy constants are much greater than those of the CoTi system sputtered with an inplane field of 0.5 kOe[57], but comparable to those of Sm-Co films flash evaporated with an inplane field of 1 kOe[43]. The intrinsic coercive forces, $_iH_c$, range from 200 Oe for $(Sm,Ti)Fe_5$ compositions to 1000 Oe for the $SmCo_5$ compositions. The samples have been deposited onto polished Al_2O_3 substrates and exhibit smooth mirror-like surfaces. No degradation with time of either the appearance or the magnetic properties have been observed.

RESULTS

In Fig. 6.1, hysteresis loops of an amorphous $SmCo_5$ composition films are shown for in the film plane measurements parallel and perpendicular to $H_{sputter}$. $H_{sputter}$ for this film was 2.5 kOe. The hysteresis loop measured parallel to $H_{sputter}$ is a regular rectangular loop with $_iH_c$ of 1000 Oe while the loop measured

perpendicular to $H_{sputter}$ is inclineed with a smaller $_iH_c$ of 500 Oe. Within the film plane 2 kOe were required to fully saturate the film parallel to $H_{sputter}$ and 10 kOe to saturate in the film plane but perpendicular to $H_{sputter}$. Large amount of inplane anisotropy observed is due to the $H_{sputter}$ field during deposition. Films of this type exhibit smooth mirror like surfaces. When appropriately crystallized such films exhibit flat-topped hysteresis loops when measured parallel to $H_{sputter}$ with $_iH_c$ values of >22 kOe.[11] Such large coercivities are due to the magnetocrystalline energy of the crystalline $SmCo_5$ phase.

The amorphous $Sm_2(CoFeZr)_{17}$ composition films also showed similar results when sputtered under the same condition as the amorphous $SmCo_5$ composition films. The inplane hysteresis loops measured parallel and perpendicular to $H_{sputter}$ for such a sample shown in Fig. 6.2. The $_iH_c$ parallel to $H_{sputter}$ was 700 Oe and inplane perpendicular to $H_{sputter}$ was 400 Oe. The inplane field required to saturate the sample perpendicular to $H_{sputter}$ was 5 kOe while only 600 Oe saturated the sample parallel to $H_{sputter}$. This type of film had a smooth mirror-like surface. Proper crystallization has been shown to raise the $_iH_c$ to 20 kOe range but the loops measured parallel to $H_{sputter}$ were not as flat-topped as

the crystalline $SmCo_5$ films.[5]

In Fig. 6.3, inplane hysteresis loops for an amorphous $(SmTi)Fe_5$ system film with composition $Sm_{0.075}Ti_{0.092}Fe(0.833)$ are shown. This sample was sputtered from three arc melted targets of the same composition so that a uniform composition was obtained onto the substrate. For the inplane loop parallel to sputter $_iH_c$ was 500 Oe and inplane perpendicular to $H_{sputter}$ was 300 Oe. An inplane anisotropy field for perpendicular versus parallel to $H_{sputter}$ saturation of 5 kOe was observed.

In Fig. 6.4, inplane hysteresis loops for a similar (SmTi)Fe system film with a composition of $Sm_{0.069}Ti_{0.098}Fe_{0.833}$ are shown. Two major differences were made in the synthesizing these samples. The sample was a subregion of a substrate sputtered so as to create a composition gradient spaning the (SmTi):Fe = 1:5 range and the $H_{sputter}$ employed was 1.75 kOe. The $_iH_c$ values inplane parallel and perpendicular to $H_{sputter}$ were 700 Oe and 500 Oe respectively. The field required to saturate inplane parallel and perpendicular to $H_{sputter}$ were 1.5 and 3 kOe respectively.

All the hysteresis loops are either smooth rectangular loops when measured parallel to $H_{sputter}$ or inclined loops when measured inplane and perpendicular to $H_{sputter}$. There was no evidence of any

mix phases and or mixed compositions in these amorphous films. Most of the Co based films have high moments and external fields perpendicular to the film plane did not saturate the films in that direction. The inplane remanant moments parallel to $H_{sputter}$ were at least an order of magnitude larger than the inplane remanant moments perpendicular to $H_{sputter}$.

DISCUSSION

The amorphous films reported were sputtered with a magnetic field $H_{sputter}$ applied in the substrate plane during the deposition. For the systems reported the hysteresis loops measured in the film plane and parallel to $H_{sputter}$ exhibit rectangular loops and inclined loops when measured in the plane but perpendicular to $H_{sputter}$. The large degree of inplane anisotropy is evident from the very different field values required to saturate the films inplane parallel versus perpendicular to $H_{sputter}$. The induced inplane anisotropy was created during the deposition due to the presence of the $H_{sputter}$ field. This anisotropy may arise because the $H_{sputter}$ applied during the deposition selectively favors those interatomic distances that give positive contributions to the exchange energy. This then induces effective fields within these amorphous states in the direction of $H_{sputter}$. The results of these induced fields are the inclined loops inplane but perpendicular to $H_{sputter}$ and the very small ratios of the inplane remanant moments perpendicular versus parallel to $H_{sputter}$. This consistent with the larger inplane anisotropy for the (SmTi)Fe samples of Fig. 6.3 with $H_{sputter}$ = 2.5 kOe versus the lower anisotropy for the Fig. 6.4 sample where $H_{sputter}$ = 1.75 kOe. The slightly higher Ti content of the Fig. 6.4 sample versus the Fig. 6.3 sample increase the coercive forces

slightly which is same trend exhibited in crystalline samples.

The saturation moments, anisotropy fields, and anisotropy constants, for magnetizing these compositions in the film plane parallel versus perpendicular to $H_{sputter}$, are summarized in table 2. The in the film plane squareness ratios M_r/M_s remanent moment to saturation moment, when originally magnetized in the film plane parallel and perpendicular to $H_{sputter}$ are summarized in table 3.

Although there is no long range order, there is a correlation between the coercive forces of these amorphous films with the corresponding coercive forces of crystalline films. The largest amorphous $_iH_c$, 1000 Oe, was obtain for the amorphous $SmCo_5$ composition, followed by 700 Oe for $Sm_2(CoFeZr)_{17}$ compositions, and then 500 Oe for $(SmTi)Fe_5$ compositions. The corresponding $_iH_c$ values we have reached in crystalline forms are > 22 kOe for $SmCo_5$, 20 kOe for $Sm_2(CoFeZr)_{17}$, and 24 kOe for $(SmTi)Fe_5$. [11,8] The presence of short range order in these systems give rise to the broad amorphous hump seen in the X-Ray diffraction patterns. The 3d transition metal electrons overlap the localized 4f electrons of the Sm atom to produce in analogy to the crystalline state. The absence of long range order however does not allow the full crystal field energy of the crystalline state to develope and the coercive forces are down an order of magnitude from the crystalline values. The

anisotropy constants were roughly constant for these systems at about 1.5×10^6 erg/cc when $H_{sputter}$ = 2.5 kOe. This also supports the fact that the induced inplane anisotropy is related predominantly to $H_{sputter}$ and only slightly to the details of the different composition. For the sample of Fig. 5.4 for which the lower value of $H_{sputter}$, 1.75 kOe, was used a lower value of 0.8×10^6 erg/cc was obtained for the inplane anisotropy constant.

Chapter 7

FILMS WITH LARGE PERPENDICULAR ANISOTROPY

7.1 INTRODUCTION

We have successfully synthesized perpendicular anisotropy crystalline phases of $Sm(FeTi)_2$, $Nd_2Fe_{14}B$, and $SmCo_3$ in thin film form by selectively thermalized RF sputtering.[9,16] Magnetic and X-Ray data of these phases reveal that easy axes align perpendicular to the film plane.

Nd-Fe-B and $SmCo_3$ exhibit hard magnetic properties with high coercivities while $Sm(FeTi)_2$ with its low coercivity seems more like perpendicular recording material for either conventional or thermomagnetic recording. These two different class of perpendicular magnetic anisotropy film systems will be discussed separately in this chapter.

7.2 PERPENDICULAR MAGNETIC ANISOTROPY IN $Sm(FeTi)_2$ FILMS

INTRODUCTION

Ever since the realization of perpendicular recording can be used to achive high density recording,[58] numerous crystalline film systems have been synthesized with perpendicular magnetic anisotropy. These include films such as Co,[59] Co-Cr,[60-62],Co-Ru,[63] Co-V,[64] Co-O,[65] Co-Cr-Ru,[66] Co-Ni-Mn-P,[67] Fe-Nd-Ti,[68] Fe-N,[69] and $BaFe_{12}O_{19}$,[70] thin films.

We had successfully synthesized new $Sm(FeTi)_2$,[9] magnetic thin films which exhibited large perpendicular anisotropy of 5×10^6 erg/cc. The saturation flux of the new phase was 4.6 kG and perpendicular remanant was 3 kG. External fields, up to 18 kOe were not large enough to saturate the sample in the film plane and estimated effective anisotropy field was about 35 kOe. Also those samples exhibited a large perpendicular to parallel remanant ratio of 3. No substrate bias was needed to produce the perpendicular anisotropy phase as required for most of the previously mentioned

systems. Samples were first deposited onto room temperature substrates and then crystallized to reveal the perpendicular anisotropy phase. Films made without Ti or directly synthesized onto heated substrate did not show the large perpendicular anisotropy.

Film samples had been sputtered by selectively thermalized RF sputtering from a set of three colinear targets. The crystallization was performed in-situ right after sputtering. The magnetic data were taken with a vibrating sample magnetometer at room temperature and structure and composition determination were done with Cu radiation using Si(Li) detector.

In Fig. 7.1, a plot of $_iH_c$ versus Fe concentration is shown. For samples that were sputtered amorphous and then crystallized, a peak of $_iH_c$ when measured perpendicular to the film plane was observed corresponding to a $Sm(FeTi)_2$ cubic phase. For samples that were sputtered crystalline directly as in hot substrate deposition, a peak of $_iH_c$ measured parallel to the film plane was observed at the $(SmTi)Fe_5$ composition as we discussed in chapter 4.

In Fig. 7.2, the hysteresis loops of the $Sm(FeTi)_2$ film are shown. The perpendicular loop (a) was a typical square loop of a perpendicular anisotropy film with $_iH_c < 4*Pi*M_s$. The perpendicular remanant to parallel remanant ratio was equal to 3 and the external

field necessary to saturate the sample in the film plane(anisotropy field) was estimated to be 25 kOe. The saturation flux was 4.6 kG and perpendicular remanant was 3 kG. It clearly indicates that the above film was associated with large perpendicular anisotropy and the estimated intrinsic perpendicular anisotropy constant was 5 x 10^6 erg/cc.

In Fig. 7.3, a X-Ray diffraction trace of this sample is shown. It exhibits a cubic structure as that of $SmFe_2$. We group Ti with the Fe because the observed lattice is 2% larger than that the $SmFe_2$ lattice and the Ti possibly go into Sm sites. Only the (220) and (311) reflections were observed. A grain size average of 350 A (+ 20%) was estimated from the broadning of the peaks.

In Fig. 7.4, the remanant magnetization of the sample after initially magnetized to 18 kOe external field is shown. After the sample initially magnetized perpendicular to the plane and in plane, then rotated in zero field, moment relaxes perpendicular to the plane in spite of large demagnetization energy(= $2*Pi* M^2$). It clearly demonstrated that the easy axis preferentially align perpendicular to the plane.

DISCUSSION

In general magnetic anisotropy of cubic RFe_2 compounds were of

about two order of magnitude smaller than uniaxial R_2Co_{17} and RCo_5. But $TbFe_2$ and $SmFe_2$ exhibited anisotropies comparable to that of uniaxial crystals because of large anisotropic 4f charge density of the R^{3+} ion and strong Fe-Fe and Fe-R interactions. For example, magnetic anisotropy and anisotropy field of $TbFe_2$ were 7.6 x 10^7 erg/cc and 100 kOe respectively. Even though there was no such measurement done on $SmFe_2$ so far due to unavailability of single crystal, the observed perpendicular anisotropy of 5 x 10^6 erg/cc was not unusual for $SmFe_2$ system. The total observed anisotropy was the sum of intrinsic and magneto elastic anisotropies. The exact origin of perpendicular anisotropy of $Sm(FeTi)_2$ is not known at the moment. Since $SmFe_2$ ($TbFe_2$ the other) has one of the largest magnetorestrictive coefficient (1.56 x 10^{-3}), the contribution from magneto elastic anisotropy could be significant.

7.3 HIGH $_iH_c$ PERPENDICULAR ANISOTROPY Nd-Fe-B FILMS

INTRODUCTION

Film samples of $Nd_2Fe_{14}B$ which exhibited perpendicular anisotropy had been synthesized by selectively thermalized sputtering onto heated substrates.[16] Minor hysteresis loops measured with fields up to 20 kOe perpendicular to the film plane exhibited a remanant moment of 7.5 kG and an intrinsic coercive force, $_iH_c$, of 14.8 kOe at room temperature. The easy axis of magnetization was perpendicular to the film plane which correlated with a preferential texturing of the c-axis out of the film plane as observed by X-Ray diffraction. Effective large perpendicular anisotropy constant of 1.2×10^7 erg/cc had been observed.

Among the rare earth transition metal permanent magnet systems, the $Nd_2Fe_{14}B$ bulk sample exhibits the highest energy product of 45 MGOe. High energy product materials in thin films usually aligned the easy axis onto the substrate planes. Good examples are the $SmCo_5$ sputtered films which we had studied extensively.[11] Perpendicular anisotropy requires the easy axis to be normal to the film plane and is generally not possible if the saturation magnetization is very large. For the moment to align perpendicular to the plane, the intrinsic anisotropy must be positive and be large enough to overcome the demagnetization energy $2*Pi*M^2$. Perpendicular anisotropy crystalline phases, for example: Fe_xN,[69] $Sm(Fe,Ti)_2$,[9] Co-Cr,[60] exhibits either low or moderate saturation fluxes and loose

their perpendicular anisotropy as the flux increases. It is therefore surprising that $Nd_2Fe_{14}B$ film magnet can be sputtered with large effective perpendicular anisotropy of 1.2×10^7 erg/cc by controlling the sputtering parameters in spite of its large saturation magnetization.

The high energy product $SmCo_5$ hexagonal phase cannot be sputtered with perpendicular anisotropy. In contrast, the $Nd_2Fe_{14}B$ complex tetragonal phase gives more degrees of freedom in crystal orientation that can be controlled by varying the sputtering condition. In this chapter, only the details of perpendicular anisotropy sputtering are discussed since the high energy product sputtering was disscussed in the previous chapter.

EXPERIMENT

Approximately 1.5 micron thick film samples had been RF sputtered from a set of colinear $Nd_2Fe_{14}B$ bulk targets obtained from the Cruecible Research Center. The sputtering gas pressure of 150 microns Ar was sufficiently high to thermalize the sputtered atoms to the substrate temperature before deposition. The substrates were heated to the desired temperature to achieve direct crystallization. No subsequent heat treatment was employed after direct crystallization. Sputtering rate was controlled by the

target bias voltage. The film compositions were checked by X-Ray fluorescence. X-Ray diffraction was performed with Cu radiation. Details of the experiment were discussed elsewhere.[6]

RESULTS AND DISCUSSION

The hysteresis loop measured perpendicular to the film plane for an as sputtered $Nd_2Fe_{14}B$ film deposited at 700 C substrate temperature with a sputtering rate of 0.9 A/sec is displayed in Fig. 7.5 (solid line). The observed moment at 18 kOe was 9.2 kG. This combined with a relative low coercivity of 7.3 kOe gave an inclined shape to the otherwise square loop because of the demagnetization 4*Pi*M. The dash line represents measurement parallel to the film plane. The remanant moment of the dash line is 3.5 kG compared to 7.2 kG in the solid line indicating the c-axis prefer to align more perpendicular to the film plane. The X-Ray diffraction is shown in Fig. 7.6 where it is observed that (105),(214) are the prominent peaks suggesting a preferential texturing of the c-axes normal to the film plane.

Film sputtered under the same condition but at a higher rate gave c-axes preferentially aligned onto the film plane. In Fig. 7.7, the magnetic responses of a $Nd_2Fe_{14}B$ sputtered under the same condition as the film in Fig. 7.5 but with a rate of 2 A/sec is

shown. The parallel to plane direction had attained a higher moment compared to the normal to plane direction. This suggests that the c-axes are more aligned onto the film plane. This is consistent with the X-Ray diffraction pattern as shown in Fig. 7.8, where the (031) line is larger than the (222) line. The presence of the (310) line also indicates c-axes aligned more onto the film plane. The most striking difference of Fig. 7.6 and Fig. 7.8 is that most major peaks occured at angles from 34 to 46 degrees in Fig. 7.6 whereas most major peaks occured at lower angles from 28 to 33 degrees in Fig. 7.8. These correspond to d-spacings of 1.973 A to 2.637 A in the low rate sputtered film and 2.715 A to 3.187 A in the high rate sputtered film. This illustrated that low rate sputtering produced a relative close pack stacking sequence than high rate sputtering. This is again consistent with the fact that low rate sputtering produces a c-axis preferential texture normal to the film plane since the c-axis is the more closely stacked direction in the $Nd_2Fe_{14}B$ tetragonal phase. The low rate sputtering allows relatively more Ar atoms bombardment when compared to the sputtered atoms flux. This Ar pseudo compression certainly favors more close stacking sequence. In high rate sputtering where the c-axis is more aligned onto the film plane, it is also consistent that the lattice favors larger d-spacings so as to minimize the stored magnetic energy. Therefore it is concluded that low rate sputtering is essential in producing perpendicular anisotropy $Nd_2Fe_{14}B$ films.

The hysteresis loop measured perpendicular to the film plane for an as sputtered Nd2Fe14B film deposited at 800 C substrate temperature with a 0.6 A/sec sputtering rate is displayed in Fig. 7.9 (solid line). The flux at 20 kOe external field is 8.5 kG and the perpendicular remanant at zero applied field is 7.5 kG. The coercive force is 14.8 kOe as a result of higher deposition temperature. The magnetization versus internal effective field, after correction for the demagnetization factor, is shown as cross points. The high $_iH_c$ and remanant moment makes these film magnets unique among the perpendicular anisotropy materials. The area bounded by the magnetization curves in the easy (solid line) and hard (dash line) directions gave an effective perpendicular anisotropy constant of 1.2×10^7 erg/cc. An X-Ray diffraction trace is shown in Fig. 6.10. The prominent peaks are (214), (204), and (105) reflections. This indicated a preferential texturing of the c-axis normal to the film plane. Comparing to Fig. 7.6, this also shows more c-axis texturing normal to the film plane.

CONCLUSION

In this report, we have established that low rate sputtering is essential to produce perpendicular anisotropy and high deposition temperature is necessary to produce high coercivity in the $Nd_2Fe_{14}B$ phase. The $Nd_2Fe_{14}B$ system is unique in that large values of the

static energy product and extreme values of effective anisotropy constant can be obtained in the same compound. The ratio of the intrinsic perpendicular anisotropy constant (15 x 10^6 erg/cc) to the demagnetization energy ($2*Pi*M^2$ = 2.8 x 10^6 erg/cc) gives a Q value of 5.3.

7.4 PERPENDICULAR ANISOTROPY $SmCo_3$ FILMS

INTRODUCTION

Film samples of $SmCo_3$ which exhibit large perpendicular anisotropy have been synthesized in thick film form by direct hot substrate sputtering from elemental targets. In the Sm-Co system, only the $SmCo_3$ phase could be synthesized with perpendicular anisotropy, while other Co rich film phases such as Sm_2Co_7 and $SmCo_5$ exhibited inplane anisotropy. [11] Since the $SmCo_3$ is a rhombohedral with a = 5.050 A and c = 24.59 A, it resembles a long cylindrical shape just like the $Nd_2Fe_{14}B$ phase that were discussed earlier. Therefore, the prefered orientation would be the c-axis perpendicular to the film plane in hot substrate sputtering with low

rate. Among systems that exhibit perpendicular anisotropy, the $SmCo_3$ phase has the highest Curie temperature of 1050 K. Combined with a large perpendicular remanent of 5.2 kG, $SmCo_3$ films could be an excellent candidate for flux generation film magnet where hightemperature tolerance is required.

RESULTS

In Fig. 7.11, the hysterisis loop of a $SmCo_3$ sample crystallized at 650 C is shown. The solid line was measured perpendicular to the film plane direction, while the dash line was measured parallel to the film plane direction. The solid line loop was as measured and no demagnetization correction was employed. The perpendicular remanent was 5.2 kG and coercive force was 6.2 kOe. Saturation flux and calculated lattice parameters agreed with the bulk values.[71] X-Ray diffraction pattern was shown in Fig. 7.12 with only (111), (201) being observed and this suggested a c-axis coming out of the film plane. This is consistent with the magnetization data, where 18 kOe applied feild in the film plane could not saturate the sample.

CONCLUSION

Perpendicular $SmCo_3$ film magnets were sputtered with intrinsic perpendicular anisotropy constant of $8.2*10^6$ erg/cc and a Q value of 7.6. Unlike $SmFe_2$ and $Nd_2Fe_{14}B$ which have low Curie temperatures of 650 k and 580 k respectively, $SmCo_3$ has a Curie temperature of 1050 K. Thus, the magnetic properties of the perpendicular $SmCo_3$ film phase are less temperature dependent and these films could be an important class in film magnet technology application.

Chapter 8

CONCLUSIONS

Samples of rare earth transition metal systems of the type Sm-Co, Sm-Ti-Fe and Nd-Fe-B were synthesized in thick film form either by directly sputtering onto hot substrate in a magnetic field or by sputtering amorphous state and then crystalizing in a magnetic field. By employing, what we termed, selectively themalized sputtering, the desired phases were directly synthesized onto heated substrates, so that samples were highly textured and stable on the Al_2O_3 substrate surfaces. The in the substrate plane applied magnetic field during sputtering had been used to achieve a partial preferential alignment of the c-axes within the film plane for crystalline films and also were used to synthesize large in the film plane anisotropy amorphous films. Film compositions were determined by X-Ray fluorescence, Auger electron analysis and Electron microprobe analysis. It was observed that low oxygen content in the film (below 2 at %) was essential to produce single phase film magnets. The crystal phase determination was being studied by X-Ray diffraction. For those films that had bulk counterparts, the X-Ray diffraction pattern resembled the bulk X-Ray patterns. It was

observed that the relative intensities of the X-Ray peaks, i.e., the texturing, could be control by varying the sputtering parameters such as sputtering rate, $H_{sputter}$, sputtering presure, and substrate temperature, provided that the sputtering gas pressure was high enough to thermalize the sputtered atoms. A model based on hard spheres collision was used to account for the thermalization effect. A magnetic field $H_{sputter}$ of 1.75 or 2.5 kOe was applied along the substrate plane during annealing or hot sputtering to promote c-axis alignment. A qualitative model relating the grain size, magnetic energy and thermal energy was used to describe the $H_{sputter}$ effect.

The sputtering rate effect was corelated with the relative Ar (sputtering gas) bombardment flux to the sputtered atoms flux. In the $SmCo_5$ case with almost cubic shape, the c-axis is always aligned onto the film plane and sputtering rate could only control (100) or (110) texturing. In the $Nd_2Fe_{14}B$ case with long cyclinderical shape, the sputtering rate could control the c-axis alignment in that low rate gives perpendicular to film plane alignment and high rate gives onto film plane alignment.

We had successfully fabricated high energy product film magnets of up to 21 MG-Oe based on the $Sm_2(CoFeZr)_{17}$ system. Samples have been directly crystallized onto heated substrates in the presence of an applied inplane magnetic field of 2.5 kOe. These films possessed

flat topped hysteresis loops and exhibited a maximum coercive force of 7 kOe and an inplane remanant of 10 kG. The coercive force of these film magnet system could be controlled by using different annealing conditions because coercivity depends on the grain size of these materials.Thus, film magnets with intrinsic coercivity of 16 kOe were obtained when synthesized in finer grain forms, by sputtering amorphous first and then annealing at 750 C for one hour.

Samples of $SmCo_5$ film magnets exhibited large uniaxial inplane anisotropy of 10^7 erg/cc when synthesized by sputtering amorphous first and then annealing in the presence of $H_{sputter}$ of 2.5 kOe. The easy axis of magnetization was parallel to the $H_{sputter}$. Applied external measuring feilds of upto + 22 kOe were not large enough to rotate the magnetization by any significant amount away from the easy axis.

The Sm-Ti-Fe film magnet system exhibited interesting magnetic properties for several different Fe concentrations. For Fe rich region a new ternary phase with intrinsic coercivity in the 20 kOe range had been observed. This phase was synthesized by annealing and X-Ray data revealed a tetragonal phase with a= 8.285 A and c= 12.500 A. We interpreted this as a $Sm_2Fe_{14}Ti$ in analogous to the well known $Nd_2Fe_{14}B$ phase. The Ti played the role of B in the $Nd_2Fe_{14}B$ structure and acted as a stabilizing agent. The saturation

flux of this phase estimated to be 16 kG. The Curie temperature of this new ternary phase was found to be 630 K which is about 50 C higher than that of $Nd_2Fe_{14}B$. Samples sputtered onto hot substrate exhibited a maximum coercive force of 10 kOe and a static energy product of 12 MG-Oe.

For lower Fe concentration as in the $Sm(FeTi)_2$, we had successfully fabricated film magnet that had large perpendicular anisotropy of 5.5 x 10^6 erg/cc. The perpendicular remanant was 3 kG. The analogous system, $SmCo_3$ also exhibited perpendicular anisotropy of 10^6 erg/cc and the remanant was 5 kG. The Curie temperature of this film magnet was found to be 1050 K, which is about 400 C higher than that of other perpendicular anisotropy film phases, such as, $SmFe_2$ and $Nd_2Fe_{14}B$,

The $Nd_2Fe_{14}B$ iron based permanent magnet had been successfully sputtered in the thin film form with intrinsic coercive force up to 16 kOe and either with high static energy product of 15 MG-Oe or with largest known effective perpendicular anisotropy constant of 1.2 x 10^7 erg/cc. It had been observed that for deposition rates less than 1.8 A/sec the film exhibited easy axis of magnetization perpendicular to the plane, while for deposition rates greater than 1.8 A/sec the easy magnetization axis was in the film plane. The precise dependance of c-axis(easy axis) texturing versus sputtering

rate is expected to be system dependent. The intrinsic coercivity of these films was observed to increase with the deposition temperature up to 800 C.

In addition to the above hard magnetic films we have also investigated the induced inplane anisotropy of amorphous rare earth-transition metal systems. We have achieved the highest inplane anisotropy, in any amorphous material known, of 2 x 10^6 erg/cc. This was observed in $SmCo_5$, $Sm_2(CoFeZr)_{17}$ and $(SmTi)Fe_5$ phases.

In conclusion, we have demonstrated the means of fabricating film magnets with special anisotropies in various rare earth-transition metal systems. All these films were chemically stable and have not shown any degradation for several years.

TABLE 1

Comp.	Str. Type	Symm.	Sp. Group	R site	M site	M
RM_2	$MgCu_2$	cub	Fd3m	8(a)	16(d)	Ni,Co Fe
	$MgZn_2$	hex	P63/mmc	4(f)	2(a),6(h)	Mn
RM_3	$PuNi_3$	Rh	R3m	3(a),6(c)	3(b),6(c) 18(h)	Ni,Co Fe
	$CeNi_3$	hex	$P6_3/mmc$	2(c),4(f)	2(a),2(b) 2(d),12(k)	Ni,Co
R_2M_7	Ce_2Ni_7	hex	$P6_3/mmc$	$4(f_1),4(f_2)$	2(a),4(e) 4(f),6(h) 12(k)	Ni,Co
	$GdCo_7$	rh.	R3m	$6(c_1),6(c_2)$	3(b),6(c) 6(c),9(e) 12(h)	Ni,Co
R_6M_{23}	Th_6Mn_{23}	tetr	Fm3m	24(e)	4(b),24(d) 32(f_1) 32(f_2)	Fe,Mn
RM_5	$CaCu_5$	hex	$P6_3/mmc$	1(a)	2(c),3(g)	Co,Ni Zn,Cu
R_2M_{17}	Th_2Ni_{17}	hex	$P6_3/mmc$	2(b),2(d)	6(g),12(j)	Ni,Fe
	Th_2Zn_{17}	rh	R3m	6(c)	6(c),9(d) 18(f),18(h)	Ni,Co Fe
RM_{12}	$ThMn_{12}$	tetr	$I4_1/mmc$	2(a)	8(f),8(i) 8(j)	Mn

TABLE 2

COMPOSITION	$4\pi M_s$ (kG)	H_A (kOe)	K_A (10^{+6} erg/cc)
$SmCo_5$	10.3	10.6	2.6
$Sm_2(CoFeZr)17$	15.2	5.8	2.2
SmTiFe(.075,.092,.833)	16.4	5.0	1.5
SmTiFe(.069,.098,.833)	14.2	3.1	1.4

TABLE 3

In-plane M_r/M_s:	Parallel to H_s,	Perpendicular
$SmCo_5$	0.91	0.14
$Sm_2(CoFeZr)_{17}$	0.90	0.15
SmTiFe(.075,.092,.833)	0.99	0.22
SmTiFe(.069,.098,.833)	0.94	0.19

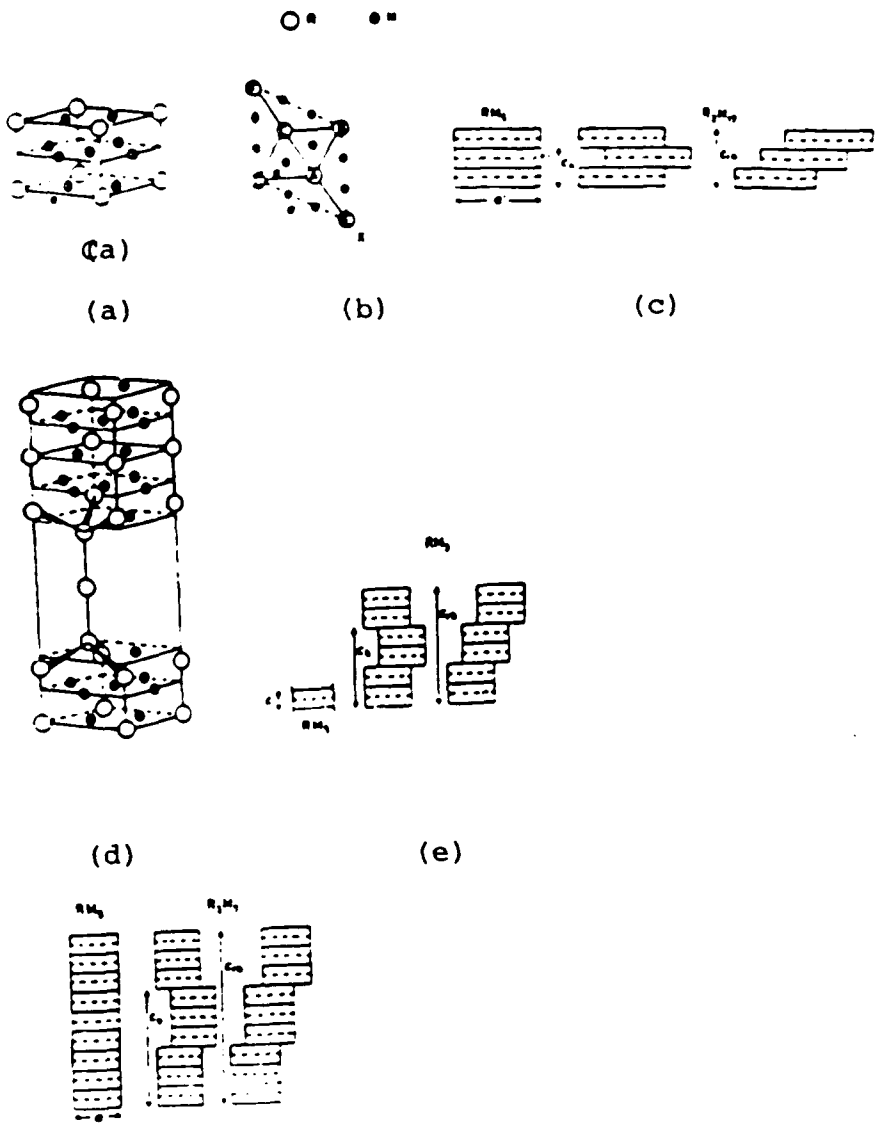

Fig. 2.1

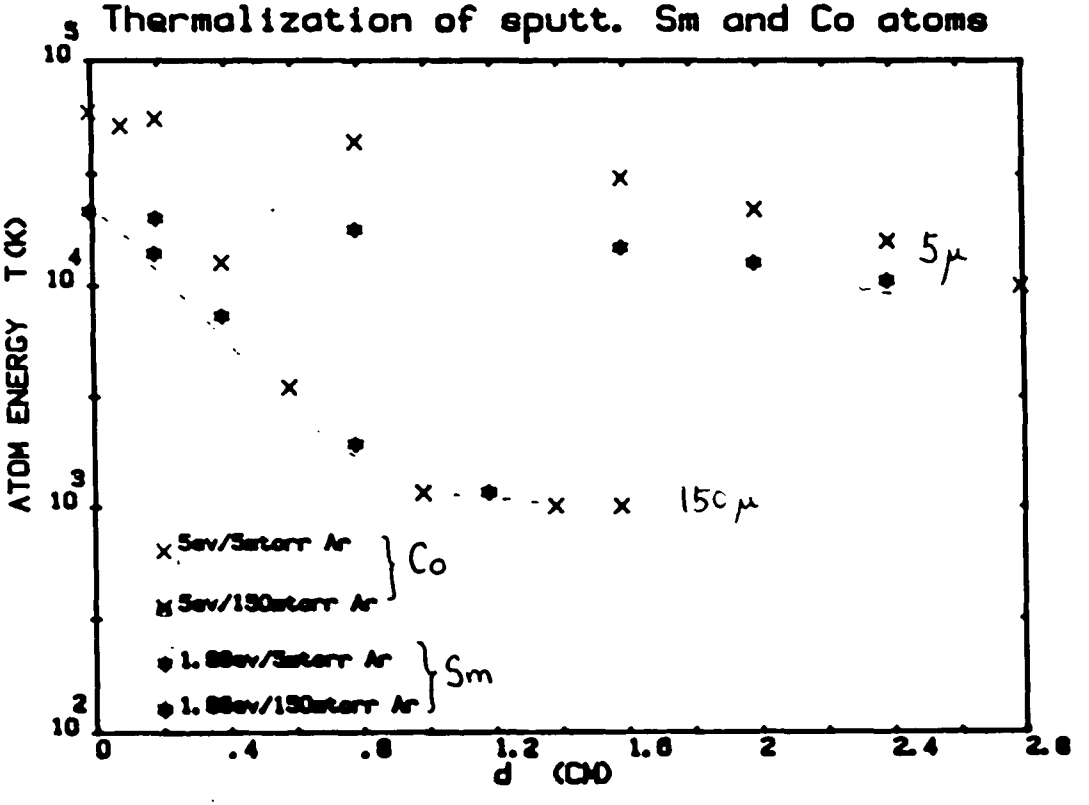
Thermalization of sputt. Sm and Co atoms
ATOM ENERGY T(K)
10^5
10^4
10^3
10^2
5μ
150μ
5ev/3mtorr Ar
5ev/150mtorr Ar
1.8ev/3mtorr Ar
1.8ev/150mtorr Ar
Co
Sm
0
.4
.8
1.2
1.6
2
2.4
2.8
d (CM)

Fig. 3.1

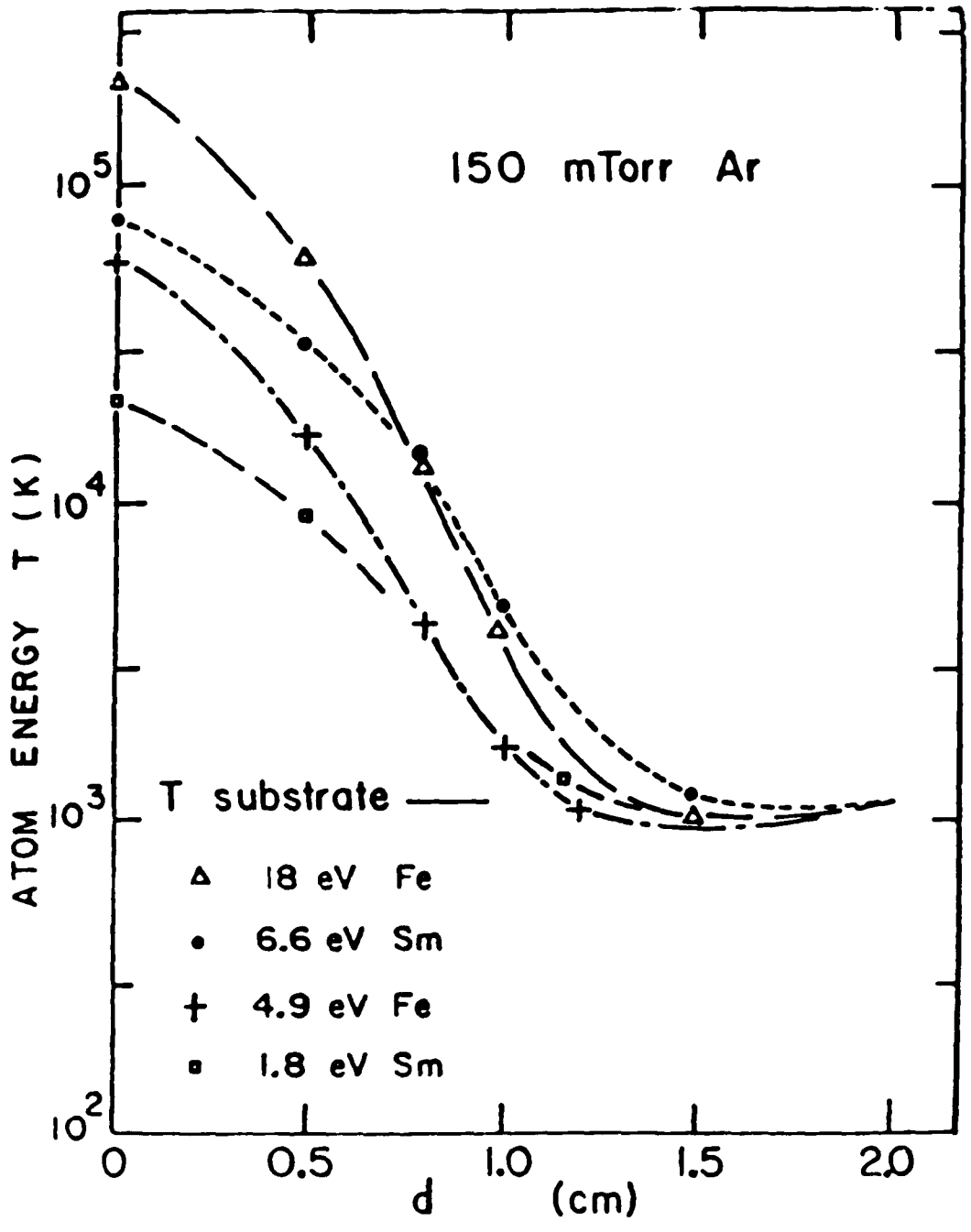
150 mTorr Ar
ATOM ENERGY T (K)
10^5
10^4
10^3
10^2
T substrate
18 eV Fe
6.6 eV Sm
4.9 eV Fe
1.8 eV Sm
0
0.5
1.0
1.5
2.0
d (cm)

Fig. 3.2

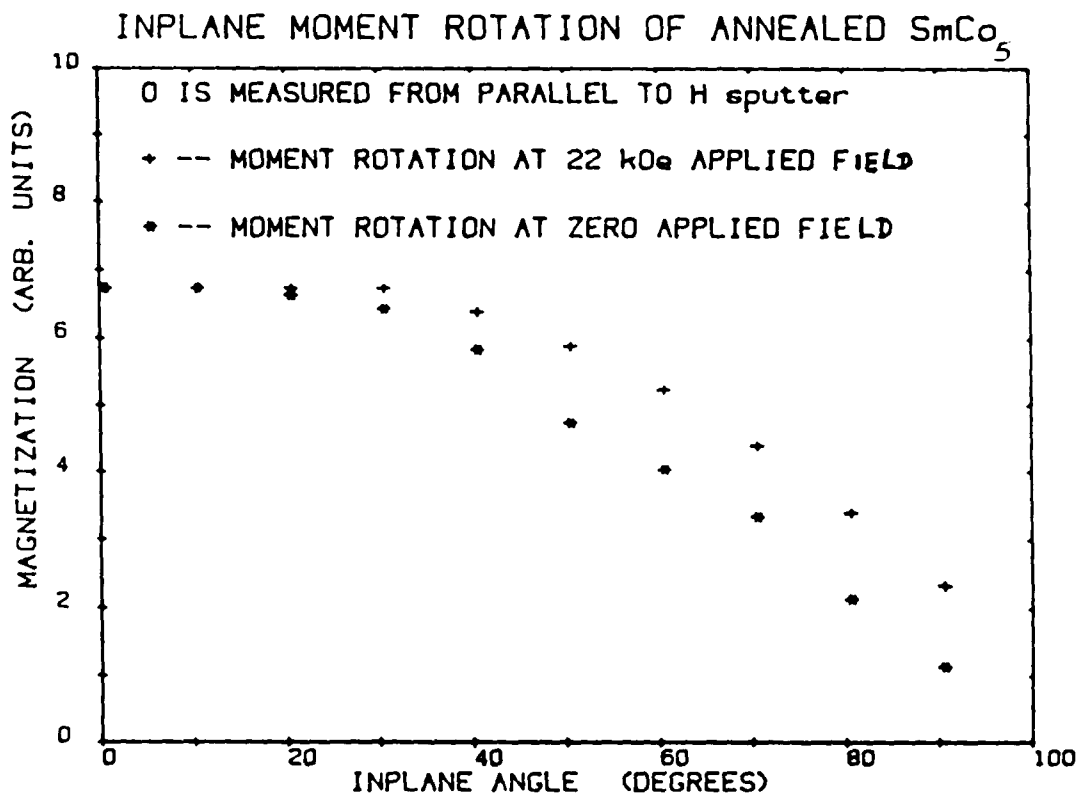
INPLANE MOMENT ROTATION OF ANNEALED SmCo5
0 IS MEASURED FROM PARALLEL TO H sputter
+ -- MOMENT ROTATION AT 22 kOe APPLIED FIELD
* -- MOMENT ROTATION AT ZERO APPLIED FIELD
MAGNETIZATION (ARB. UNITS)
0
2
4
6
8
10
0
20
40
60
80
100
INPLANE ANGLE (DEGREES)

Fig, 3.3

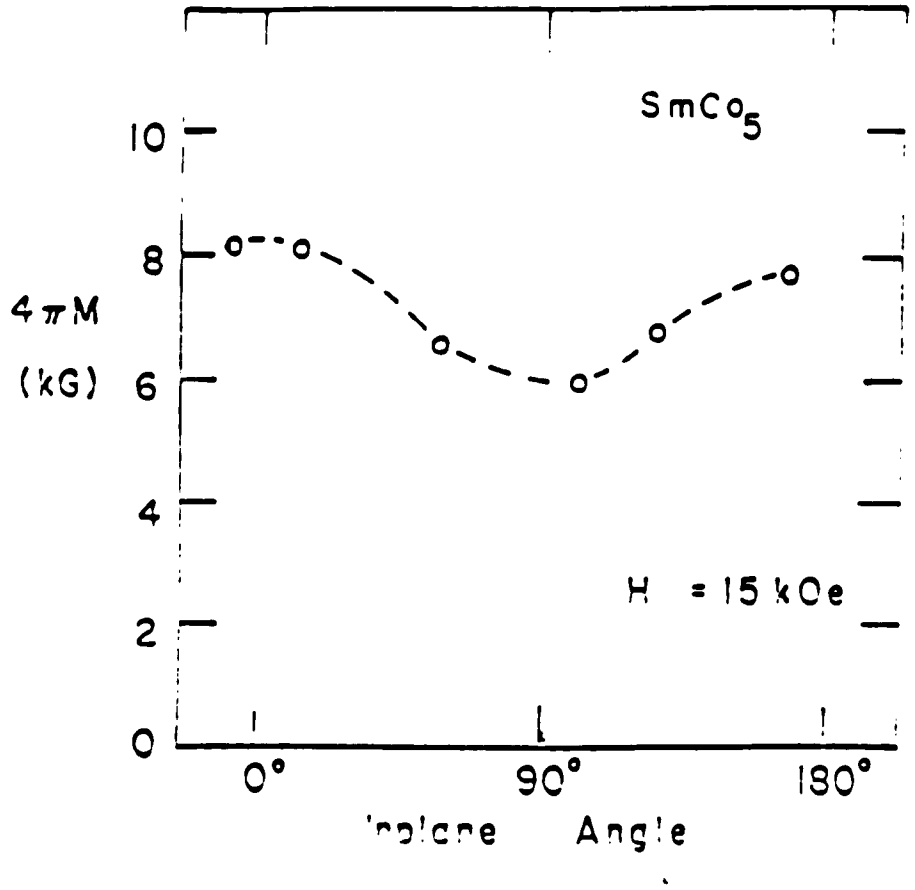

Fig. 3.4

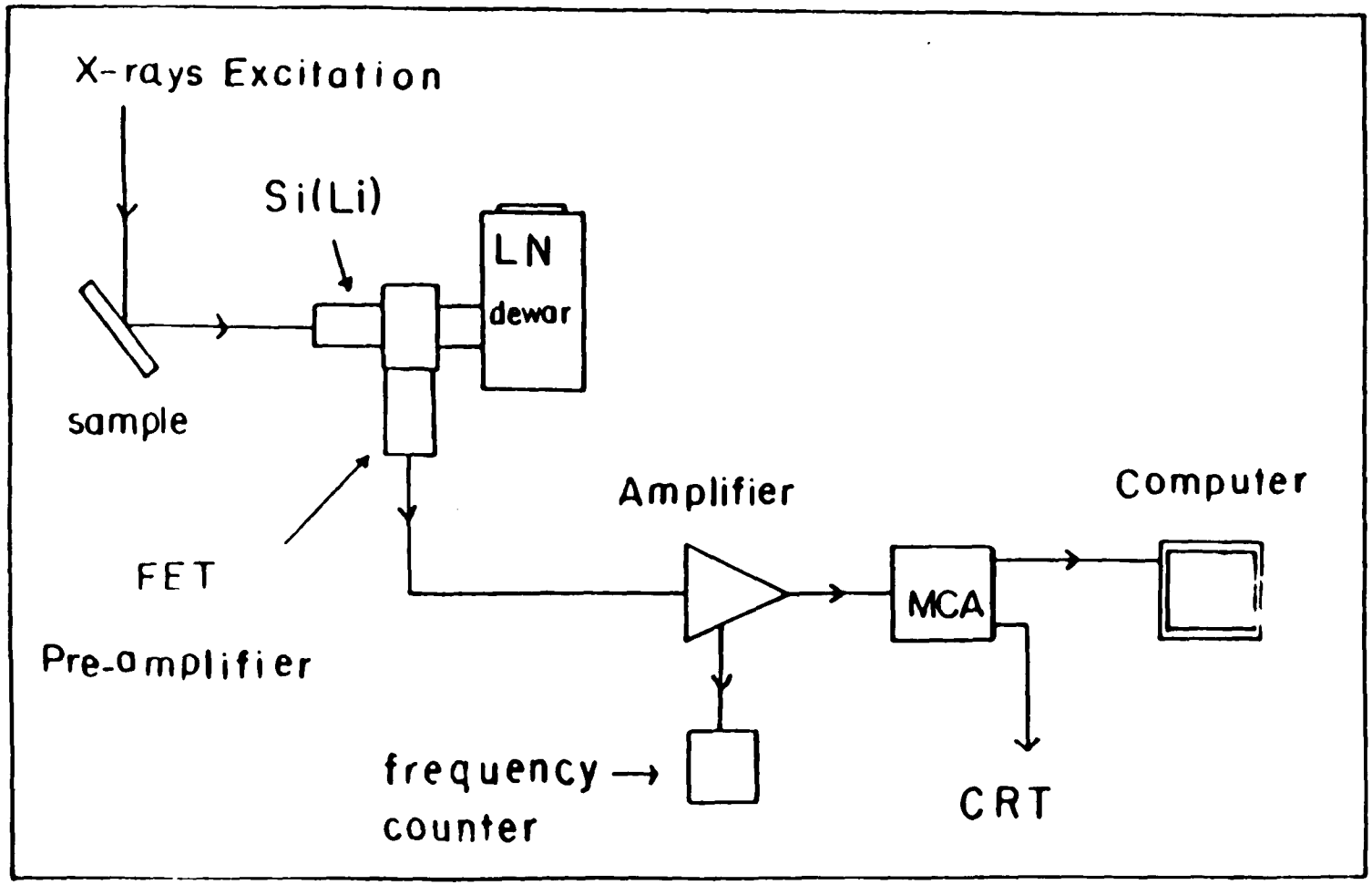
X-rays Excitation
Si(Li)
LN
dewar
sample
FET
Pre-amplifier
Amplifier
Computer
MCA
frequency →
counter
CRT

Fig. 3.5

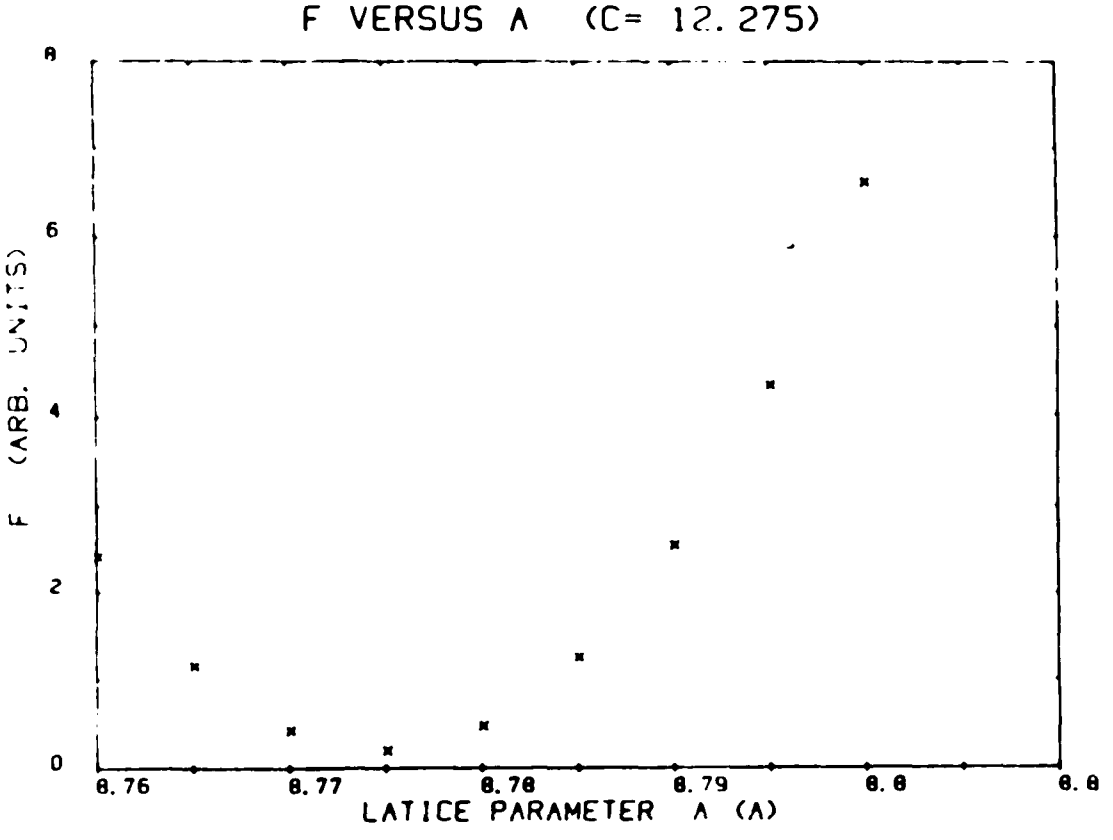
F VERSUS A (C= 12.275)
F (ARB. UNITS)
0
2
4
6
8
8.76
8.77
8.78
8.79
8.8
8.8
LATICE PARAMETER A (A)

Fig. 3.6

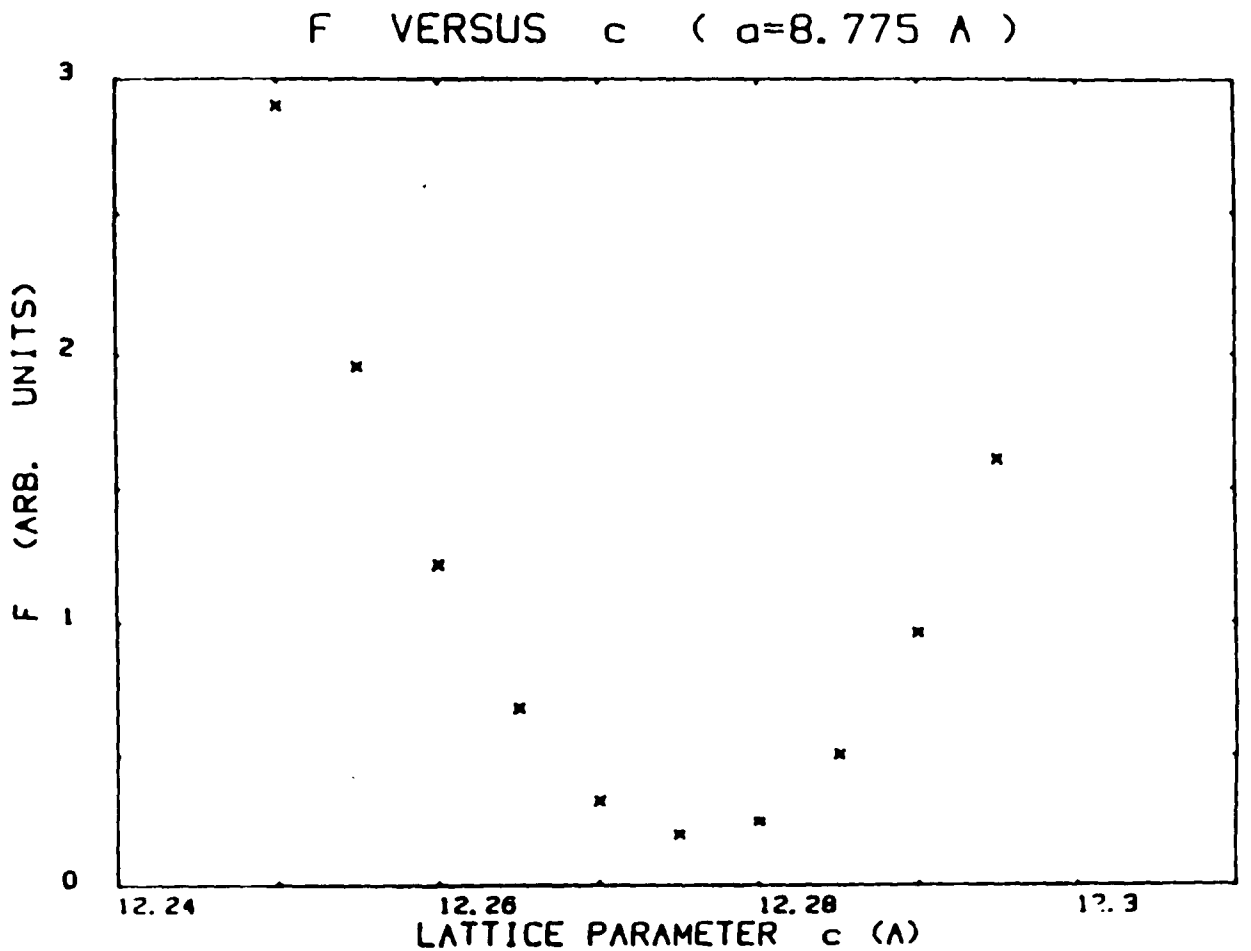
F VERSUS c (a=8.775 A)
F (ARB. UNITS)
3
2
1
0
12.24
12.26
12.28
12.3
LATTICE PARAMETER c (A)

Fig. 3.7

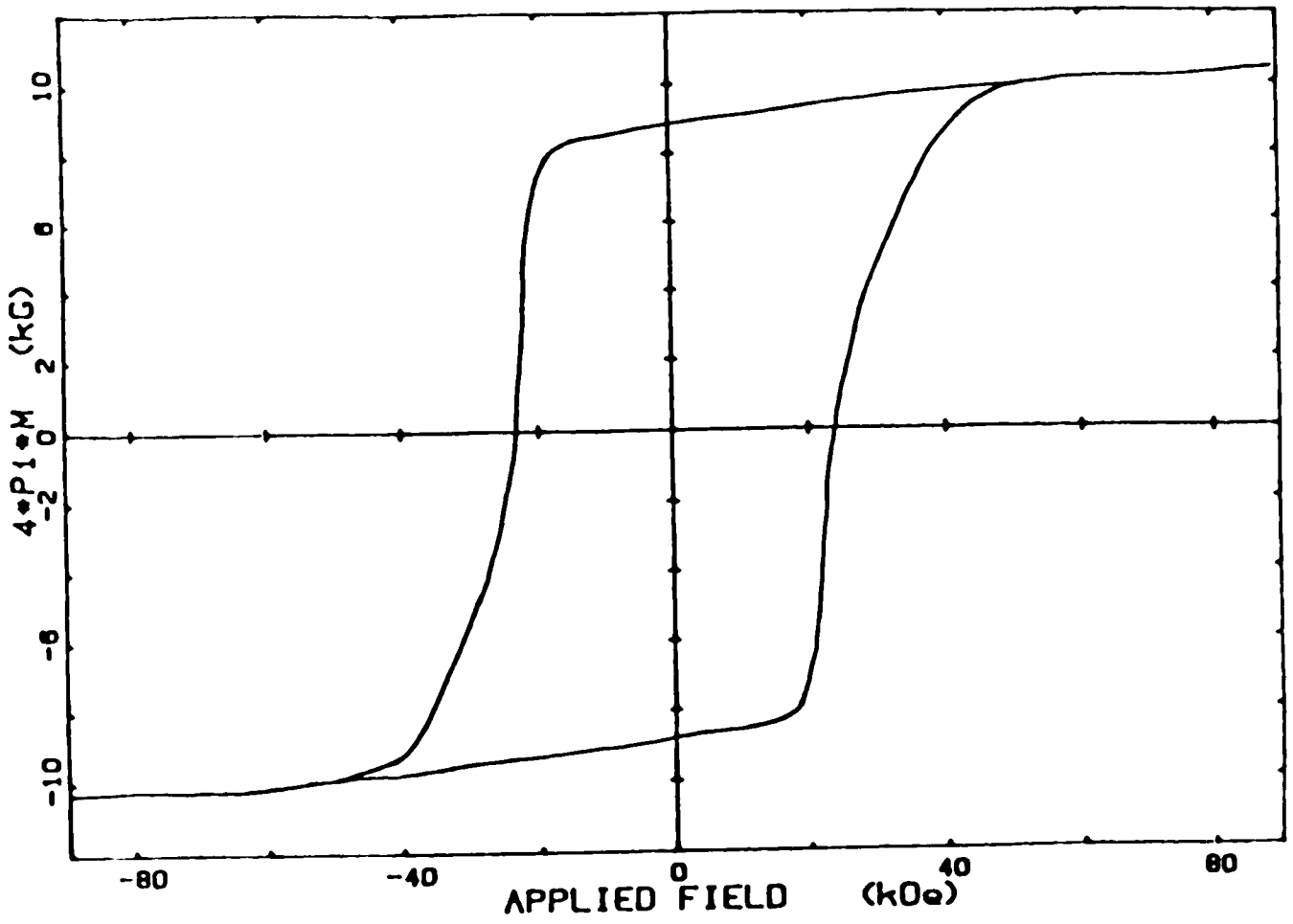

Fig. 4.1

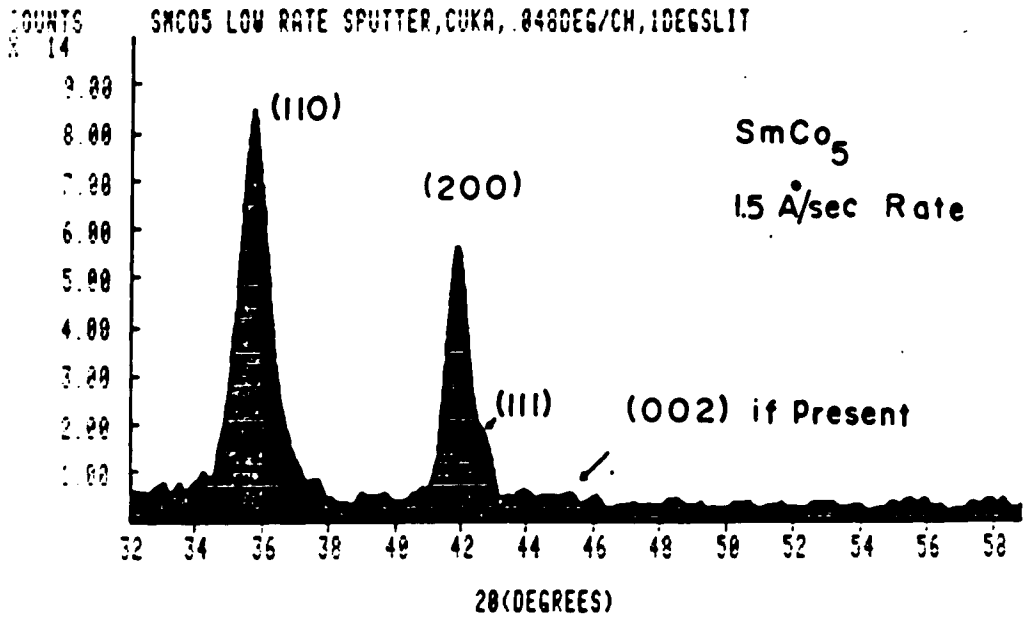
COUNTS
X 14
SMCO5 LOW RATE SPUTTER,CUKA,.048DEG/CH,1DEGSLIT
9.00
8.00
7.00
6.00
5.00
4.00
3.00
2.00
1.00
(110)
(200)
(111)
(002) if Present
SmCo5
1.5 Å/sec Rate
32
34
36
38
40
42
44
46
48
50
52
54
56
58
2θ(DEGREES)

Fig 4.2

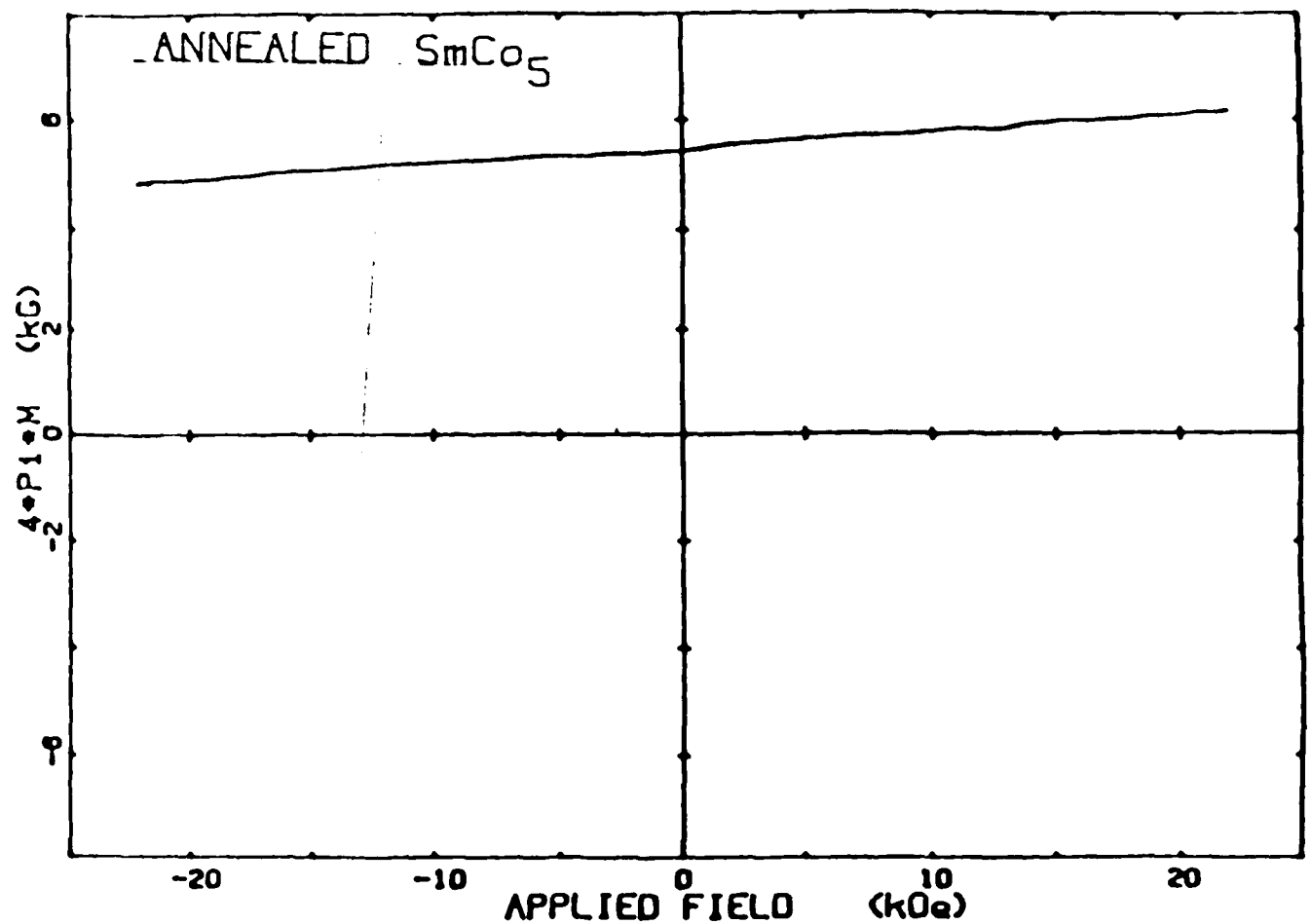

Fig. 4.3

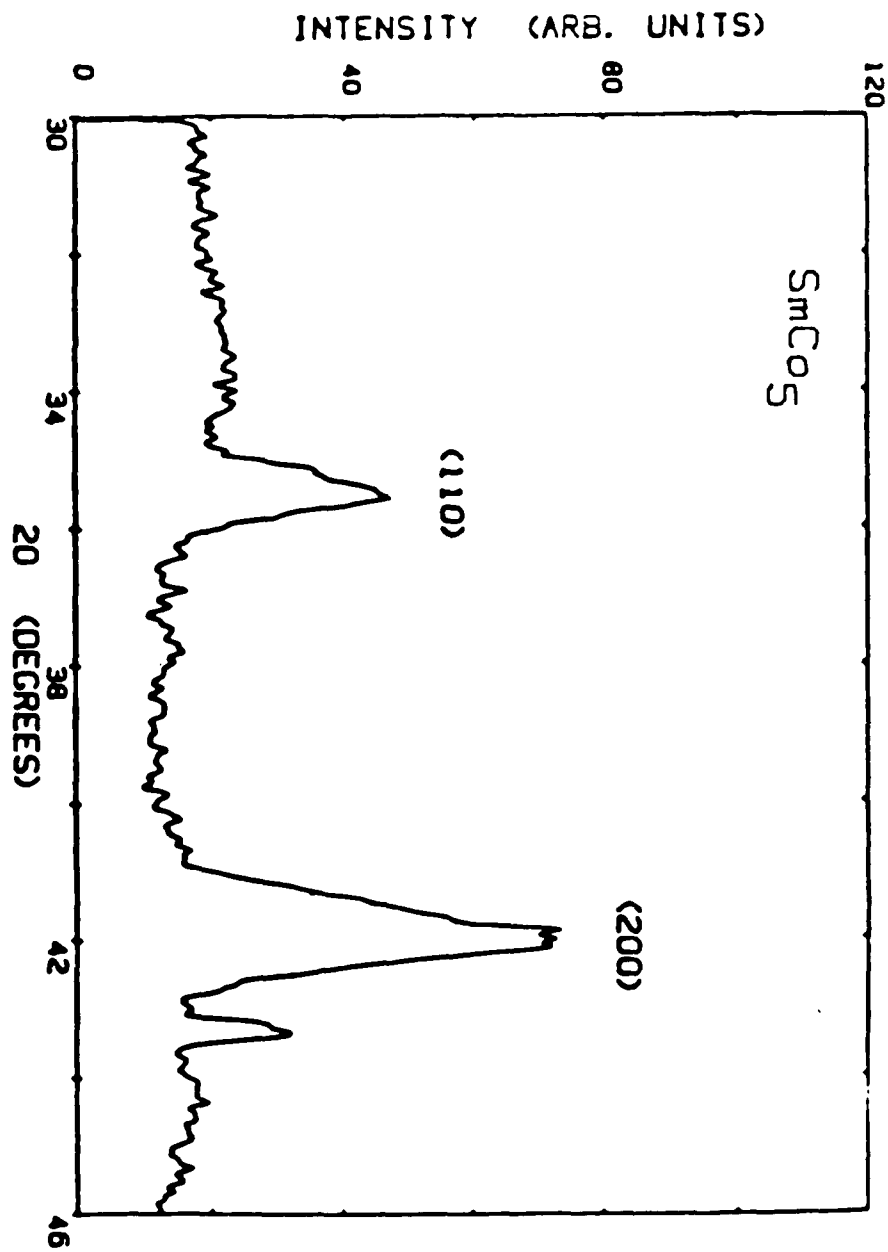
INTENSITY (ARB. UNITS)
0
40
80
120
30
34
38
42
46
2θ (DEGREES)
SmCo5
(110)
(200)

Fig. 4.4

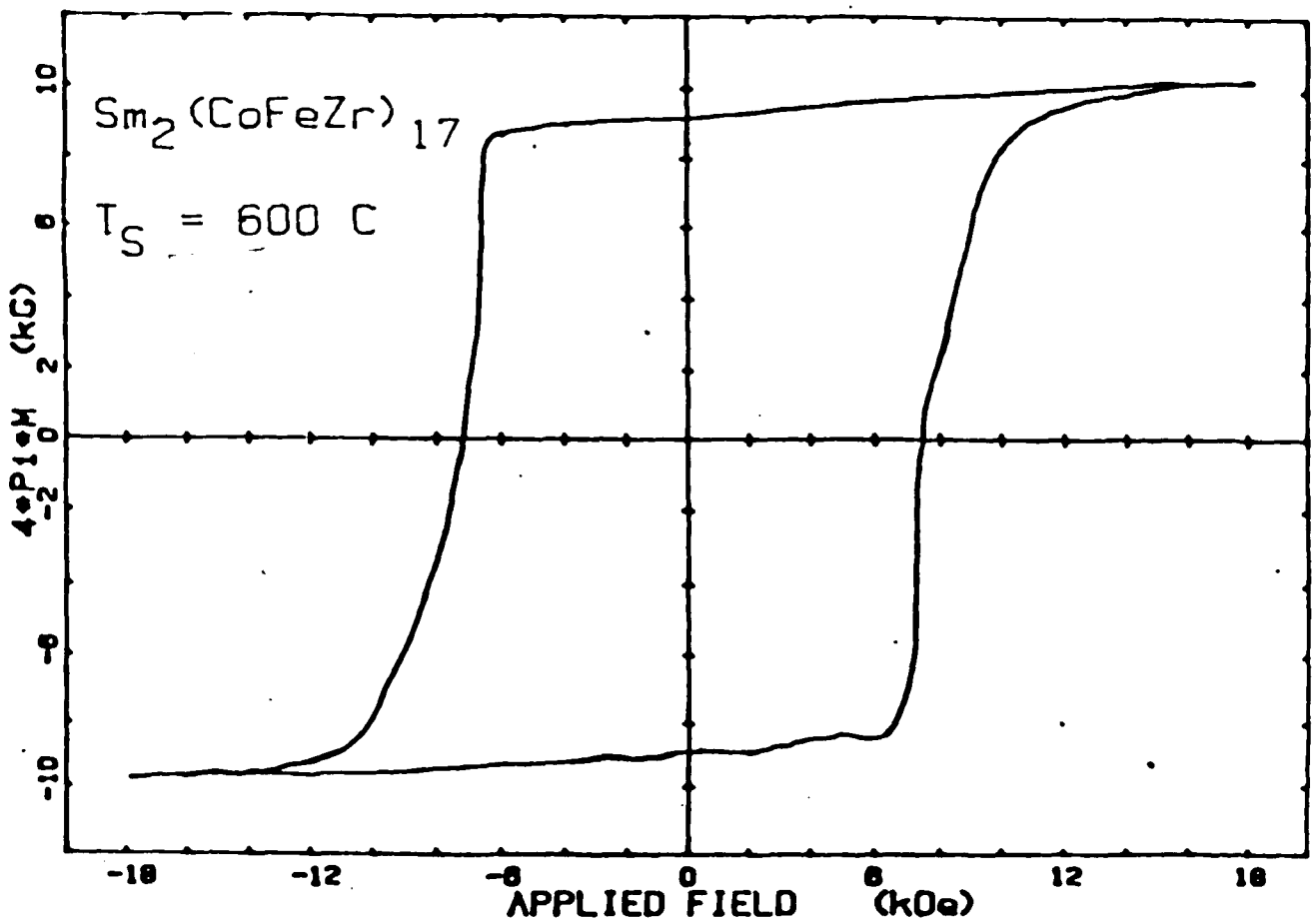
Sm2(CoFeZr)17
TS = 600 C
4•PI•M (kG)
10
6
2
0
-2
-6
-10
-18
-12
-6
0
6
12
18
APPLIED FIELD (kOe)

Fig. 4.5

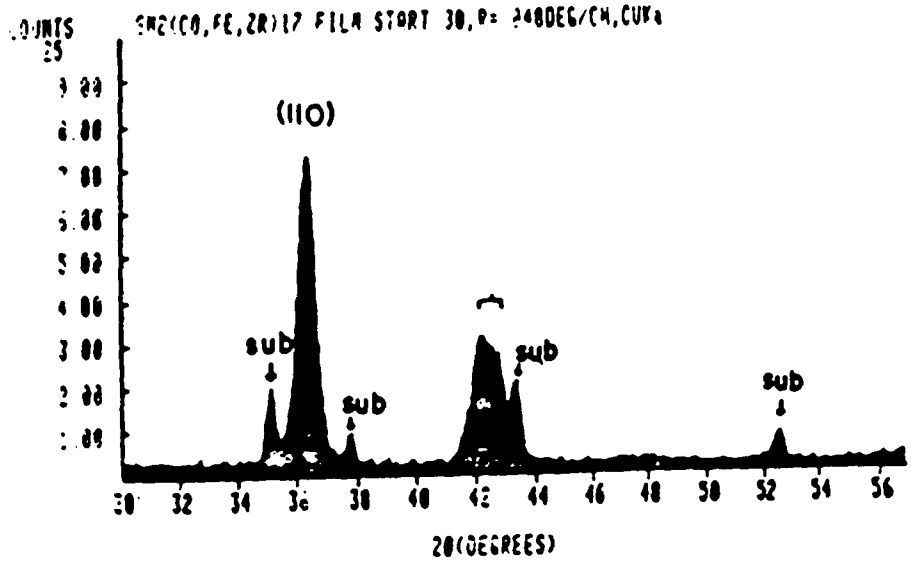
(110)
sub
sub
sub
sub
30
32
34
36
38
40
42
44
46
48
50
52
54
56
2θ(DEGREES)

Fig. 4.6

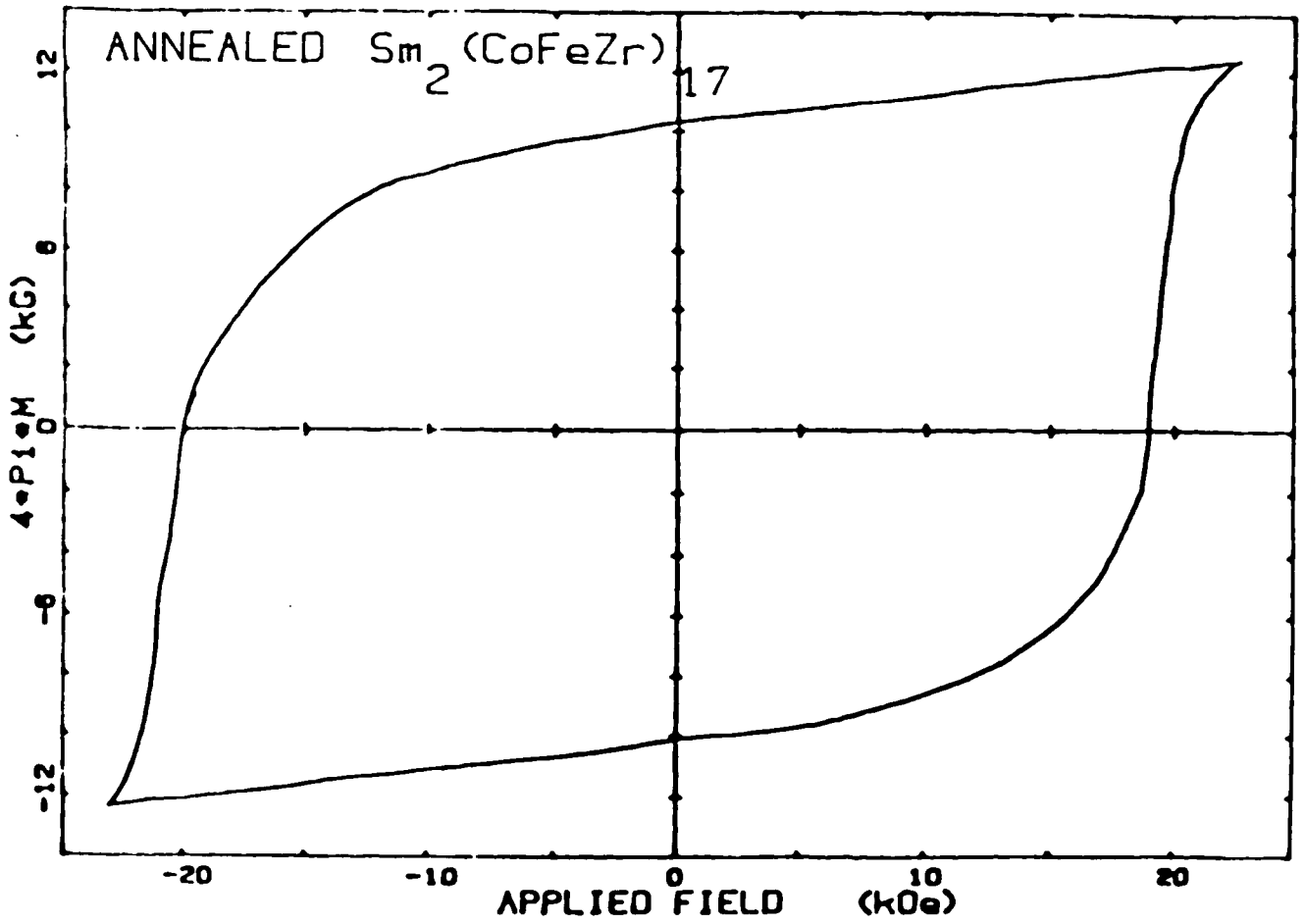
ANNEALED Sm2(CoFeZr)17
4•PI•M (kG)
12
8
0
-8
-12
-20
-10
0
10
20
APPLIED FIELD (kOe)

Fig. 4.7

Fig. 4.8

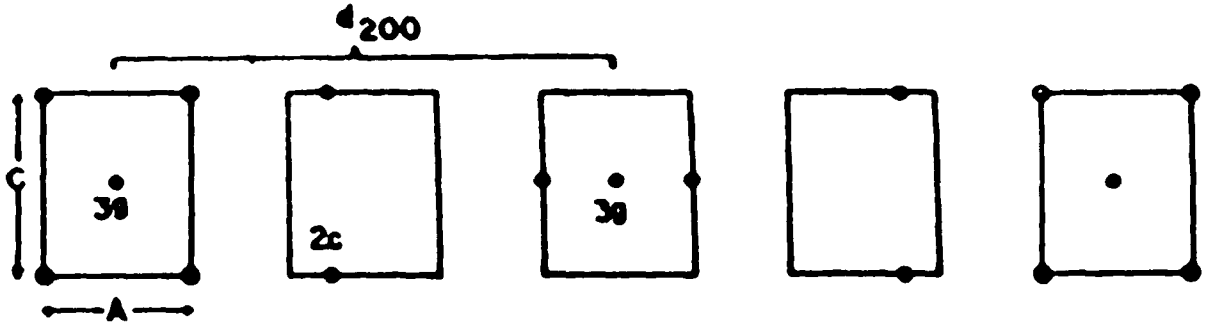

o Sm • Co (200) Stacking Sequence of $SmCo_5$

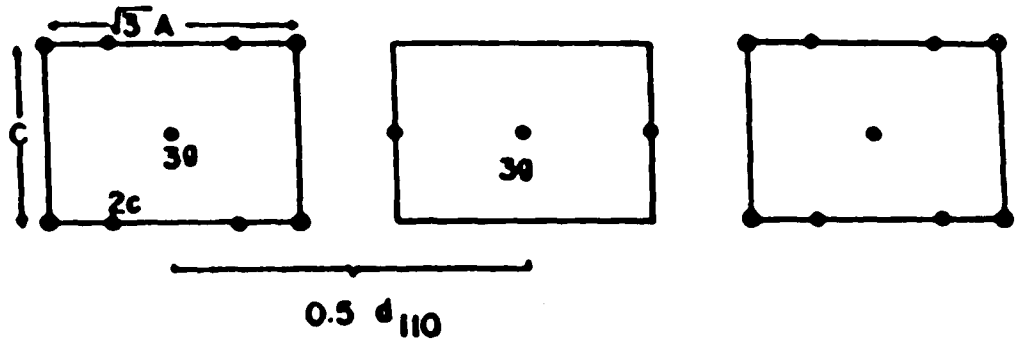

(110) Stacking Sequence of $SmCo_5$

Fig. 4.9

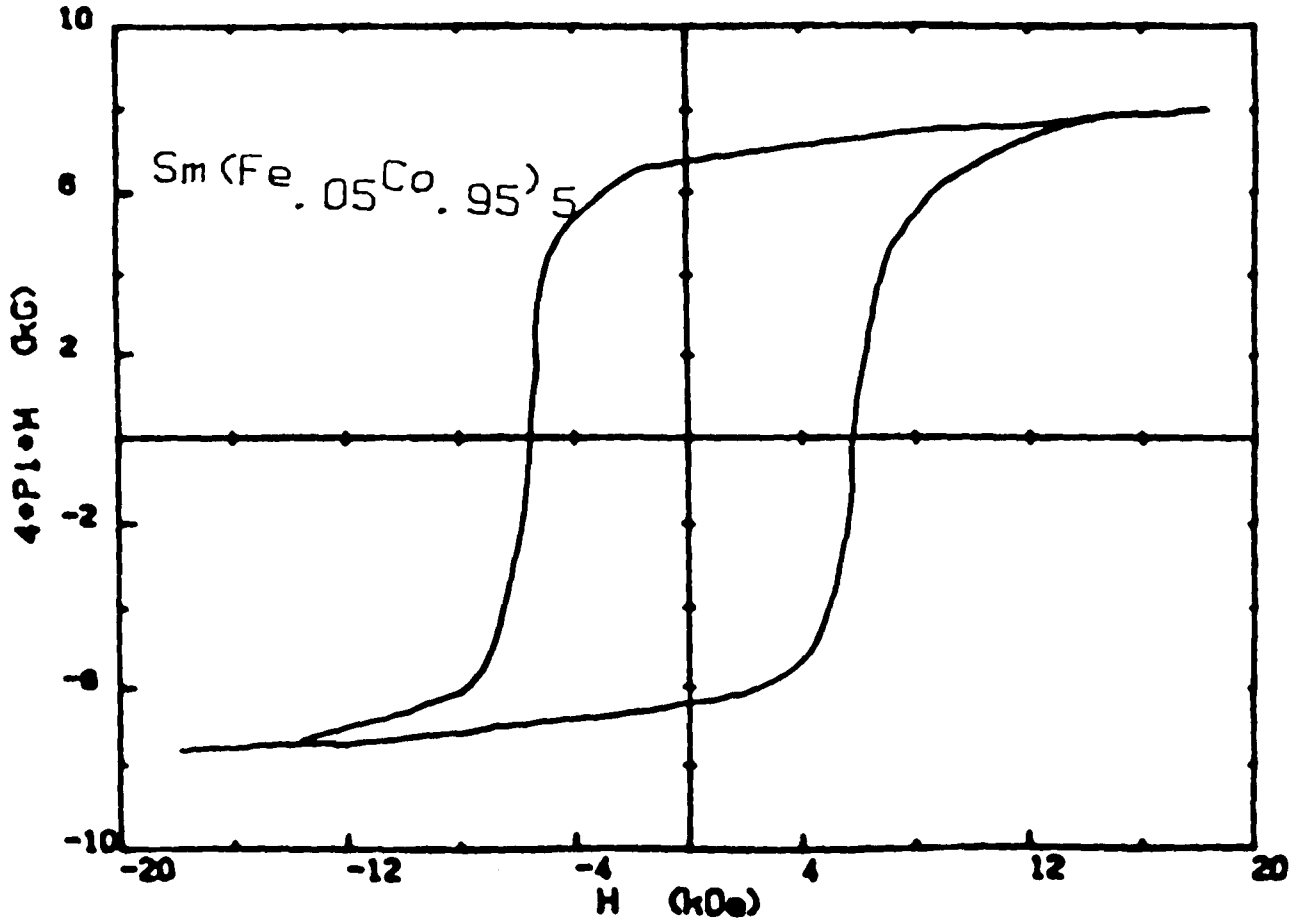

Fig. 4.10

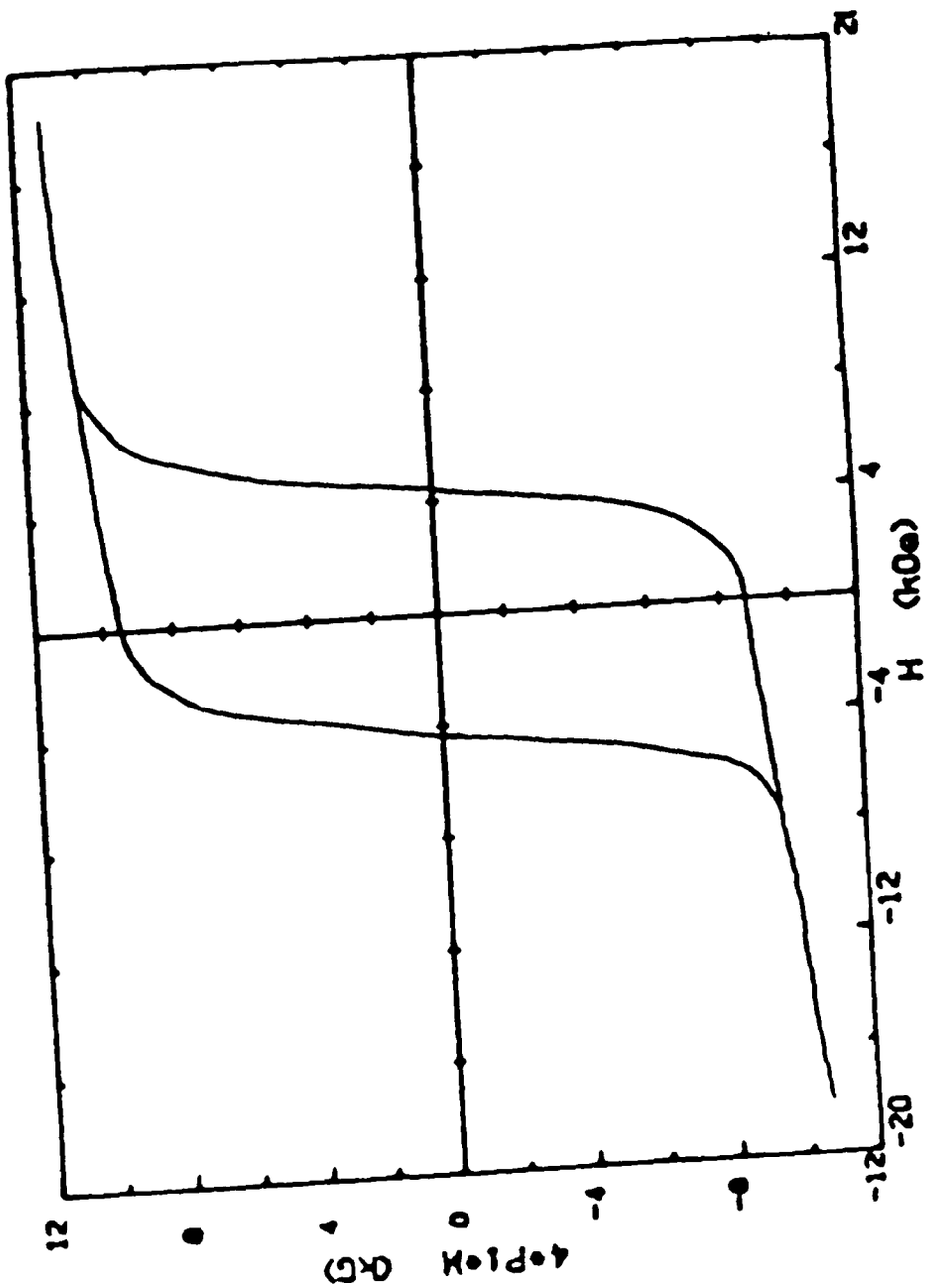

Fig. 4.11

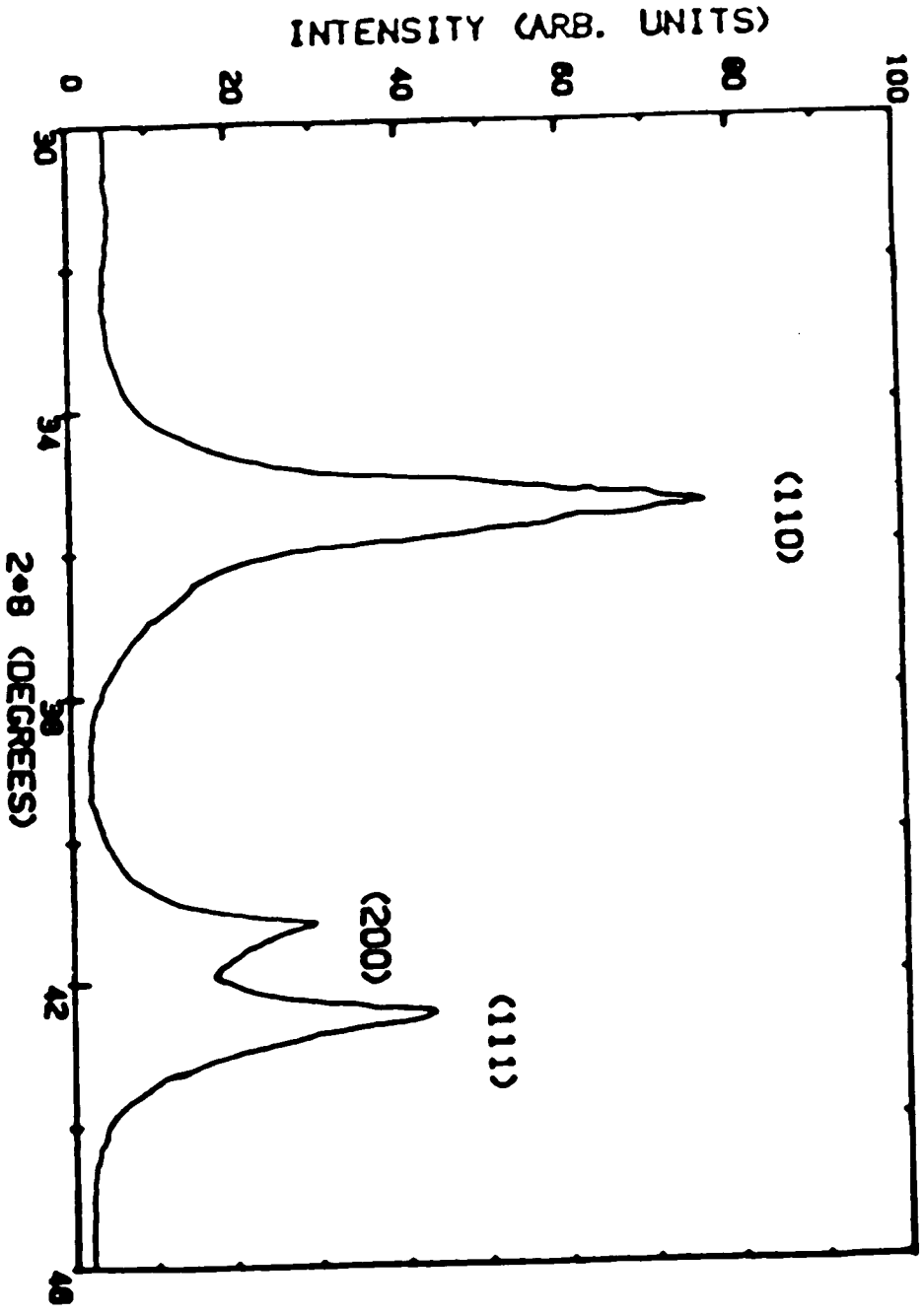
INTENSITY (ARB. UNITS)
0
20
40
60
80
100
30
34
38
42
46
2θ (DEGREES)
(110)
(200)
(111)

Fig. 4.12

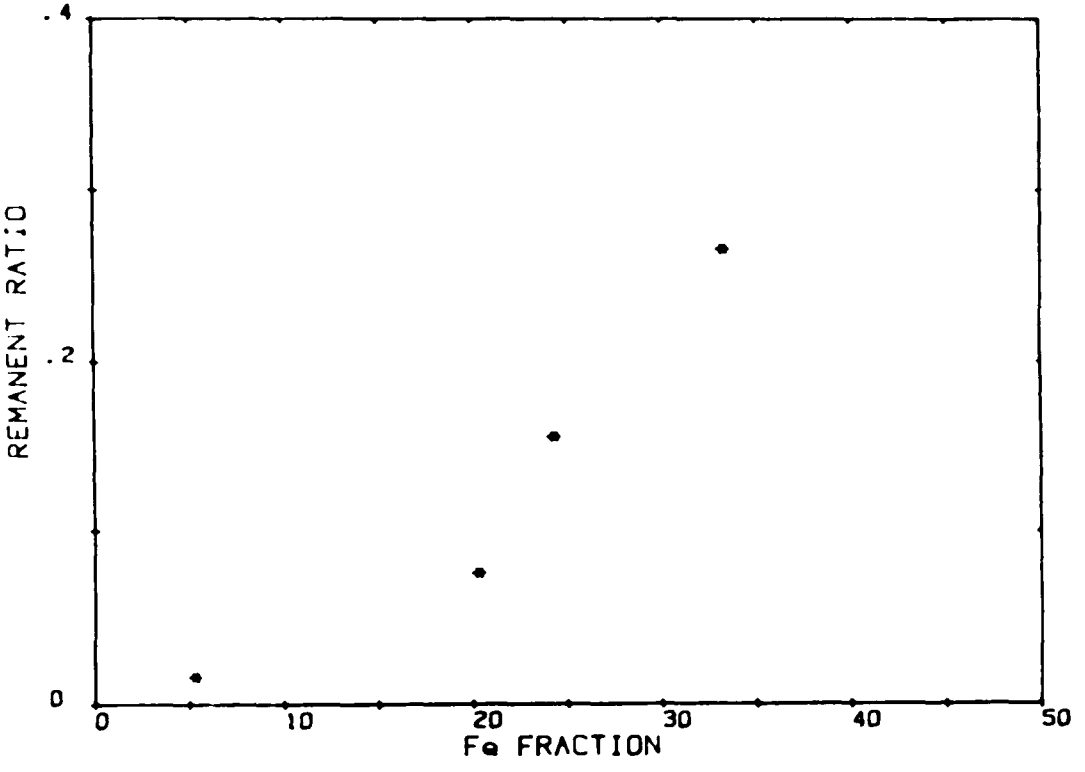

Fig. 4.13

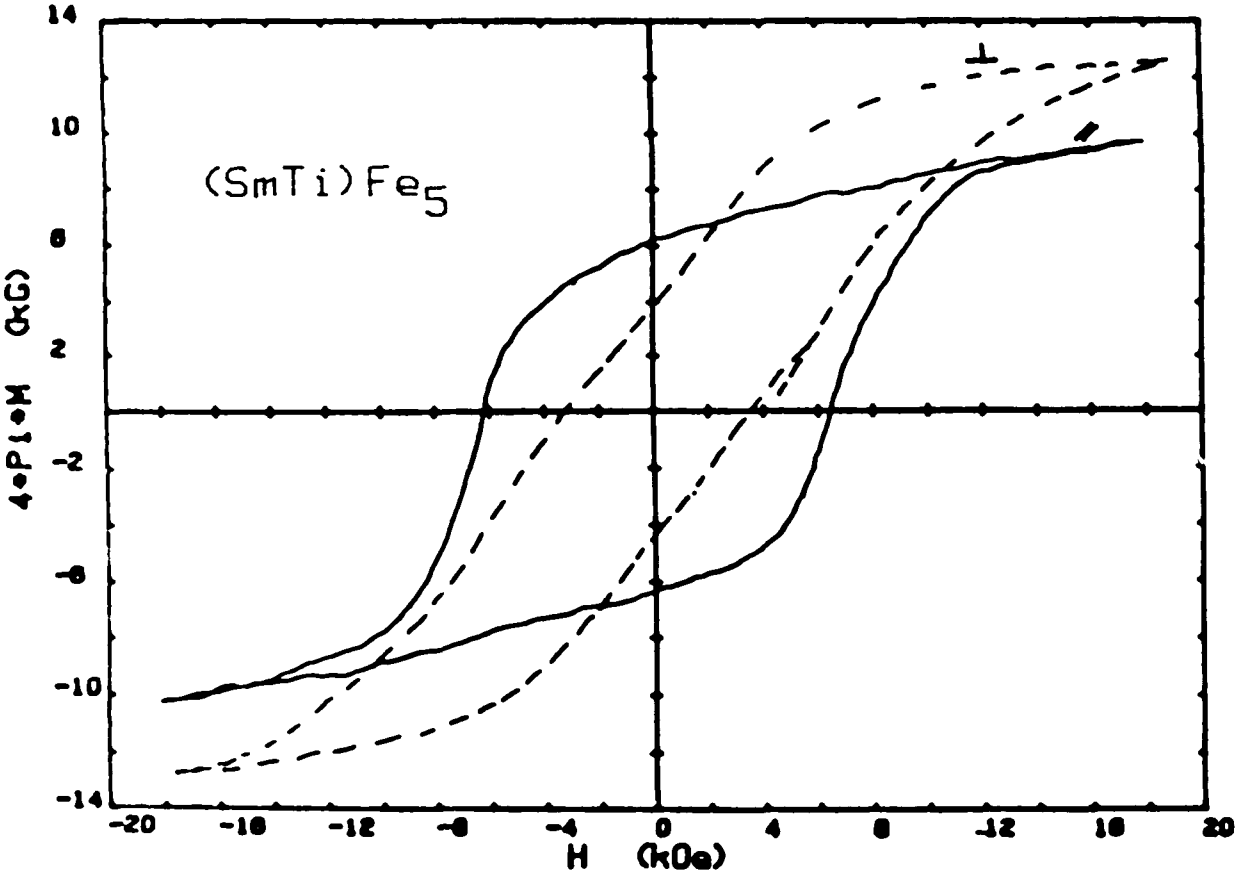

Fig. 4.14

Table I. X-Ray diffraction lines observed in reflection for Cu K_α radiation from Ti and O stabilised $SnFe_5$ phases crystallised onto heated substrates.

	2θ (°)	d (Å)	Hexagonal Index
O Stabilised $SnFe_5$	37.22	2.416	(110)
	42.85	2.111	(111)
	43.25	2.092	(200)
	48.30	1.885	(201)
Ti Stabilised $SnFe_5$	37.40	2.405	(110)
	42.87	2.111	(111)
	43.22	2.094	(200)
	48.21	1.887	(201)

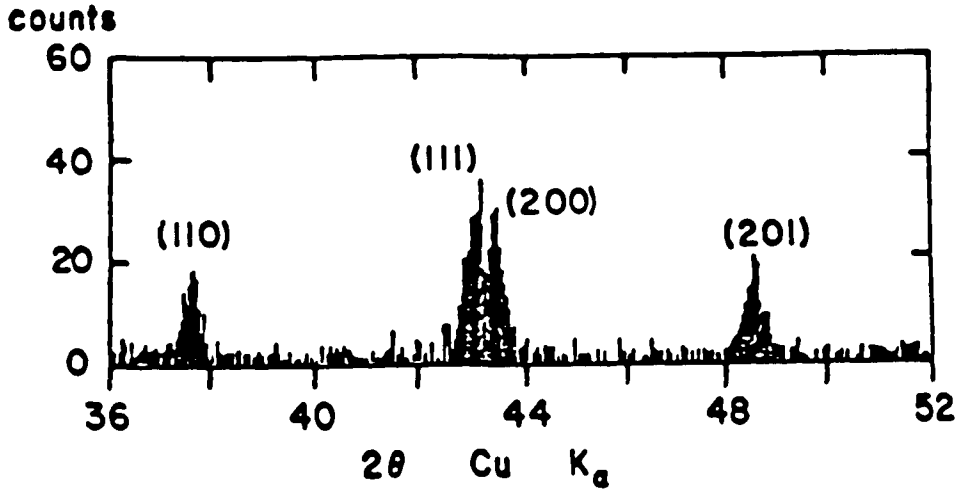

Fig. 4.15

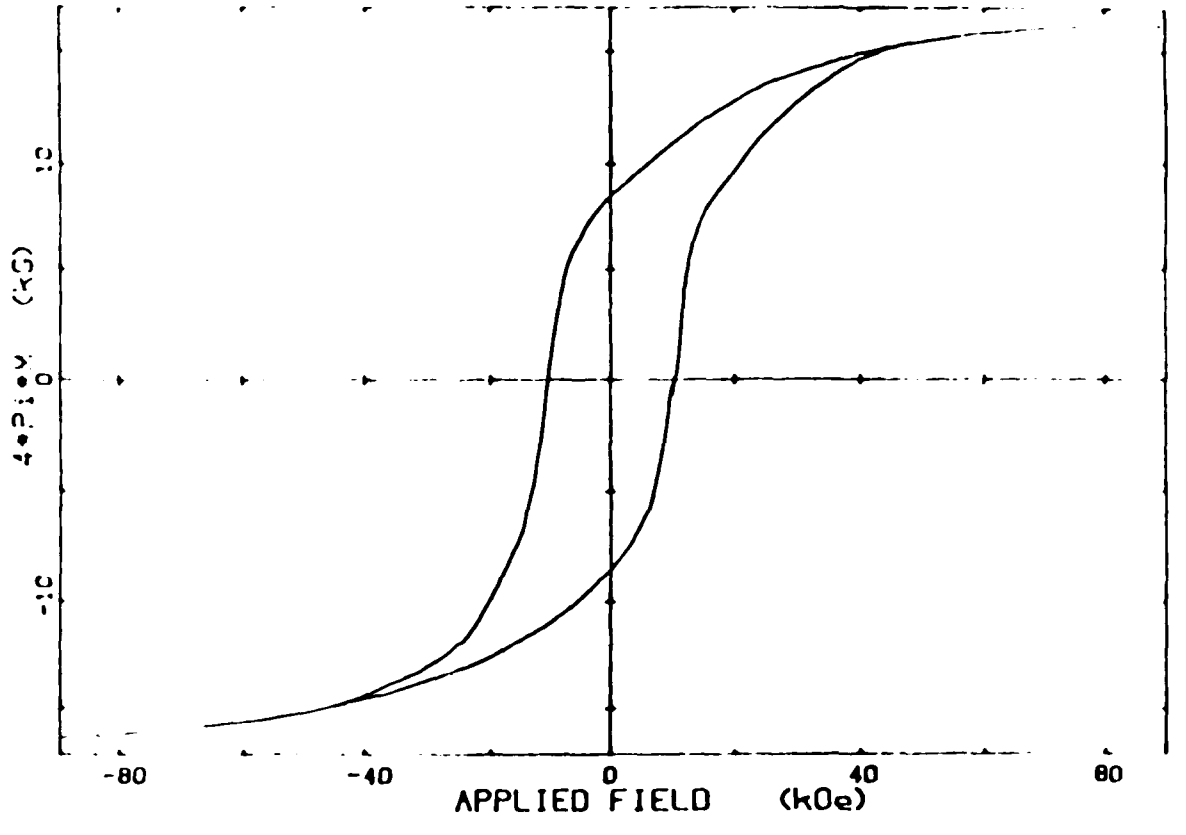

Fig. 4.16

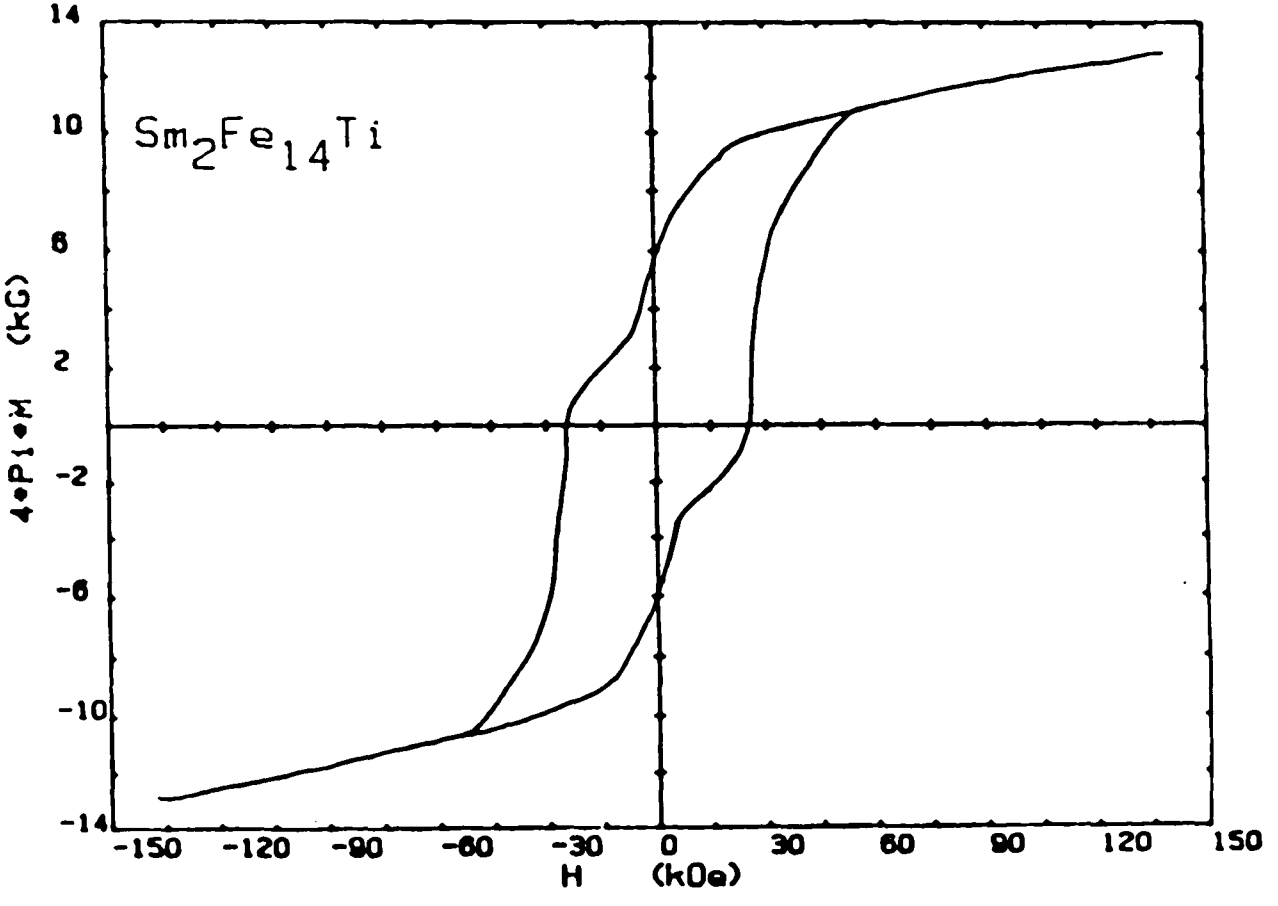
$Sm_2Fe_{14}Ti$
14
10
6
2
-2
-6
-10
-14
4•Pi•M (kG)
-150
-120
-90
-60
-30
0
30
60
90
120
150
H (kOe)

Fig. 4.17(a)

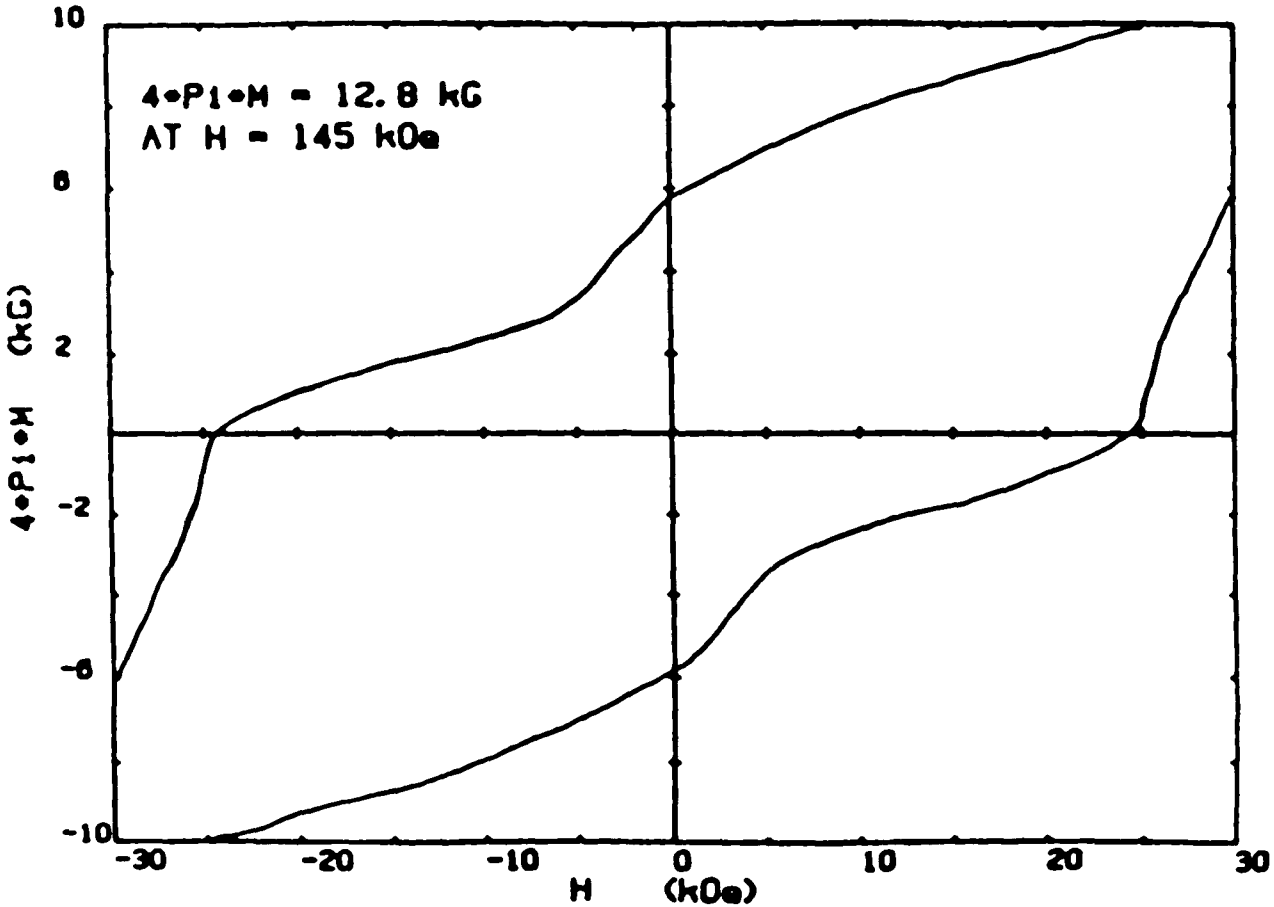

Fig. 4.17(b)

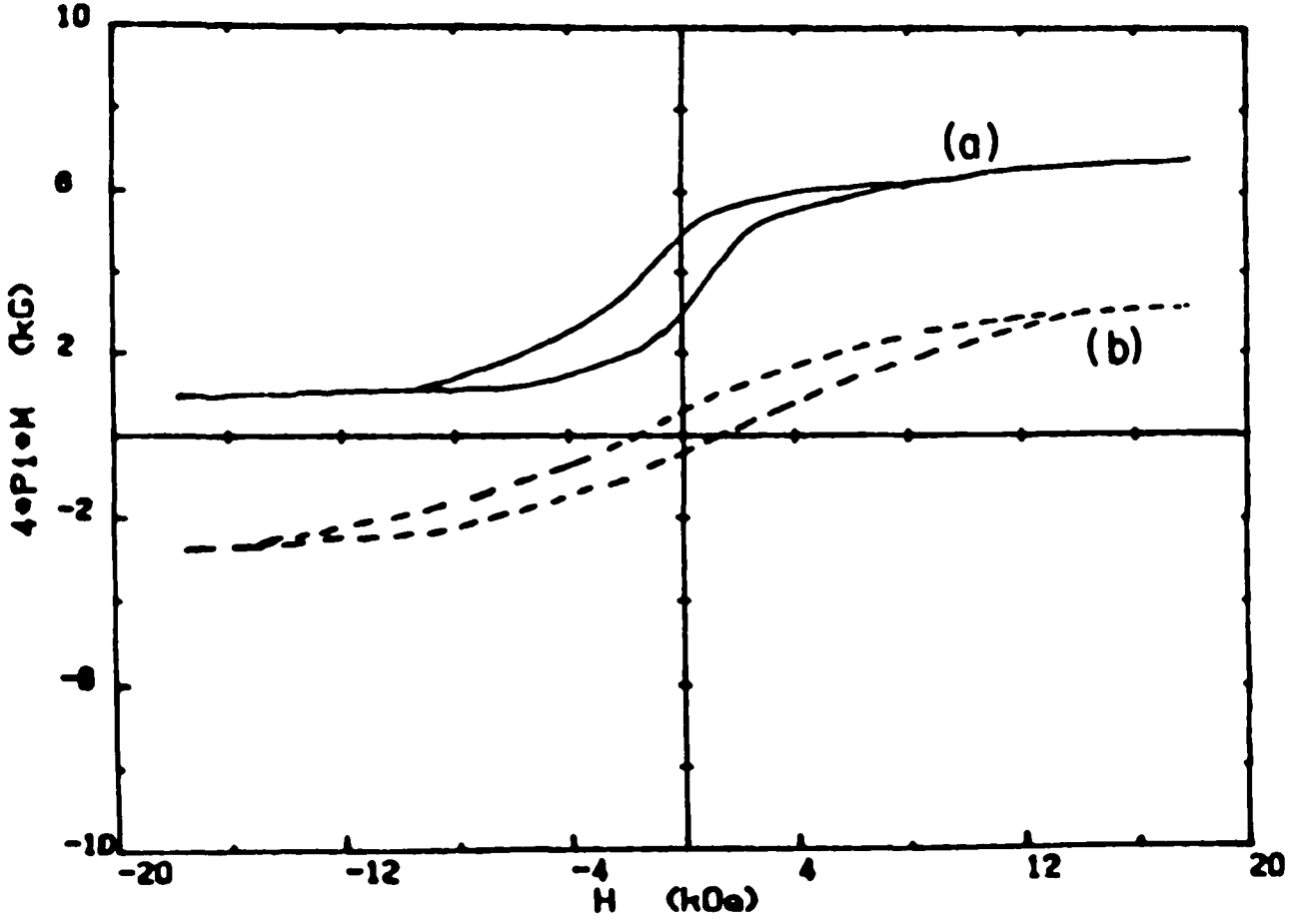

Fig. 4.17(c)

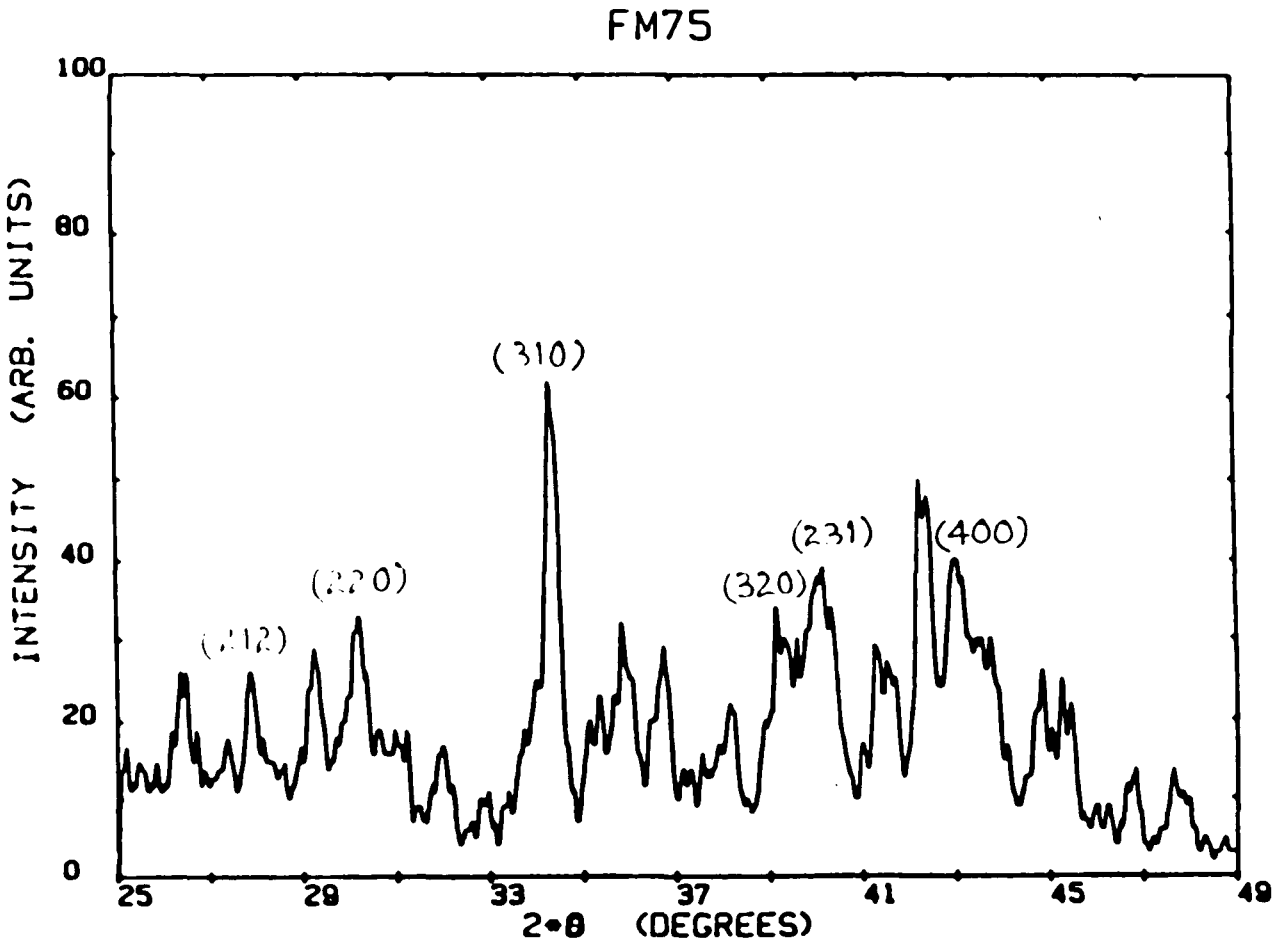
FM75
INTENSITY (ARB. UNITS)
100
80
60
40
20
0
25
29
33
37
41
45
49
2•θ (DEGREES)
(310)
(231)
(400)
(320)

Fig.4.18

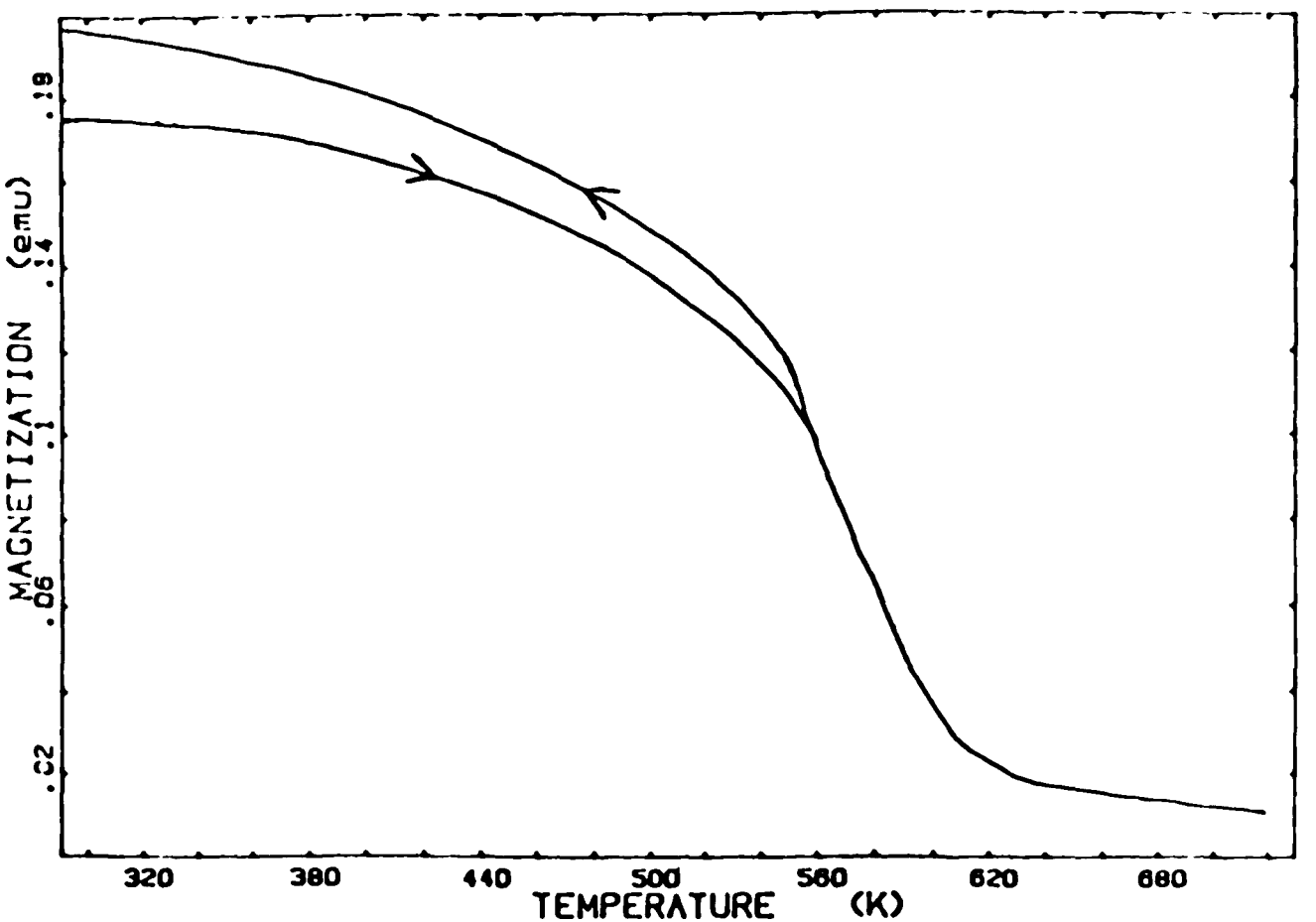
MAGNETIZATION (emu)
.18
.14
.1
.06
.02
320
380
440
500
560
620
680
TEMPERATURE (K)

Fig. 4.19

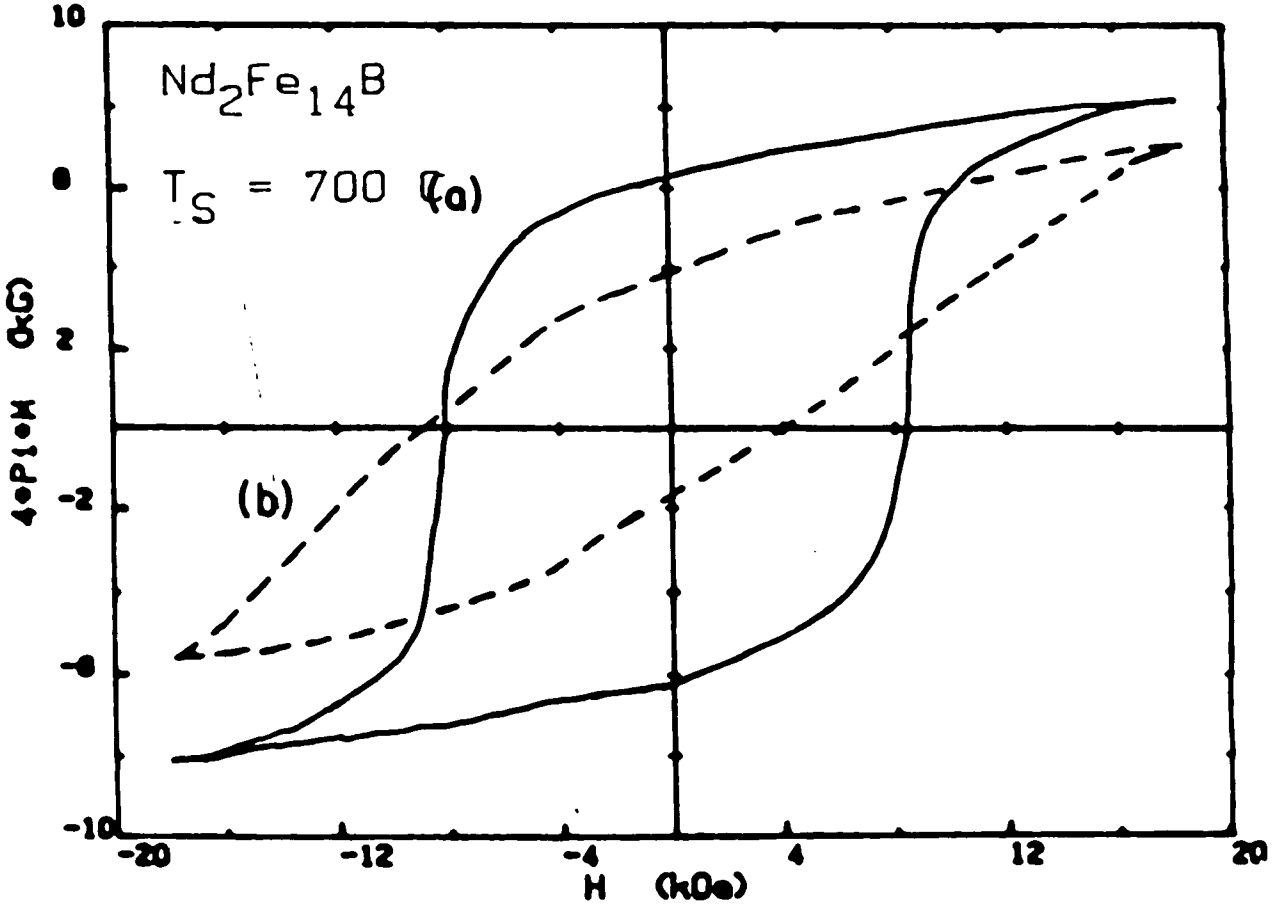

Fig. 5.1

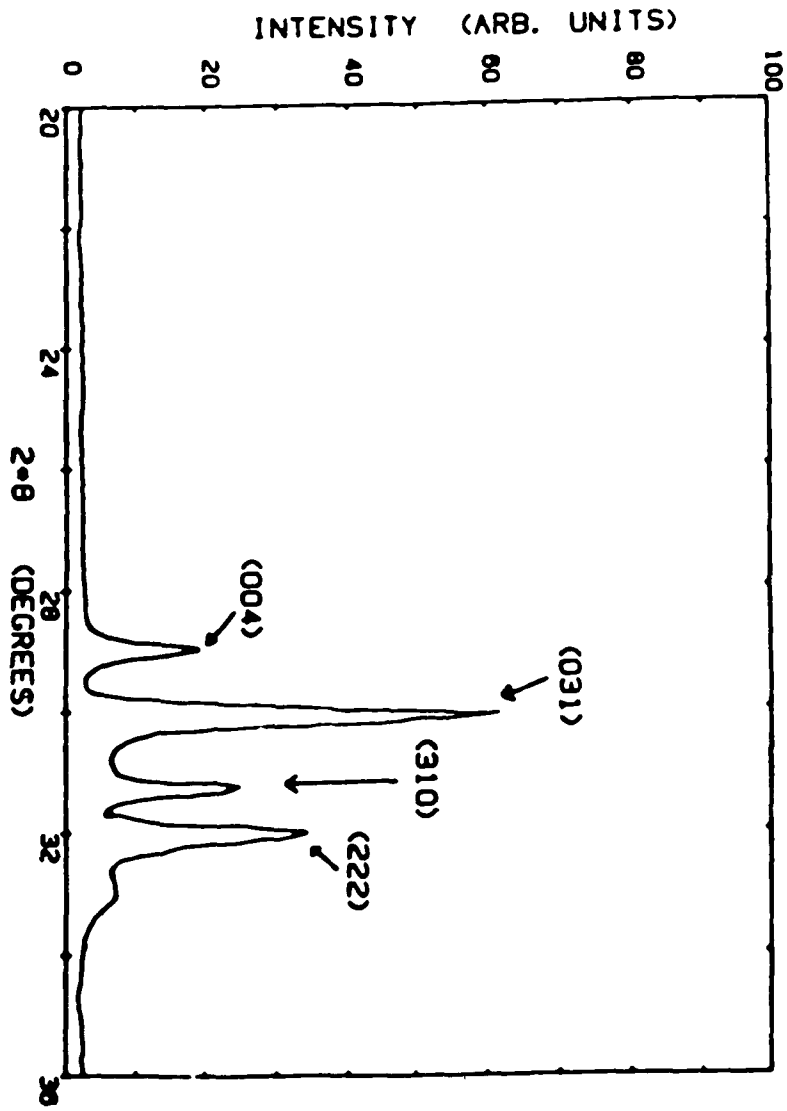
INTENSITY (ARB. UNITS)
0
20
40
60
80
100
20
24
28
32
36
2θ (DEGREES)
(004)
(031)
(310)
(222)

Fig. 5.2

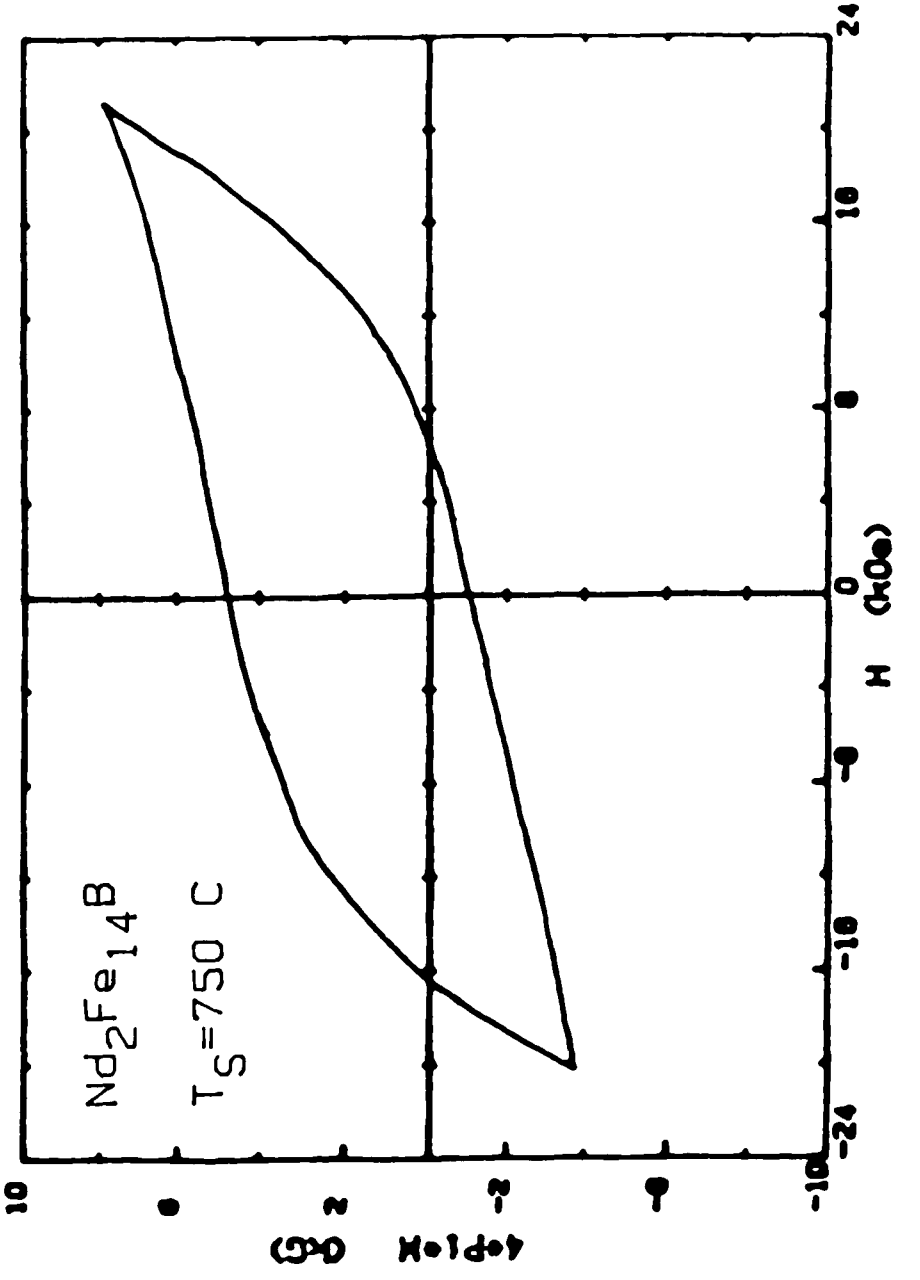

Fig. 5.3

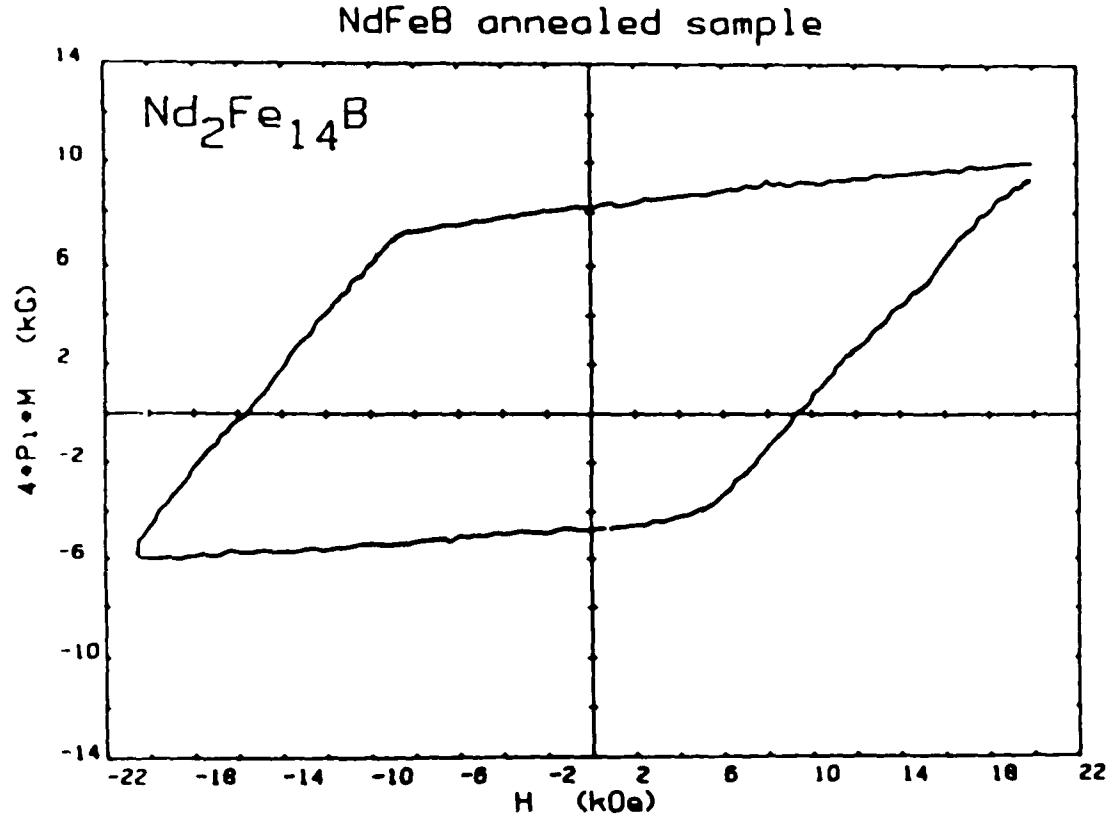
NdFeB annealed sample
$Nd_2Fe_{14}B$
14
10
6
2
-2
-6
-10
-14
4•Pi•M (kG)
-22
-18
-14
-10
-6
-2
2
6
10
14
18
22
H (kOe)

Fig. 5.4

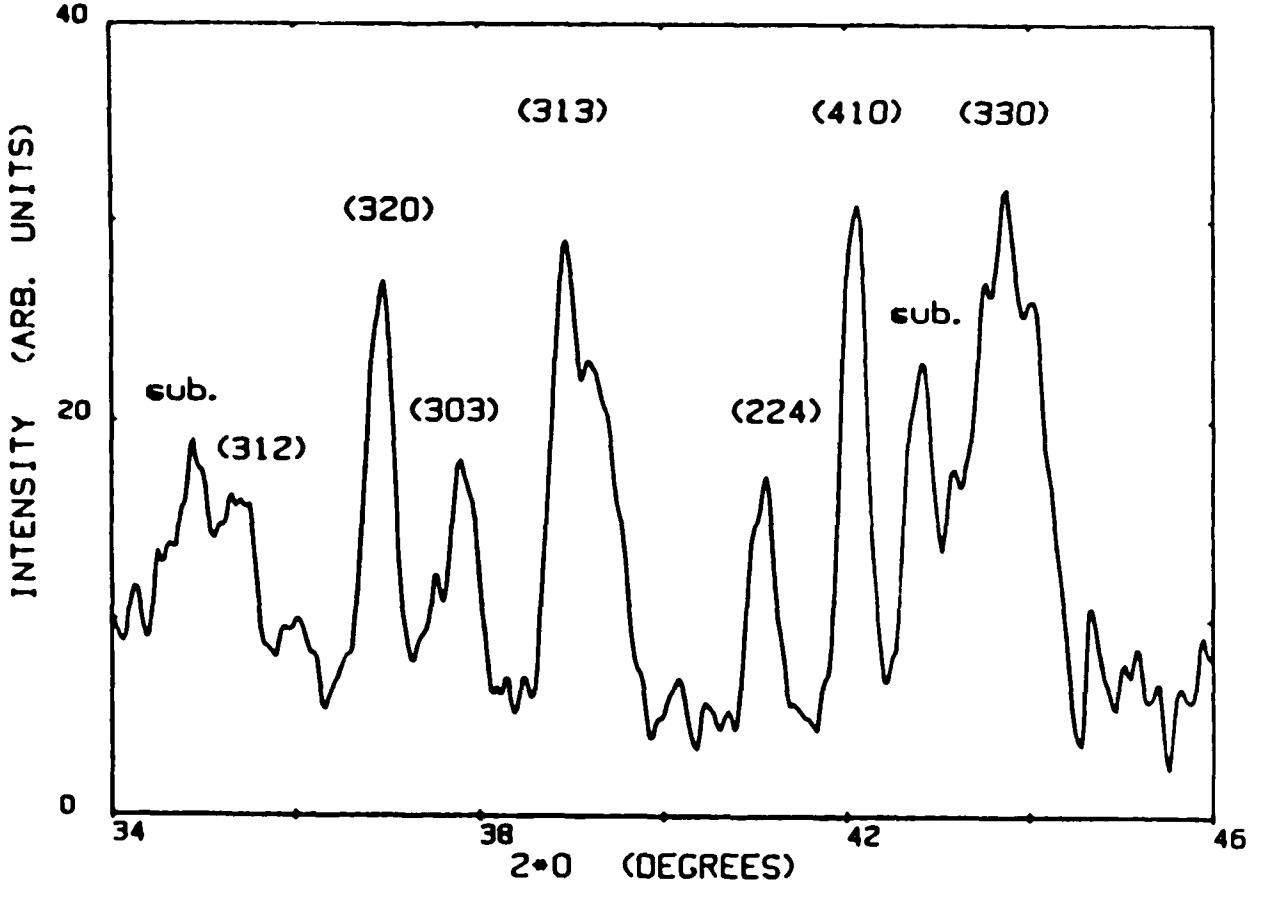
40
20
0
INTENSITY (ARB. UNITS)
(313)
(410)
(330)
(320)
sub.
(312)
(303)
(224)
sub.
34
38
42
46
2•0 (DEGREES)

Fig. 5.5

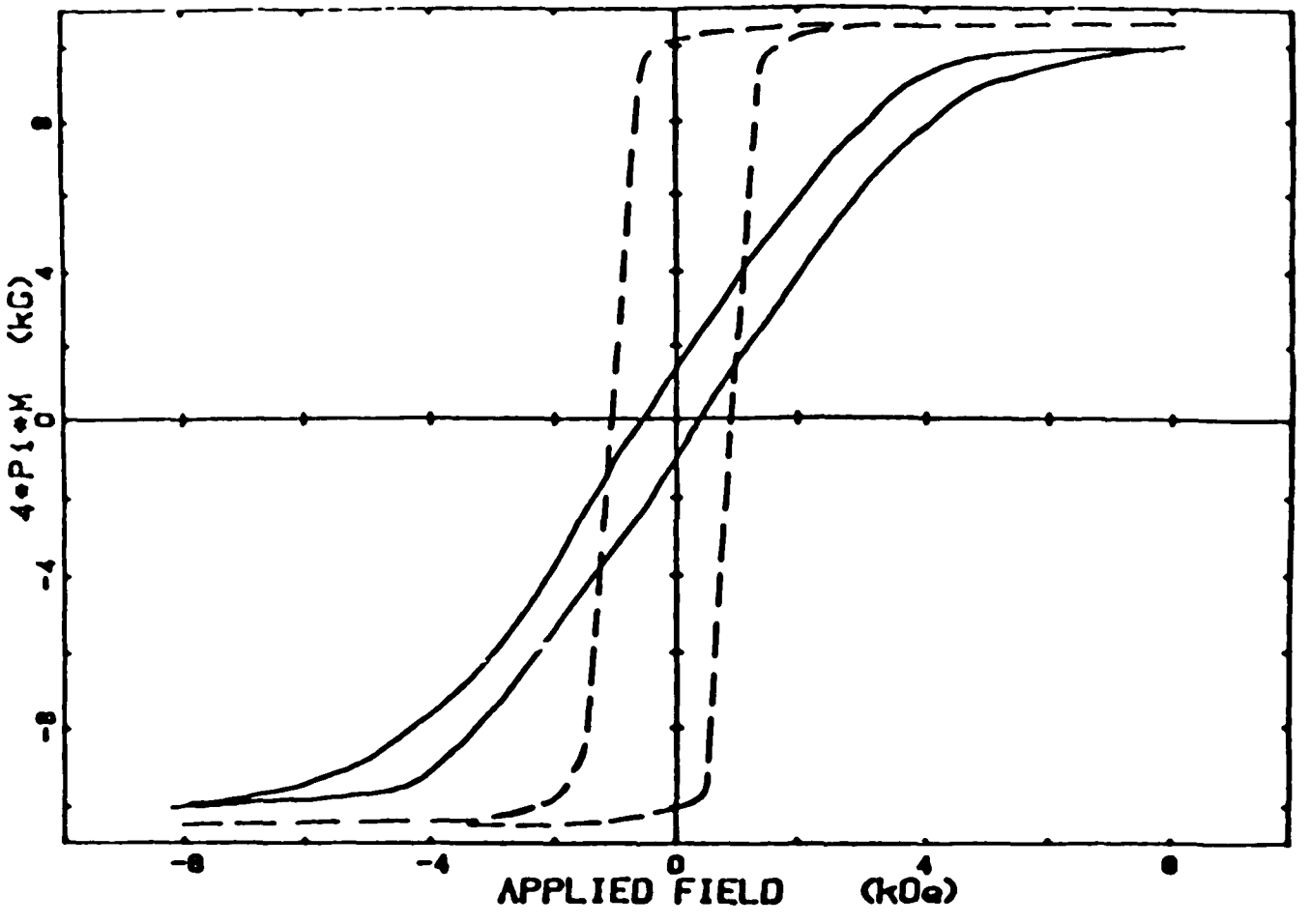

Fig. 6.1

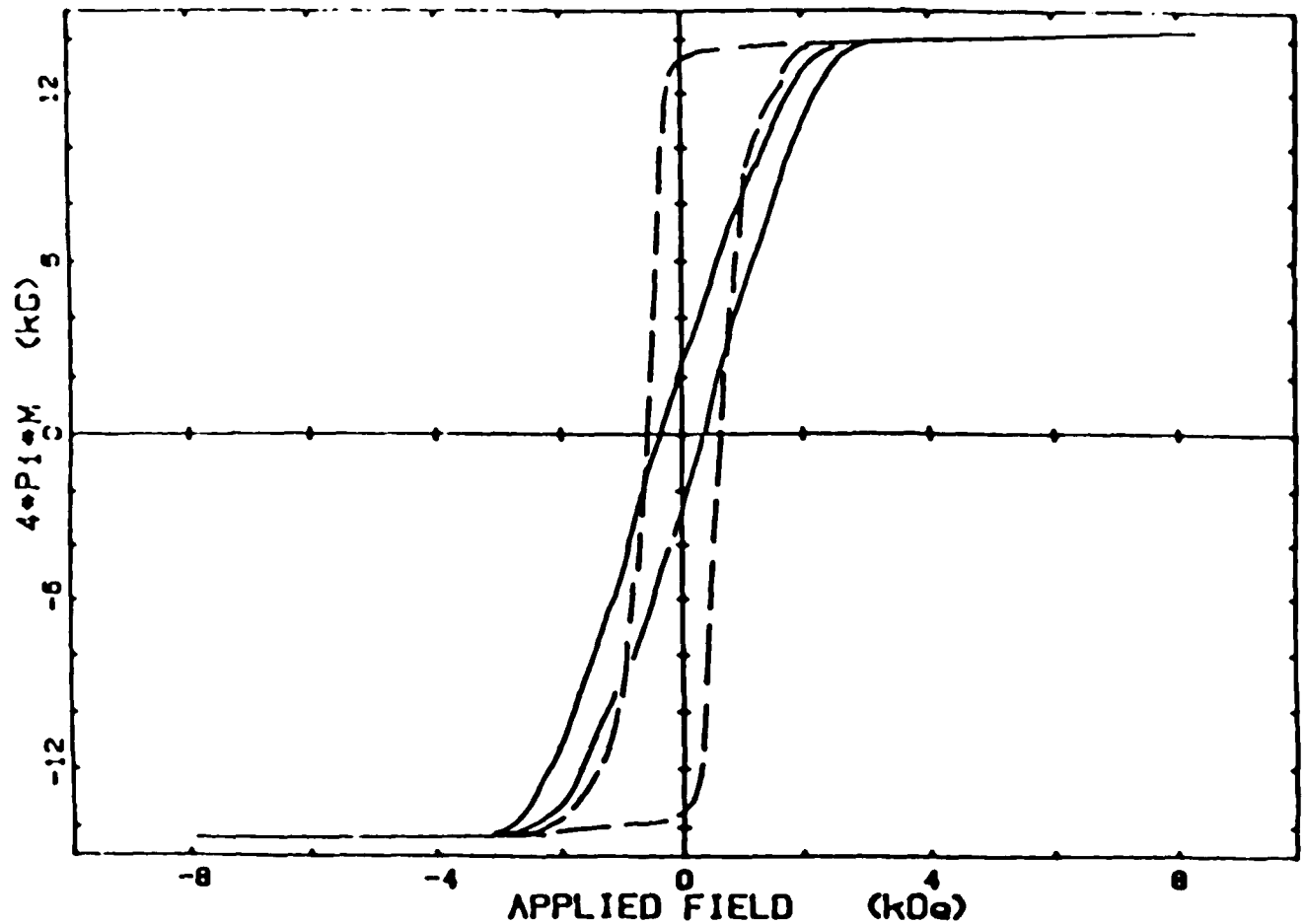

Fig. 6.2

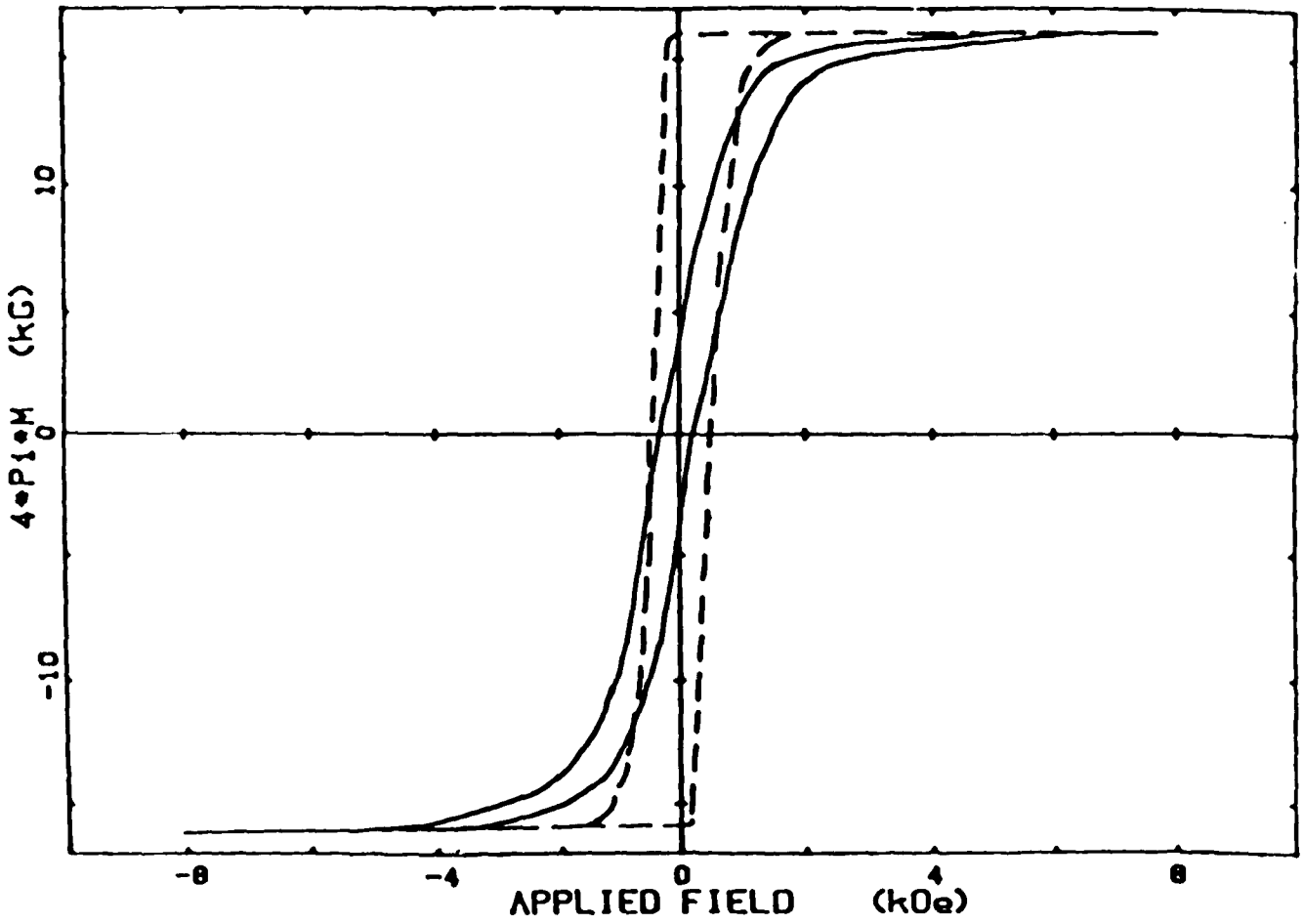

Fig. 6.3

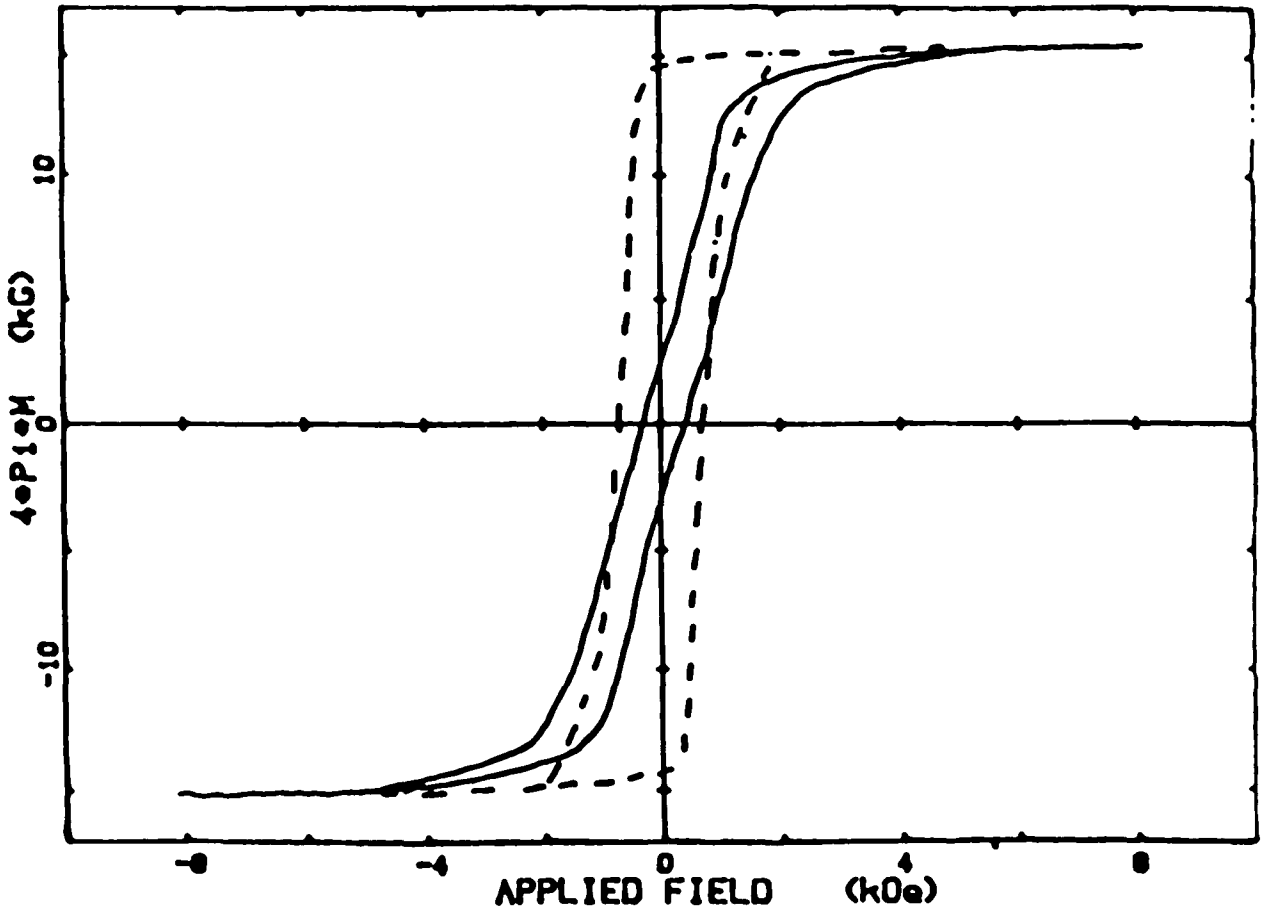

Fig. 6.4

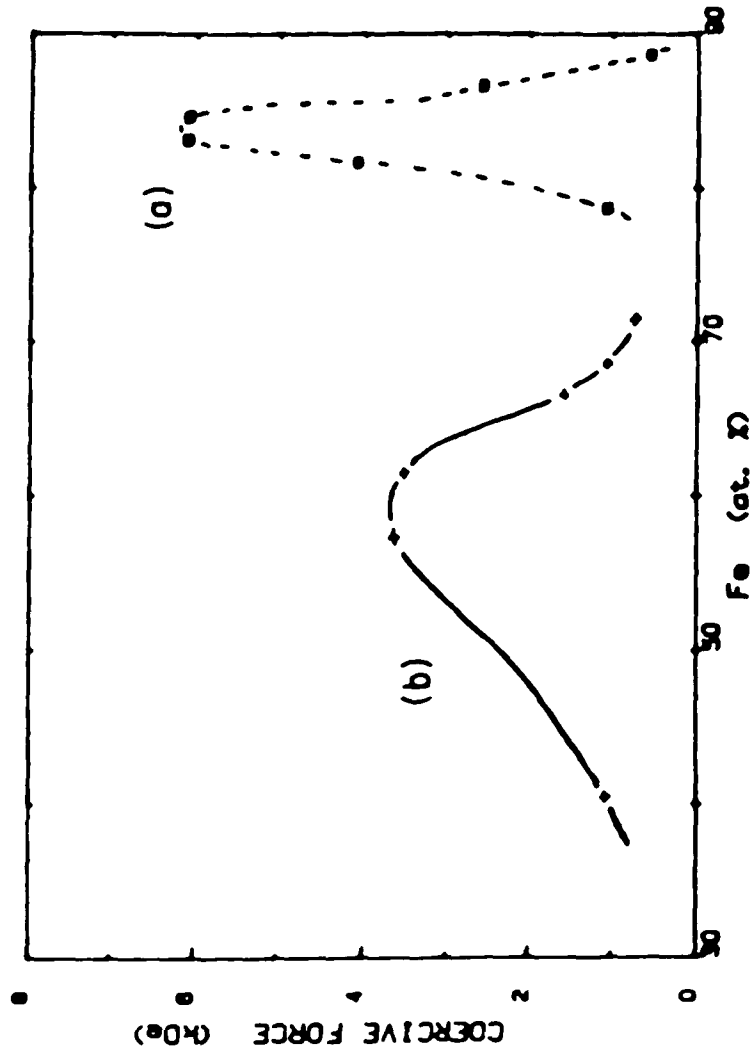

Fig. 7.1

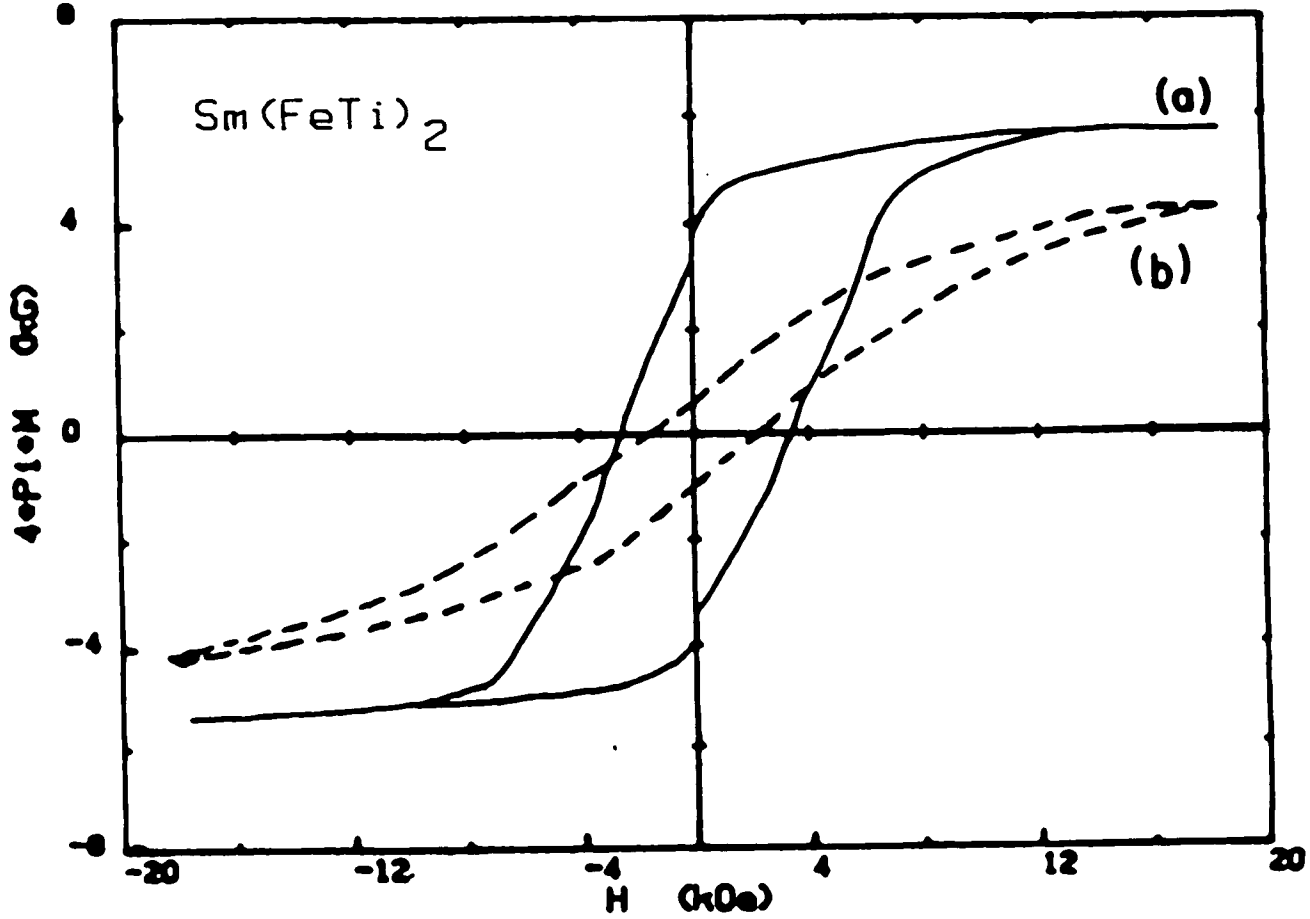

Fig. 7.2

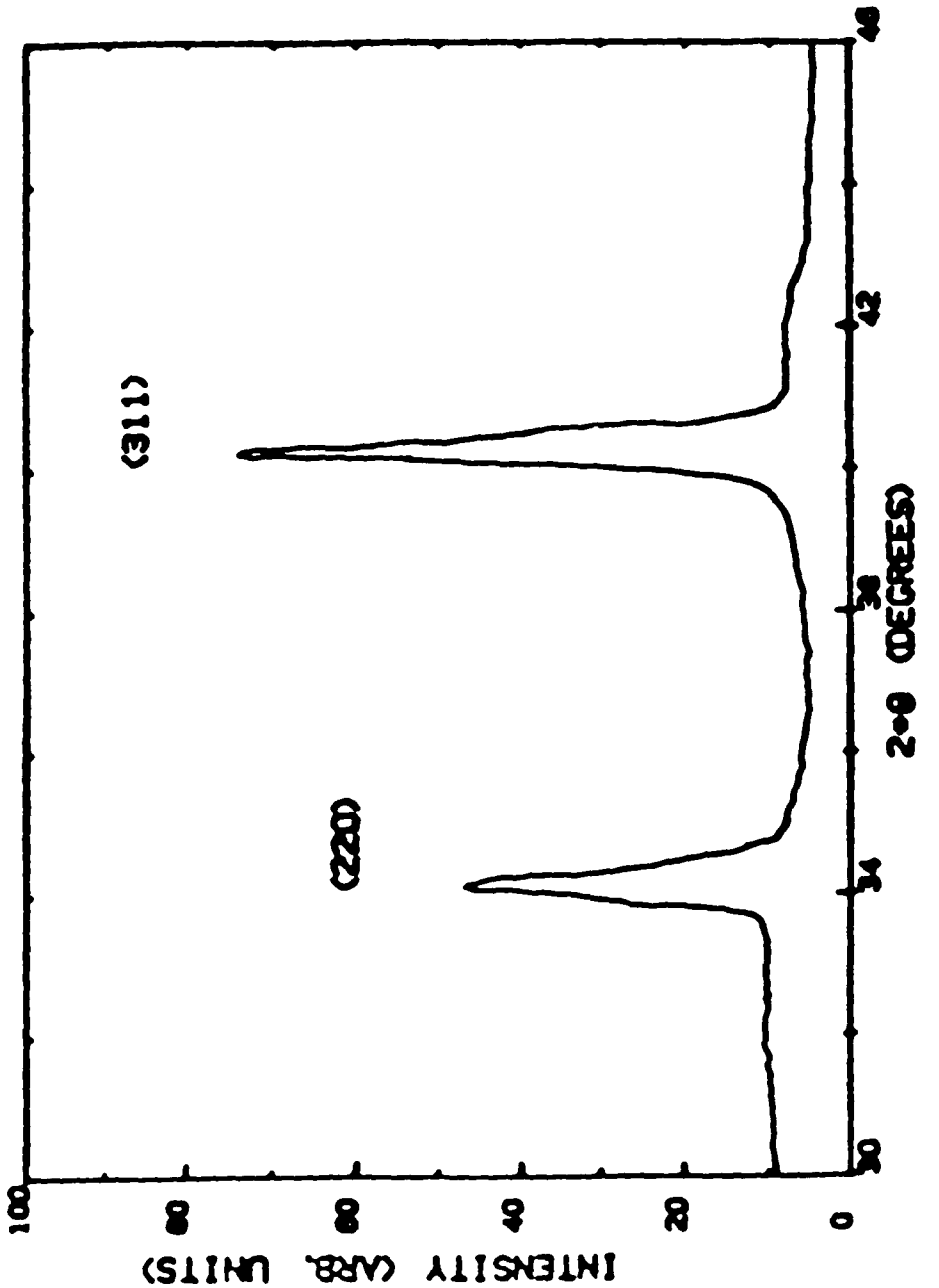
(311)
(220)
INTENSITY (ARB. UNITS)
2θ (DEGREES)
100
80
60
40
20
0
30
34
38
42
46

Fig. 7.3

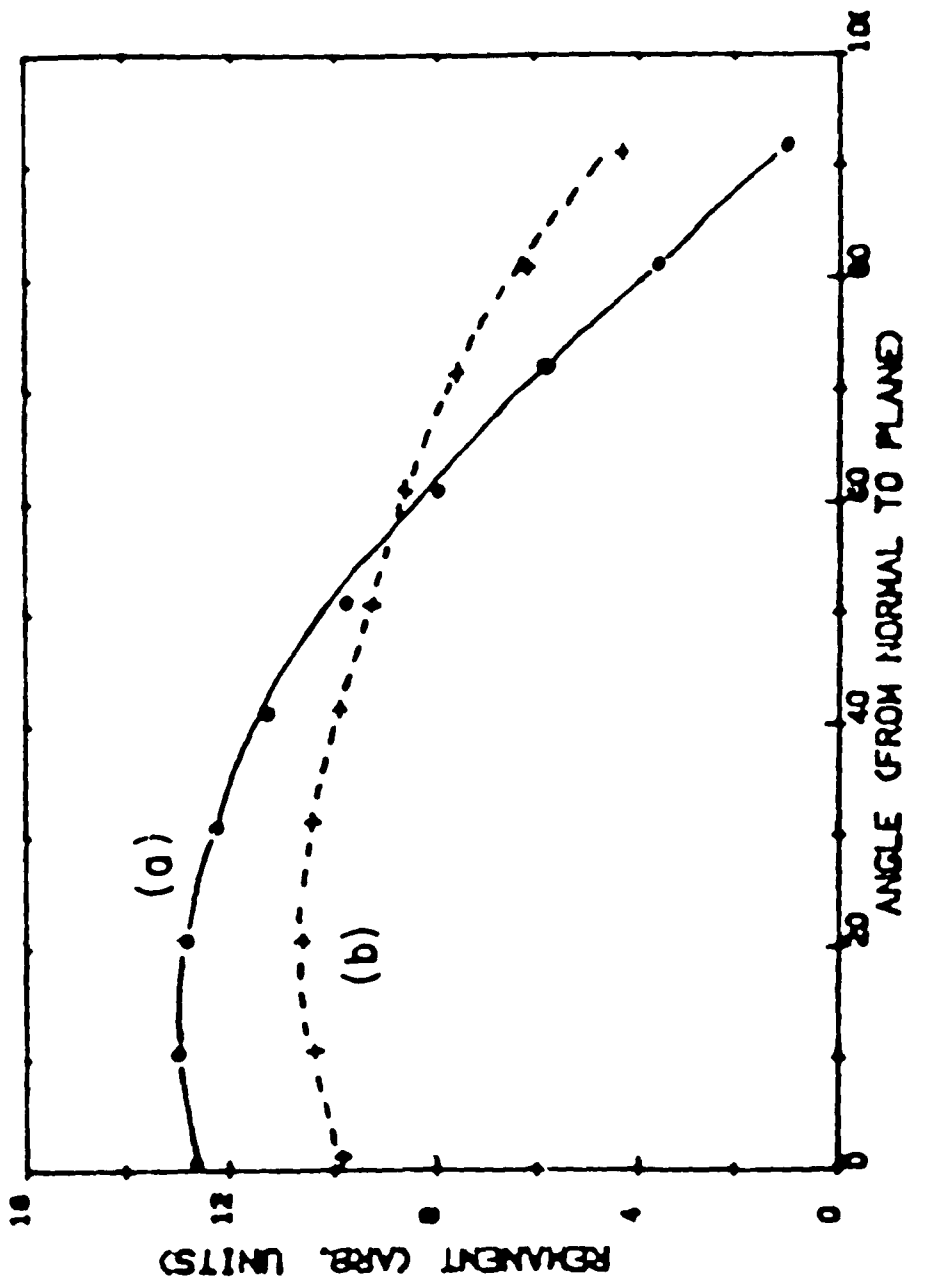

Fig. 7.4

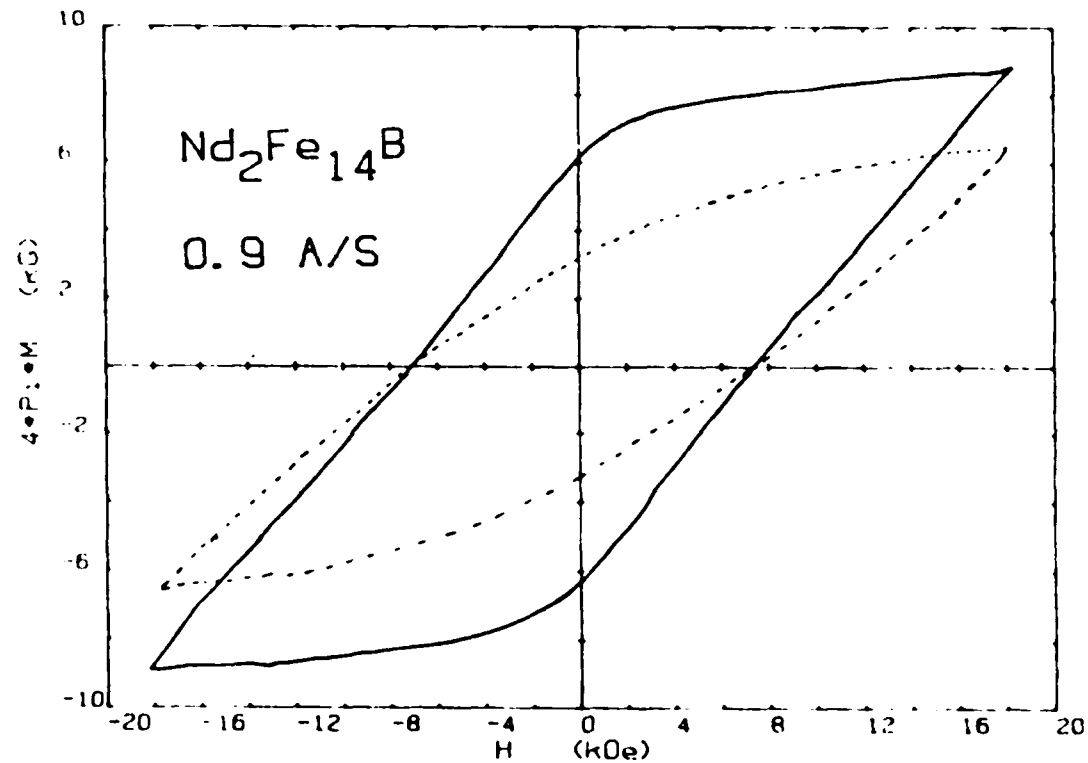

Fig. 7.5

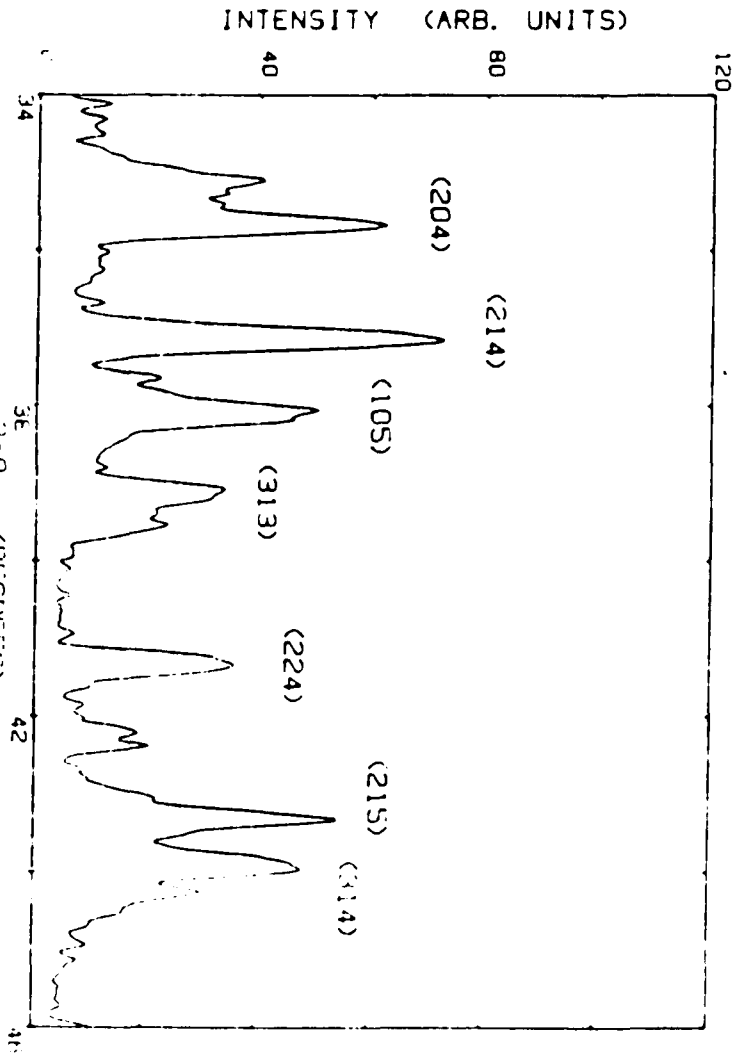
INTENSITY (ARB. UNITS)
40
80
120
34
38
42
2•θ (DEGREES)
(204)
(214)
(105)
(313)
(224)
(215)
(314)

Fig. 7.6

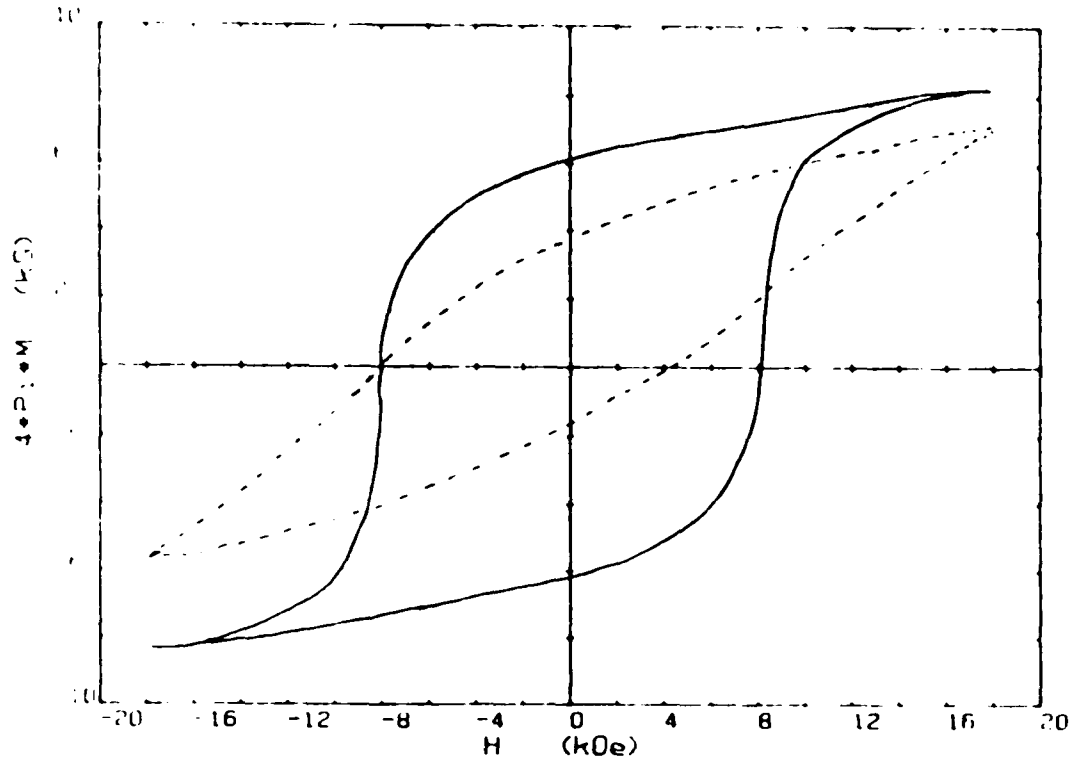

Fig. 7.7

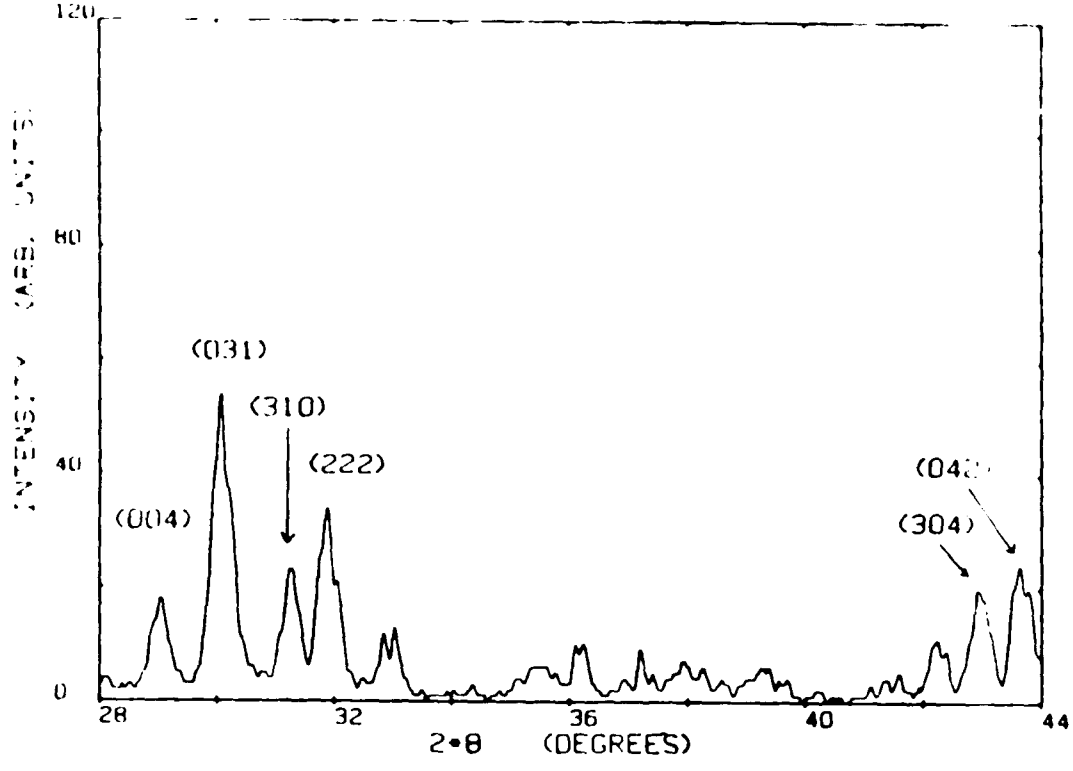
120
80
40
0
INTENSITY (ARB. UNITS)
(031)
(310)
(222)
(004)
(042)
(304)
28
32
36
40
44
2•θ (DEGREES)

Fig. 7.8

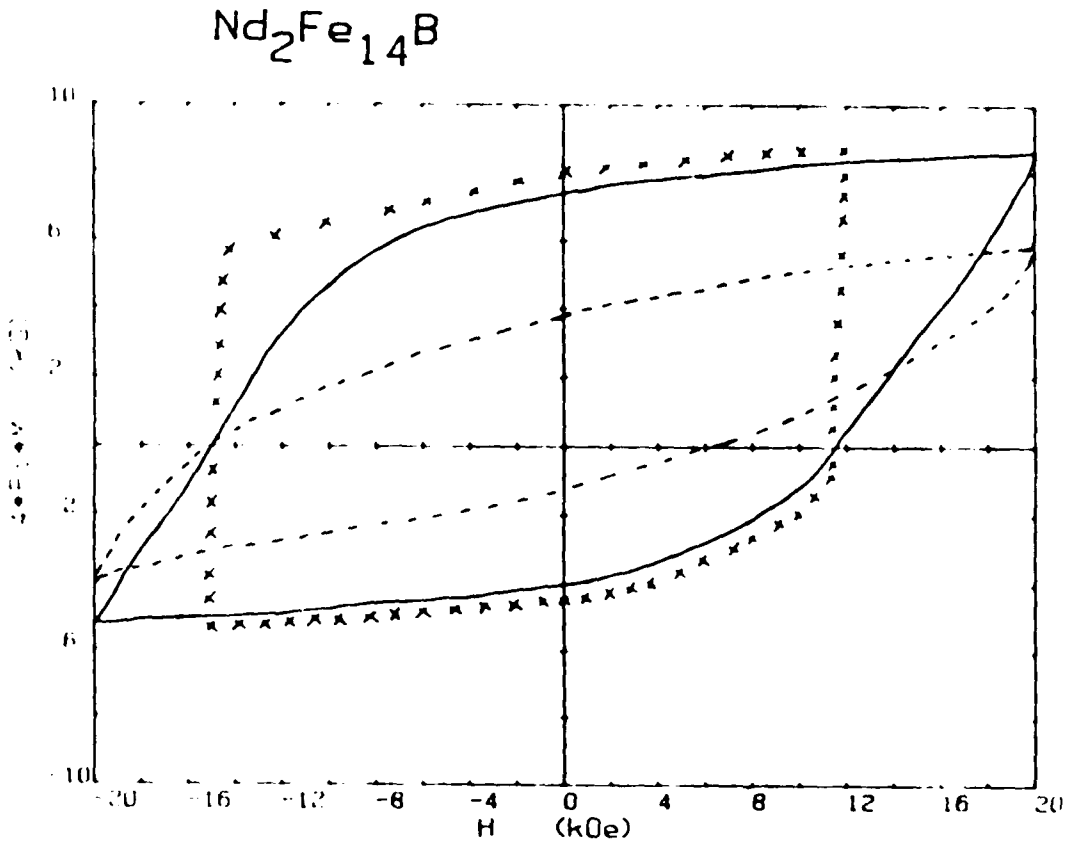

Fig. 7.9

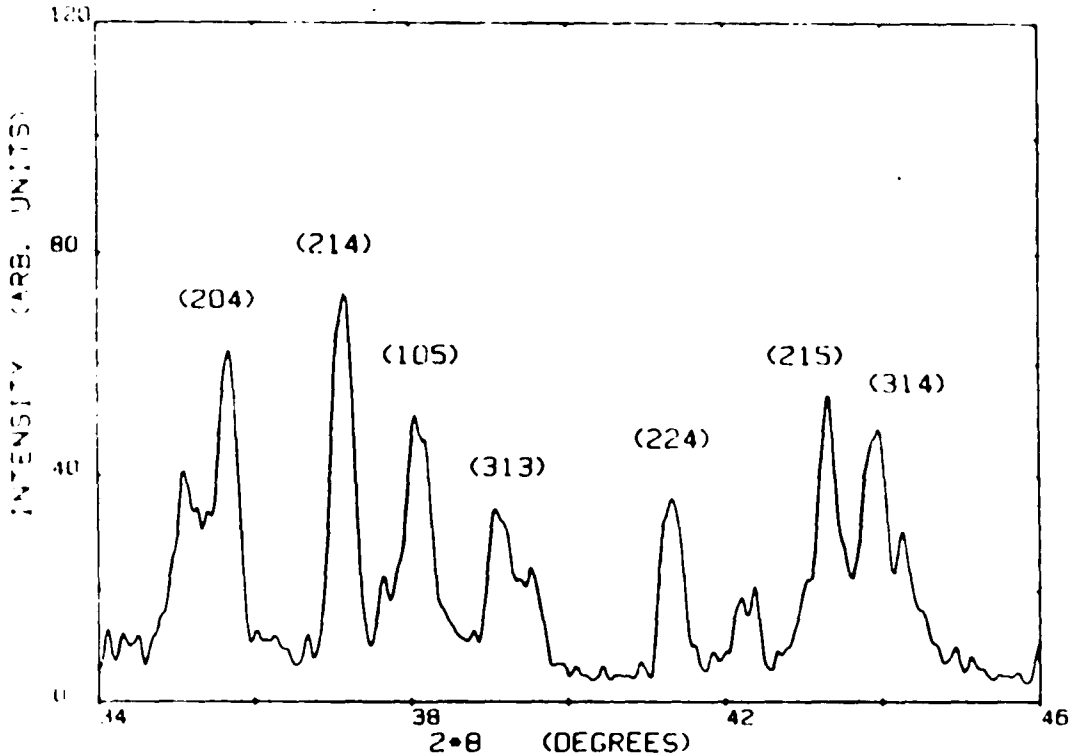
120
80
40
0
INTENSITY (ARB. UNITS)
(204)
(214)
(105)
(313)
(224)
(215)
(314)
34
38
42
46
2•8 (DEGREES)

Fig. 7.10

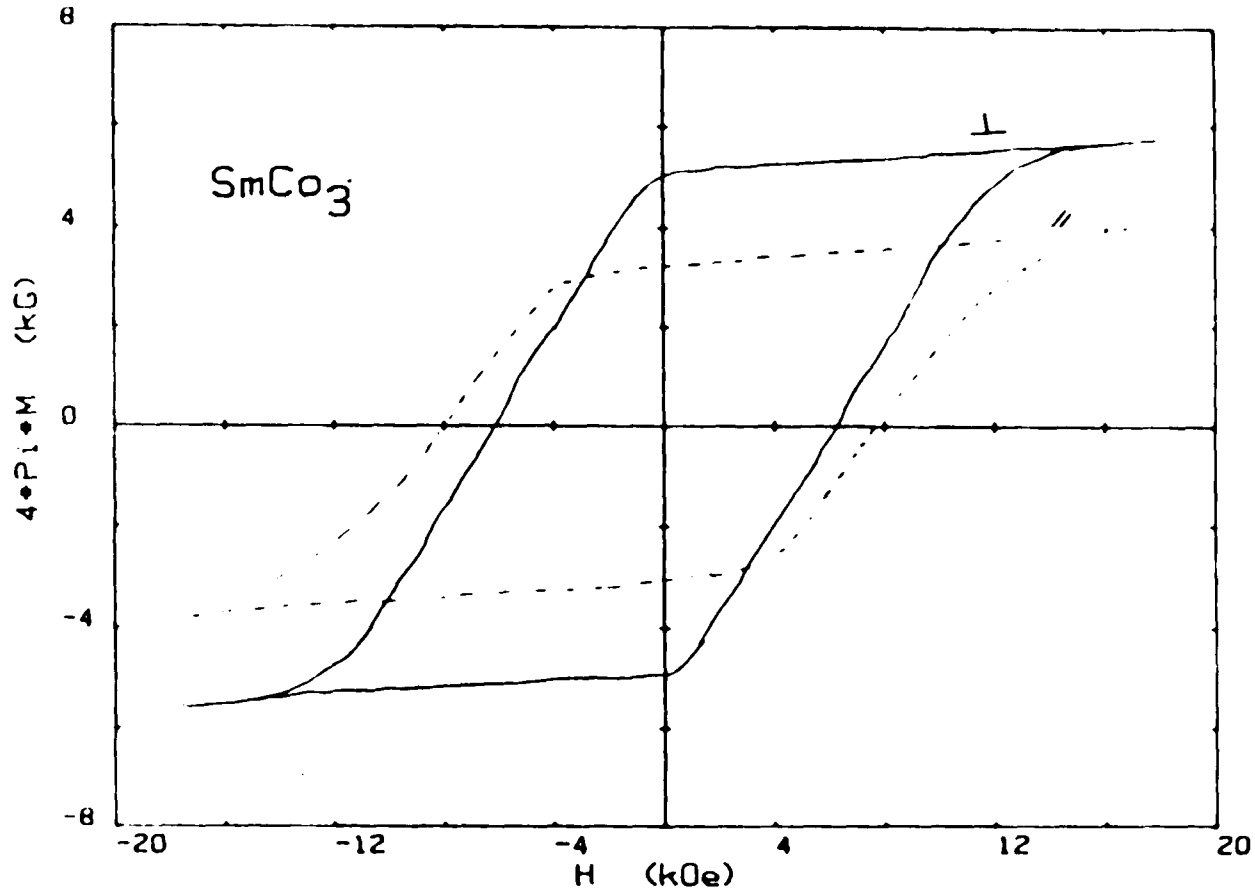

Fig.7.11

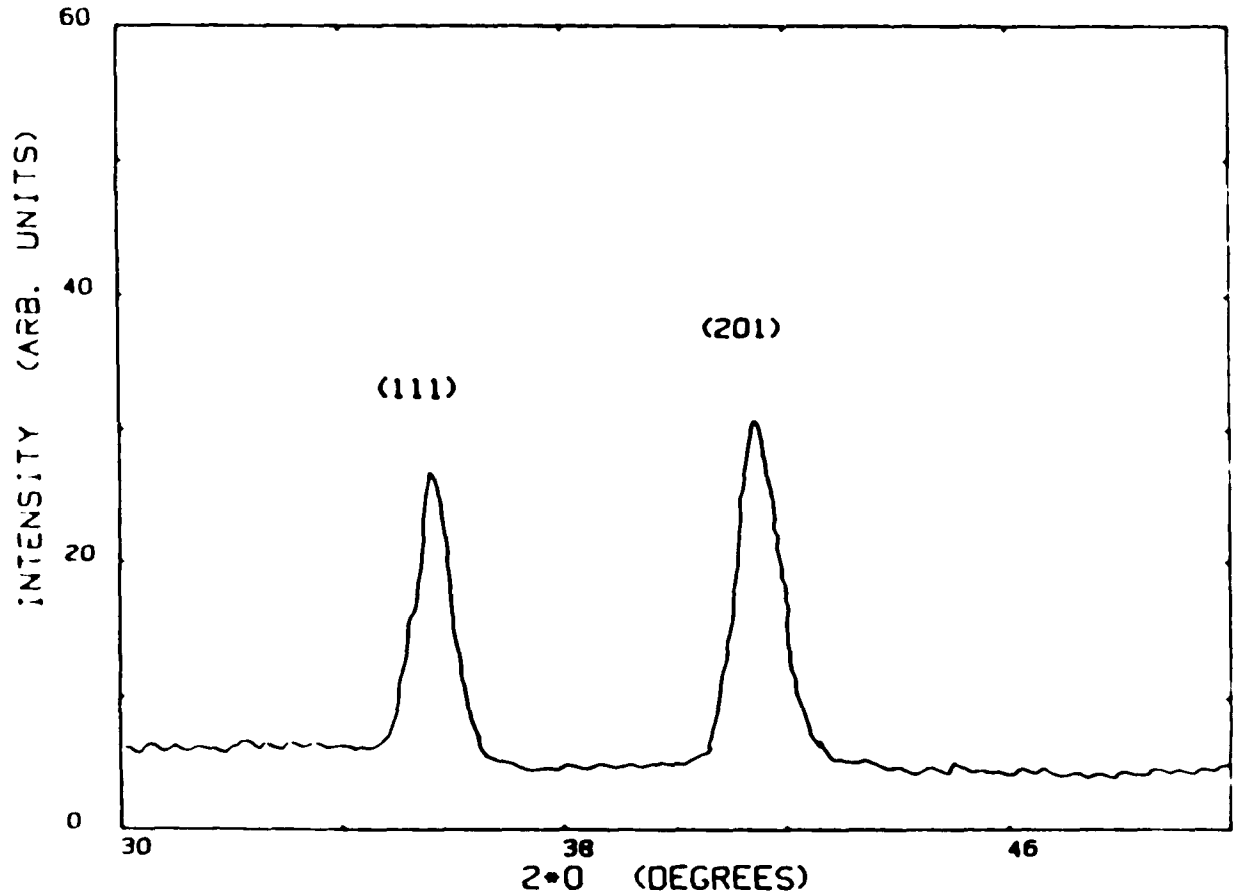

Fig. 7.12

REFERENCES

1. D.E. Speliotis, and J.J. Becker, J. Appl. Phys. 41, 1055 (1970).

2. M. Merches, S.G. Sankar and W.E. Wallace, J. Appl. Phys. 49, 2055 (1978).

3. R.S. Perkins, S. Strassler, and A. Menth, AIP Conf. Proc. 29, 610. (1975).

4. M.V. Satyanarayana, W.E. Wallace, and R.S. Craige, J. Appl. Phys. 50, 2324 (1979).

5. K.H.J. Buschow, J. Lees Common Metals 25, 131 (1971).

6. F.J. Cadieu, T.D. Cheung, S.H. Aly, L. Wickramasekara, and R.G. Pirich, J. Appl. Phys. 53, 8338 (1982).

7. F.J. Cadieu, T.D. Cheung, L.Wickramasekara, and S.H. Aly, J. Appl. Phys. 55, 2611 (1984).

8. T.D. Cheung, L. Wickramasekara, and F.J. Cadieu, J. Magn.& Magn. Mat. 54-57, 1641(1986).

9. L. Wickramasekara, T.D. Cheung, and F.J. Cadieu, J. Magn.& Magn. Mat. 54-57, 1679 (1986).

10. R.W. Lee, J. Appl. Phys. 52, 2549 (1981).

11. F.J. Cadieu, T.D. Cheung, and L. Wickramasekara, J. Appl. Phys. 57, 4161 (1985).

12. R.W. Lee, Appl. Phys. Lett. 46, 790 (1985).

13. M. Sagava, S. Fujimura, H. Yamamoto, Y. Matsuura, and K. Hiraga, IEEE Trans Magn. MAG-20, 1584 (1984).

14. Y. matsuura, S. Hirosawa, H. Yamamoto, S. Fujimura, and M. Sagawa, Appl. Phys. Lett. 46, 308 (1985).

15. F.J. Cadieu, T.D. Cheung, and L. Wickramasekara, J.Magn & Magn. Mat. 54-57, 535(1986).

16. F.J. Cadieu, T.D. Cheung, L. Wickramasekara, and N. Kamprath, IEEE Trans Magn. MAG-22, 752 (1986).

17. S.H. Aly, T.D. Cheung, L. Wickramasekara and F.J. Cadieu, J.

Appl. Phys. 57(6), 2147 (1985). Also S.H. Aly, Ph.D thesis, 1985, CUNY.

18. T.D. Cheung, L. Wickramasekara, and F.J. Cadieu, J. Appl. Phys. 57, 3598 (1985).

19. K.H.J. Buschow, Chapter 4, Ferromagnetic materials,vol.1, North Holland,(1980).

20. W.B. Pearson, A Hand Book of Lattice Spacing and Structures of Metal and Alloys,Pergamon Press,Oxford (1958).

21. W.B Pearson, The Crystal Chemistry of Lattice Spacing and Physics of Metals and Alloys, Willey Interscience,NY (1972).

22. W.E. Wallace, Rare Earth Intermetallic, Academic Press, N.Y. (1973).

23. K.H.J. Buschow, Rep. Prog. Phys. 40, 1179 (1977).

24. E.C. Stoner, Proc. Royal. Soc.A, 165, 372 (1938).

25. K.H.J. Buschow, Phys. Status Sol. (a),7, 199 (1971).

26. E. Burzo, D.P. Lazar and Ciorascu M, Phys. Status Sol. (b),65(1974) K145.

27. W.E. Wallace, Prog. Rare Earth Sci.Tech. 3, 1(1968).

28. I.A. Campbell, J. Phys. F: Metal Phys. 2L,47 (1972).

29. Szpunar and Kozarzeski, Phys. stat. Sol. (b), 82, 449 (1977).

30. P. Chaudhari, J.J. Cuomo and R.J. Gambino, Appl. Phys. Letters 22,337 (1973).

31. P. Chaudhari, J.J. Cuomo and R.J. Gambino, IBM J. of Res. & Dev. 11, 66 (1973).

32. H.J. Garrett and W.G.D. Frederrck, AIP Conf. Proceedings, No. 10, Part I Mag. and Mag. Materials-1972,p.582.

33. R.J. Gambino, P. Chaudhari, and J.J. Cuomo, AIP Proceedings, No. 12, part 1 Mag. and Mag. Mate.-1974, p. 578.

34. S. Mader , J. Vac. Sci. and Tech. 2, 35 (1965).

35. J.L. Vossen, Thin Film Processes Ch.1, Academic Press (1978).

36. B. Chapman, Glow Discharge Processes, Wiely Interscience

Publishers (1980).

37. J.S. Logan et al., J. Vac. Sci. Tech. Vol. 14, 1(1977).

38. F.J. Cadieu and N. Chencinski, J. Low. Temp. Phys. 28, 535 (1977).

39. F.J. Cadieu, T.D. Cheung, S.H. Aly, L. Wickramasekara and R.G. Pirich, IEEE, MAG-19, 2038 (1983).

40. F.J. Cadieu, L.F. Cooley and D.H. Douglass, Jr.,Rev. Sci. Instr. 42, 587 (1971).

41. Austin M. Garath, Phys. Rev. 36, 248 (1930).

42. Report Air Force Materials Laboratory Contract No. F33615-73-c-5012, Batelle Pacific Northwest, 1974.

43. M. Gronau, H. Goeke, and S. Methfessel, Proc. 4th Int. Conf. on Rapidly Quenched Metals (Sendai 1981).

44. E.P. Bertin, Principles and Practice of X-Ray Spectrometric Analysis, Second Edition, Plenum press (1975).

45. R. Jenkings and J.L. De Vries, Practical X-Ray Spectrometry, Springer-Verlag,N.Y. (1967).

46. L. Bergel and F.J. Cadieu, X-Ray Spectrometry, Vol. 9, 19 (1980).

47. L.S. Birks, X-Ray Spectrochemical Analysis, First Edition, Interscience Publisher, N.Y. (1969).

48. B. Cullity, Elements of X-Ray Diffraction, Second Edition, Addision-Wesley, 1978.

49. J.R. Rodes, American Lab 5(7), 57 (1973).

50. L.S. Birks, Electron Probe Microanalysis, ed. 2, Interscience Publishers,N.Y.,190 (1971).

51. E.F. Kaeble, Hand Book X-Rays, Mcgraw-Hill Book Co. N.Y. (1967).

52. C.A. Anderson, Microprobe Analysis, John Wiley & Sons, New York, 1973.

53. F.J. Cadieu, Rare Earth Transition Metal Permanent Magnet Workshop, Fort Monmouth, N.J. 27-28 January, 1986.

54. H. Klug and L. Alexander, X-Ray Diffraction Procedures, Chapter 5, 9 (1954).

55. R.D. Nelson, Research in production of rare earth cobalt permanent magnet materials by sputter deposition, AFML F33615-73-C-5012, Wright patterson Air Force Base, OH (1974).

56. D. Mcneely and H. Oesterreicher, J. Less Common Metals 44, 183 (1976).

57. G. Suran, K. Ounadjela, J. Stern and C. Sella, J. Appl. Phys. 55, 1757 (1984).

58. S. Iwasaki, and Yoshihisa Nakamara, IEEE Trans. Magn. MAG-13, 1272 (1977).

59. T. Chen and P. Cavallotti, Appl. Phys. Lett. 41, 205 (1982).

60. S. Iwasaki, K. Ouchi, and N. Honda, IEEE Trans. Magn. MAG-16, 1111 (1980).

61. Y. Maeda, S. Hirano, and S. Yoshii, Jpn. J. Appl. Phys. 20, L457 (1981).

62. T.M. Coughlin, J.H. Judy, and E.R. Wuori, IEEE Trans. Magn. MAG-17, 3169 (1981).

63. S. Hirano, Y. Maeda, and I. Hatakeyama, Jpn. J. appl. Phys. 20, L571 (1981).

64. K. Fukuda, Y. Kitahara, F. Maruta, and J. Ezaki, IEEE Trans. Magn. MAG-18, 1116 (1982).

65. K. Nakamara, N. Tani, M. Ischikawa, T. Yamada, Y. Ota, and A. Itoh, Jpn. J. appl. Phys. 23, L397 (1984).

66. K. Kobayashi and G. Ishida, J.Appl.Phys. 52, 2453 (1981).

67. T. Osaka, N. Kasai, I. Koiwa, F. Goto, and Y. Suganuma, J. Electroche. Soc. 130, 568 (1983).

68. K. Tsutumi and H. Sugawara, Jpn. J.Appl. Phys. 23, L169 (1984).

69. Seiichi Asada and Masahiro Kitada, Appl. Phys. Lett., 46, 792 (1985).

70. M. Matsuoka, Y. Hoshi, M. Naoe, and S. Yamanaka, IEEE Trans. Magn. Mag-18 1119 (1982).

71. K.H.J. Bushow, Les elements de terres rare, I, CNRS, 101 (1970).